Designing high χ copolymer materials for nanotechnology applications: A systematic bulk vs. thin films approach

Polyxeni Angelopoulou, Ioannis Moutsios, Gkreti-Maria Manesi, Dimitri Ivanov, Georgios Sakellariou, Apostolos Avgeropoulos

▶ **To cite this version:**

Polyxeni Angelopoulou, Ioannis Moutsios, Gkreti-Maria Manesi, Dimitri Ivanov, Georgios Sakellariou, et al.. Designing high χ copolymer materials for nanotechnology applications: A systematic bulk vs. thin films approach. Progress in Polymer Science, 2022, 135, pp.101625. 10.1016/j.progpolymsci.2022.101625 . hal-04290075

HAL Id: hal-04290075
https://hal.science/hal-04290075v1

Submitted on 16 Nov 2023

HAL is a multi-disciplinary open access archive for the deposit and dissemination of scientific research documents, whether they are published or not. The documents may come from teaching and research institutions in France or abroad, or from public or private research centers.

L'archive ouverte pluridisciplinaire **HAL**, est destinée au dépôt et à la diffusion de documents scientifiques de niveau recherche, publiés ou non, émanant des établissements d'enseignement et de recherche français ou étrangers, des laboratoires publics ou privés.

Designing High χ Materials for Nanotechnology Applications: A Systematic Bulk *vs.* Thin Films Approach

Polyxeni P. Angelopoulou[1], Ioannis Moutsios[2], Gkreti-Maria Manesi[2], Dimirti A. Ivanov[3,4,5,6], Georgios Sakellariou*[1], Apostolos Avgeropoulos*[2,4]

[1] Department of Chemistry, National and Kapodistrian University of Athens, Athens, 15771 Greece;

[2] Department of Materials Science Engineering, University of Ioannina, University Campus-Dourouti, 45110 Ioannina, Greece; e-mail@e-mail.com

[3] Sirius University of Science and Technology, 1 Olympic Ave, 354340, Sochi, Russia;

[4] Faculty of Chemistry, Lomonosov Moscow State University (MSU), GSP-1, 1-3 Leninskiye Gory, 119991 Moscow, Russia;

[5] Institute of Problems of Chemical Physics, Russian Academy of Sciences, Chernogolovka, 142432 Moscow, Russia;

[6] Institut de Sciences des Matériaux de Mulhouse – IS2M, CNRS UMR7361, 15 Jean Starcky, Mulhouse 68057, France.

Table of Contents

Abstract

This review article, demonstrates the origins of self-assembly behaviour of block copolymers, towards the formation of high resolution patterns for nanolithography purposes. Comparative analysis for the microphase separation in bulk and thin films is provided, to map the fundamentals of BCPs inherent properties prior to their use in advanced applications. Following the on-going trend of the minimization of feature sizes high-χ/low-N and/or complex architecture copolymers are prepared to overcome the limitations posed from the conventional patterning techniques. Although trivial segment combinations have provided significant insight in polymer physics, their implementation in lithography is limited due to the relatively low repulsion between the constituent blocks. This fact led to the synthesis of novel BCPs with higher χ values and appealing properties. Directed self-assembly has drawn intensive attention due to low defectivity, diminished dimensions, facile processability, etching selectivity, low cost and ability to design various patterns. Recent strategies have been developed to further facilitate the use of BCPs according to the standards of micro electro mechanical systems, in conjunction with or instead of already established nanofabrication methods.

1. Introduction

Block copolymers (BCPs) have received tremendous attention due to their ability to microphase separate into various nanostructures when studied in bulk and/or thin films. A significant contributing factor to BCPs self-assembly is the immiscibility between the different covalently connected segments. The Flory-Huggins interaction parameter (χ) describes the segment-segment incompatibility, and the scientific community has recently shifted its interest[1,2] towards the enhancement of this enthalpic parameter in several BCP systems. Despite the extensive literature reports[1,2] regarding the significance of χ, only recently has a wide range of different block combinations exhibiting high χ values leading to self-assembly of the relative BCPs in the sub-10nm scale or even lower (sub-5nm) been reported.

Important questions concerning the morphology adopted in bulk and whether these structures are equilibrium topologies can be answered by considering various factors such as: molecular weight, dispersity, composition, architecture, amorphous or crystalline chains, solvent used (selective or non-selective), casting procedure, annealing temperature and duration, cooling process, sectioning, and staining procedures (if necessary). These factors can be considered more than enough for morphological studies in bulk taking into consideration the

well-studied phase diagram of simple diblock copolymers (χN vs φ, where χ is the Flory-Huggins interaction parameter between the two different segments, N is the degree of polymerization and φ is the volume fraction of one of the segments) of the PS-*b*-PI sequence, where PS is polystyrene and PI is poly(isoprene). Another phase diagram of ε vs φ_A (where ε is the elasticity parameter of the two different blocks and will be discussed further in the following chapters) has been reported for non-linear architectures of the AB_n sequence where the discrepancies between theoretically expected and experimentally observed structures were evident.

Similar questions can be made for the thin film structural characterization of the same BCPs. The factors controlling the adopted morphology are similar as in bulk with additional factors including periodicity, critical dimension size, interfacial width as well as film thickness and diffusivity of the segments on the corresponding substrate. Furthermore, a major question which has been the subject of many studieson thin films was how to improve the order, orientation and defects on the thin films topologies and major contributions were made based on: thermal annealing just below order-disorder transition (ODT) to improve diffusivity, altering the film thickness, changing the substrate chemistry and solvent vapor annealing (SVA). SVA has drawn much attention in the involved scientific community[1-3] since the kinetics of self-assembly are improved by plasticizing the polymer with the incorporation of solvent molecules. Thin films are exposed to solvent vapors well below the glass transition temperature (T_g) of both blocks, leading to a swollen and mobile film on the substrate which affords very well-ordered structures.

Block copolymer self-assembly is one of the most applicable materials-based methods to fabricate nanolithographic templates, nanowires, nanoarrays, optoelectronics and patterned memory storage media with feature sizes in the sub-10 nm regime.[4-9] Commonly utilized lithographic top-down methods (conventional photolithography, e-beam lithography, dip-pen lithography, interference lithography, ion beam lithography, nano imprint lithography etc.) have reached fundamental constrains in their ability to achieve low feature sizes, rendering alternative bottom-up approaches, necessary in order to continue minimizing the dimensions, such as BCP directed self-assembly (DSA). [10,11] The major disadvantages of nanolithographic techniques are related to the limited ability for higher resolution and to the high-cost procedures. In bottom-up nanotechnology, copolymer self-assembly leads to nanostructures or nanopatterns where the major scientific concern lies on the achievement of long-range order. [12] As a result, scientific interest has shifted towards the preparation of materials by exploiting different blocks and/or complex architecture copolymers in an effort to produce cost-effective, defect-free morphological patterns exhibiting long-range topologies.[13-15] BCPs suit this role perfectly since they inherently assemble in various periodic nanoscale structures, due to the chemical immiscibility of the covalently bonded blocks.[16,17] Copolymers are versatile nanomaterials and ideal candidates to bridge the gap between top-down and bottom-up nanotechnology owing not only to their nanometer dimensions, but also due to low-cost, facile processing and adjustable properties, flexibility and microphase separation (Fig.1).[18]

By combining the different DSA methods, types of polymers, studies in bulk or thin films, the process characteristics of each method, it has been concluded that thin film DSA methods such as interfacial interactions, solvent vapor annealing, pattern templated assembly, zone casting and electrospray deposition are suitable for almost all type of soft matter materials without any additional requirements. [19] In contrast, the respective DSA methods (shear, or electric field or magnetic field alignment, zone annealing and directional solidification) for bulk film studies have limitations and strongly depend on the type of the final material [19] and

therefore preparation of the bulk films require great care. The concise description of the techniques of choice for nanopatterning, together with corresponding benefits, limitations and applications are summarized in Table 1.

Table 1. Inherent characteristics of commonly utilized nanolithographic techniques

Technique	Half Pitch (nm)	Benefits	Limitations	Applications	Reference
Photo-Lithography	19	high throughput	not applicable for curved surfaces, expensive masks, photo sensitive polymers are required	electronic chips	20,21
NIL	10	simple, low cost, high throughput and high resolution	defects, overlay deficiency	electronic, optical, photonic devices	22
EBL or IBL	<10	high resolution, complicated patterns design, sustainable	low throughput, cost	opto-electronic devices, quantum structures, metamaterials	23
BCPs	3	High resolution, low cost, high aspect ratio, tunability, more sustainable	defects, limited patterns	device fabrication, plasmonics or metamaterials, nanoporous membranes	24,25,26

The combination of polymers DSA with top-down lithographic techniques has led to the preparation of multiscale templates for use in various aspects of nanotechnology.[27,28]

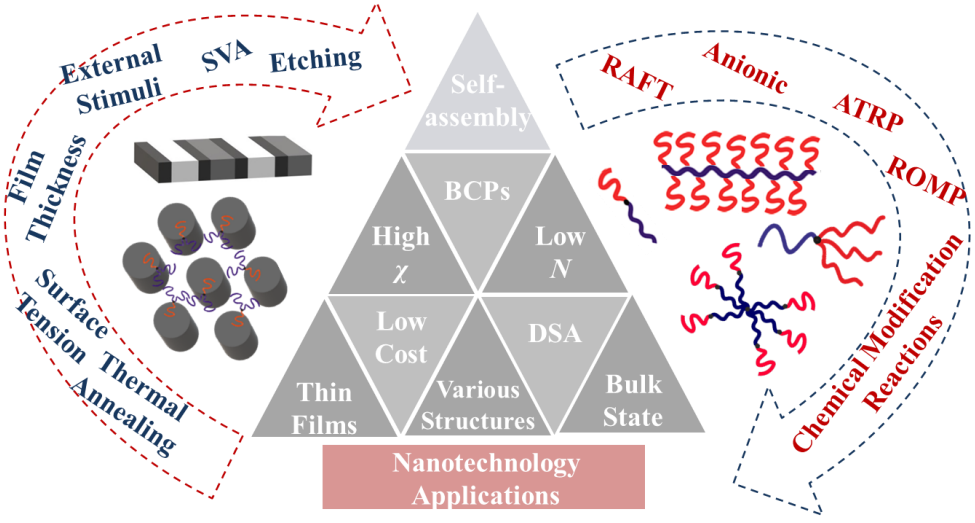

Fig. 1. Schematic illustration of BCPs properties and their potential use in nanotechnology applications.

Even though architecture complexity in block copolymers results in novel structures with variability in properties, the required mechanisms for predicting the structure/properties relationship remains challenging in such complex systems. Furthermore, their perspective has been mainly explored in the academic community and less in industry due to time consuming and/or demanding synthetic and isolation procedures of the final materials. Therefore, linear architectures have more commonly been studied in bulk and thin films, for nanotechnology related applications, compared to respective non-linear materials with identical molecular characteristics. However, in this review article the efforts made on BCP systems of complex architecture in nanotechnology applications will be described, as well.

2. Bulk self-assembly

2.1 Diblock copolymers

The simplest case of block copolymers are linear diblock copolymers where the phase behaviour is determined by the total degree of polymerization (N), the volume fraction (φ) and the segment-segment Flory-Huggins interaction parameter (χ). The entropy of mixing is affected by the first two factors, φ and N, that are related to copolymer composition and chain length, while χ is an enthalpic parameter related to the interaction between the different blocks and is inversely proportional to temperature according to the following equation, where α>0 and α, β are constants characteristic for each copolymer:

$$\chi = \frac{a}{T} + \beta \quad (1)$$

High χ values are attributed to chemically divergent segments that result in well-defined periodic nanostructures over a large-scale. Systems exhibit the highest χ values at room temperature but as temperature increases and over a critical elevated temperature (T_{ODT}), chemically dissimilar segments become miscible and microphase separation no longer occurs. When the product χN is higher than 10.5, for simple linear diblock copolymers, ordered structures ranging from spheres, to cylinders, to bicontinuous cubic structures and lamellar layers are formed and are strongly dependant on the volume fraction and the immiscibility of the segments (value of χ). The latter factor also affects the width of the inter-material dividing surface (IMDS), where the junction points are located, separating the two different blocks. Low surface width allows better organization of the structures, meaning 2D surfaces bear the junction points and have macromolecular chains completely distinct and bilaterally arranged. The localization of the junction points within the 2D surface in combination with the degree of polymerization (N), dispersity, composition and architecture complexity have an impact on the adopted morphology [16,17,29,30].

Specifically, the total number average molecular weight ($\bar{M}_n$) plays a distinct role in the self-assembly of BCPs, due to the direct association with the total degree of polymerization as can be concluded from the following equation (2), where $\bar{M}_{nA}$ and $\bar{M}_{nB}$ correspond to the number average molecular weight of each segment, while M_A and M_B correspond to the molecular weight of the two different monomeric units, respectively.

$$N = N_A + N_B = \frac{\bar{M}_{nA}}{M_A} + \frac{\bar{M}_{nB}}{M_B} \quad (2)$$

It is straightforward that lower values of $\bar{M}_n$ in combination with low or medium χ values could possibly lead to disordered structures or domains lacking long-range order. Systems exhibiting the aforementioned behavior have limited use in nanotechnology. On the other hand, copolymers exhibiting low number average molecular weights but high χ values are

more likely to self-assemble in ordered morphologies with minimum domain spacing under ambient conditions [no thermal annealing necessary according to equation (2)] [2].

The influence of dispersity ($Đ$) on the self-assembly of BCPs has been theoretically and experimentally studied and the conclusion is that narrow dispersity improves order of the adopted morphology. Several investigations regarding the shift in phase boundaries as well as the influence on $\chi N_{(ODT)}$ showcase the importance of dispersity [31-38].

Another parameter with a key role in block copolymers self-assembly is the composition or volume fraction ratio between the copolymer blocks. By modifying the volume fraction (φ), a variety of morphologies can be obtained such as: spheres of the minority component ($\varphi<0.18$) arranged in a body centered cubic (bcc) lattice in the majority component matrix, hexagonally close packed cylinders (hcp) for $0.18<\varphi<0.27$ or even more complicated cubic structures ($0.27<\varphi<0.34$) of the minority in the matrix of the majority component. For $0.34<\varphi<0.66$ the two blocks are ordered as alternating layers corresponding to the alternating lamellar morphology [16,30]. These volume fraction regimes have been reported for the most studied diblock copolymer in bulk (PS-*b*-PI) and are valid for the strong segregation limit where the IMDS is 2D [39].

Unusual morphologies in bulk have, also, been reported, theoretically and experimentally, namely the Frank-Kasper phases (σ [40,41], A15 [42], C14, C15 [43]) as well as other cubic network phases [44] (Q_{230}) and the orthorhombic Fddd space group (O_{70}) [45-47]. Such topologies are illustrated in Fig. 2.

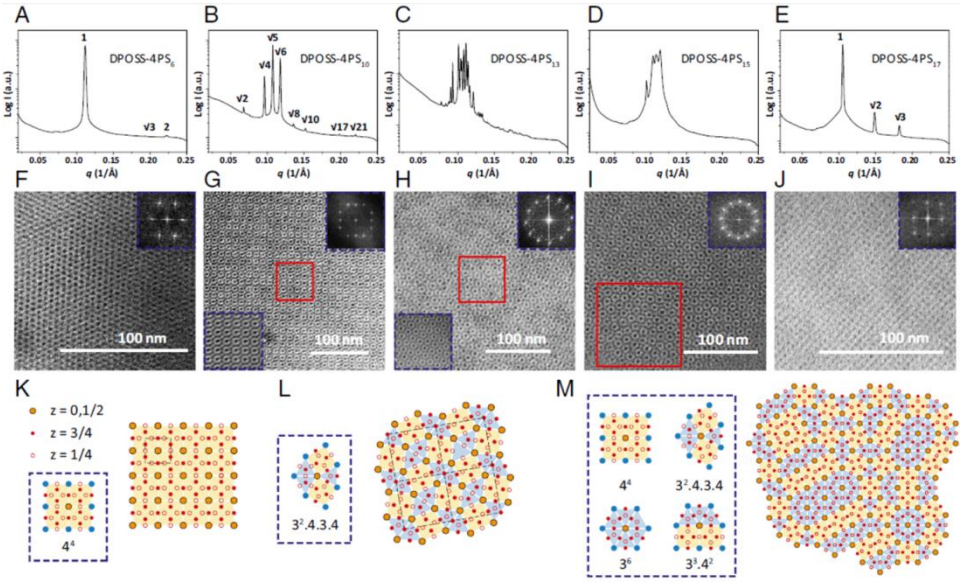

Fig.2. The self-assembly morphologies of DPOSS-4PSm giant surfactants. A-E correspond to the SAXS patterns and F-G to TEM images of five samples adopting the hexagonal close packed cylinders phase (A and F), the A15 phase (B and G), the σ-phase (C and H), the DQC phase (D and I), and the BCC phase (E and J). TEM images are taken along the[001] direction of the HEX phase in F, the [001] direction of the A15 phase in G, the [001] direction of the σ-phase in H, the [00001] direction of the DQC phase in I, and the [001] direction of the BCC phase in J. The upper right insets of the TEM images are corresponding FFT patterns and the bottom left insets in G and H show the local TEM image after Fourier filtering. Two-dimensional tiling patterns of (K) the A15 phase,(L) the σ-phase, and (M) the DQC phase are abstracted from the TEM images bounded by the red-line boxes shown in G–I, respectively. The observed basic elements and tiling numbers are summarized in the boxes [48]

Despite the microphase separated structures originating from completely amorphous BCPs, unique morphologies can also be obtained by utilizing copolymers consisting of at least one crystalline block [49]. The crystallization is affected by the following factors: composition,

molecular weight, crystallization process and incompatibility between the chemically different blocks [50]. The incorporation of crystalline or liquid-crystalline (LC) segments leads to different microstructures which are affected by the surface energy on the segregated topologies. Furthermore, block copolymers consisting of LC components can be exposed to external stimuli (electric or magnetic field, shearing) resulting in oriented patterns [51].

The self-assembly of block copolymers is severely influenced by architecture leading to various expected and more complex structures in the nanoscale. The effect of the architecture has been extensively studied indicating major discrepancies on the obtained topologies between the non-linear and the linear analogues. In the case of star block copolymers or $(A\text{-}b\text{-}B)_n$ similar structures in broadened phase boundaries can be obtained compared to their linear diblock precursors [52,53]. On the other hand, miktoarm star copolymers or AB_n self-assemble into various microdomains not obtainable for diblock copolymers with similar molecular characteristics. This behavior is attributed to the increased free energy of these systems and consequently to the stretching of the arms, causing them to shift away from the interface, leading eventually to a decrease of the interface tension and to an increased curvature between the segments [54]. In addition, Archimedean tiling patterns have been observed for non-linear architecture systems [55].

Whether the observed morphology can be considered an equilibrium structure is of great importance and interest. Copolymer self-assembly is based on the final film which will be studied with TEM and SAXS and its preparation is a combination of the following very crucial parameters: casting solvent (selective, non-selective), casting procedure, annealing temperature and duration, cooling process, sectioning and staining procedures. The phase behavior of block copolymers using selective and non-selective solvents has been thoroughly studied [56,57]. The use of neutral solvent results in simultaneous evaporation from both blocks leading to microphase separation between the chemically different segments. The exploitation of a selective solvent provokes a difference in the effective volume fraction and therefore a variety of microdomains can be obtained as shown in Fig.3 and has been reported recently in the literature [58]. The specific study justifies the fact that slow casting procedures (solvent evaporation for days) promote equilibrium structures, while accelerated casting (solvent evaporation within or less than 24h in fixed solution concentrations) can induce non-equilibrium structures, as recently reported [58]. Quick evaporation rate may result in the absence of long-range order due to inadequate time of self-assembly of the chains, especially in weakly segregated systems not thermally annealed.

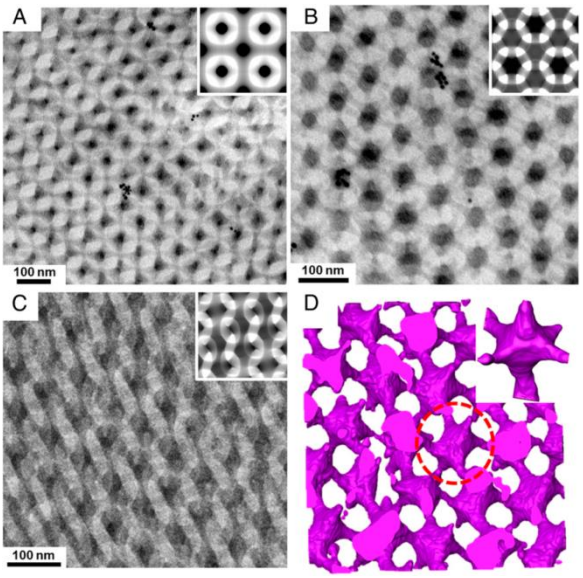

Fig. 3. TEM micrographs of PS-*b*-PDMS diblock copolymer corresponding to different projection directions: (A) [100]; (B) [111]; and (C) [321] for DP phase. All insets correspond to DP simulation images (D) Three-dimensional reconstruction images of the kinetically trapped DP phase from PS-*b*-PDMS SiO_2 along the [111] direction. The inset corresponds to the DP phase building unit [58]

Equation (1) between χ and T indicates the direct inversely proportional correlation between the BCPs self-assembly and the temperature at a given system [29]. Even though increasing the system's temperature could assist the long-range chain arrangement, there is a critical temperature (T_{ODT}) -fixed for every system-, beyond which the system undergoes an order/disorder transition. When the system is thermally annealed for several days at temperatures slightly above the highest glass transition temperature (T_g) among the two chemically different segments, the effect on the microstructure order is evident, while sufficiently elevated temperatures lead to mixed disordered domains. The self-assembly of liquid-crystalline block copolymers is highly affected by thermal annealing as well as the annealing time duration. Usually, bulk films are annealed at temperatures higher than the T_g of the liquid crystal to enable effective chain mobility during the annealing process [47].

After being thermally annealed, bulk films can either be quenched in liquid nitrogen to avoid any alternation on the formed morphology (trapping the morphology adopted at elevated temperature), especially when the system is at the weak segregation limit (WSL), or can be left to cool down gradually, when the systems are not weakly segregated. After the cooling process is completed, the bulk films can be directly studied via SAXS and should be further subjected to ultramicrotoming to obtain thin sections (thickness varying from 25nm up to 70nm depending on the blocks) when observation via TEM is necessary. Cryogenic conditions are usually employed to increase the hardness of each sample since the sectioning temperature should be performed below the lowest T_g of the blocks. For samples consisting exclusively of segments with glass transition temperature higher than ambient conditions, cryogenic conditions are not necessary.

For TEM imaging, further processing is needed if no significant difference in the electron densities between the blocks is evident, since in most cases the macromolecules studied consist exclusively of carbon and hydrogen atoms, resulting in inadequate mass thickness image contrast. The thin microtomed sections are mounted on grids (copper, carbon or gold), followed by placement on a glass slide and exposure to vapors of aqueous solution of OsO_4 or RuO_4 or iodine (and in more rare cases in other staining solutions such as: ebonite, silver sulfide, phosphotungstic acid, uranyl acetate)[59] in order to increase the mass contrast of at least one

of the segments (increased electron density). The selection of the stain depends on the functional group involved in each monomeric unit and whether pre-treatment procedures are required. It should be noted that the staining duration time is very crucial and is dependent on the chemical structure of the block [60,61].

All the above-mentioned procedures are important for the appropriate preparation of the bulk BCPs films for transmission electron microscopy (TEM) and small/wide angle X-ray scattering SAXS/WAXS analysis. Specifically, the main purpose of such in-depth studies is to provide insight on the structural properties, when combining different segments and various conformations in an effort to address possible utilization of these systems in various nanotechnology and bio-nanotechnology related applications.

2.2. Triblock Copolymers and Terpolymers

As for linear diblock BCPs, symmetric and asymmetric linear triblock copolymers (ABA and ABA' respectively) self-assembly is also determined by the segment-segment Flory-Huggins interaction parameter between the two chemically different chains (χ), degree of polymerization and volume fraction.[62-64] The major difference when compared with AB diblocks is the additional junction point, which restrains the middle block to loop and/or bridge conformations [65] and significantly affects the mechanical properties. Common and less common morphologies with feature sizes ranging between 7 to 100 nm have been reported [66-68]. Even though, coherent behaviour is expected during microphase separation between AB and ABA copolymers when studied in bulk, according to the theoretical phase diagrams, thin film self-assembly differs substantially. The fact that the free segments energy remains unaffected accounts for the phase diagrams resemblance. Commensurability as well as surface energetics are the main determinant factors for the ABA systems in thin films [66-69]. More details regarding thin film assembly will be given in the next chapters.

Linear triblock terpolymers (ABC) display well-defined three-phase morphologies, due to the presence of a third chemically different segment. It is extensively elaborated that the adopted topologies are strongly affected by the block sequence (ABC vs. BCA vs. CAB), the volume fraction ratio and the values of the three Flory-Huggins interaction parameters (χ_{AB}, χ_{AC}, χ_{BC}). Novel structures have been reported for ABC systems in bulk due to the existence of the third chemically different segment as already mentioned in the literature [62,64]. Related studies in thin films for such materials are not yet excessively reported except from a few cases which are mentioned in the following chapters.

Asymmetric linear triblock copolymer self-assembly in bulk is except for the aforementioned parameters, also significantly affected by the asymmetry factor (τ), i.e. the value of the ratio between N_A and $N_A + N_{A'}$ (N_A and $N_{A'}$ are the total monomer units of A and A' blocks). This asymmetry factor completely alters the phase diagrams related to the self-assembly of such asymmetric copolymers, and the effect increases with complexity in architecture (going from linear to non-linear architectures), as reported theoretically by Fredrickson's research group [63], which was justified experimentally by Fredrickson, Kramer and Avgeropoulos research groups [70]. Such materials have led to strong thermoplastic elastomeric behavior even with the content of the rubbery block being as low as 3% [71,72] either as pristine copolymer or as a binary blend with respective homopolymer of the hA type).

2.3. Non-Linear Copolymers

As demonstrated in the literature, the preparation of structures with sub-10nm resolution from highly immiscible BCPs displaying low N indicates a very promising pathway towards customizable applications in nanotechnology. Even though BCPs are a broad class of materials with various applications, triblock co- and/or terpolymers, miktoarm stars [AB_2, AB_3

and A_2B_2] and star block copolymers [(A-*b*-B)$_n$] have, also, been studied, due to the unique properties along with the high χ values and the small feature sizes they adopt. From the previous sections it was clear that utilization of high χ copolymers is mandatory to fabricate miniaturized nanofeatures from low N copolymers. Although, the possibility to increase the χ value of linear block copolymers has been studied adequately, this is not the case for high χ block copolymers with complex architecture. Macromolecular architecture can strongly affect the order-disorder transition temperature (T_{ODT}), the domain spacing, the stability of the morphologies and the phase boundaries of copolymers, as well as, the thickness-dependent properties in polymeric thin films [52,73-79]. In this section, the impact of macromolecular architecture of BCPs will be discussed with respect to the microphase separation.

2.3.1 Star-Block Copolymers

Star-block copolymers exhibit higher T_{ODT} values when compared to linear BCPs as evidenced by theoretical studies. χN_{ODT} is predicted to be lower in star-block compared to diblock copolymers, and is significantly decreased when the number of arms increases (Fig.4). This means that segregation strength in these copolymers can appear higher, while even smaller nanodomains can be obtained. The reduced χN_{ODT} value is attributed to entropic penalties due to configurational constraints based on the multiple chains anchoring from the same junction point, as well as, on overcrowding effect leading to similar chain stretching almost parallel to the interface, concluding to limitation of defects/dislocations and increased structure order even in low molecular weights. In star-block copolymers, nanodomain periodicities appear close to those of the precursor diblock copolymer comprising the arms. [73][74][78][80][81-87] It is important to note that avoiding the influence of the overall of the star-block copolymer on the domain periodicity appears as a promising route for the miniaturization of nanofeatures. It is known that properties connected to low molecular characteristics of short-chain linear BCPs can hinder the applicability of respective materials in industrial applications due to mechanical instability, increased possibility of dewetting in thin films or inconvenient low glass-transition temperatures. These drawbacks may be overcome by the influence of the star-block architecture as described above. Additionally, in such copolymers, complex architecture can have an impact on the phase boundaries, also evident in other topologically complex copolymers (Fig.5)[52]. For example, it is suggested that for star-block copolymers, the double gyroid morphology can occur for a wider range of volume fractions if the arm number is increased.[77] Alterations of the stability of morphologies in the phase diagram are of high importance, when, nanoporous materials are required. Asymmetric lamellae have, also, been observed in such copolymers. Furthermore, studies suggesting that thin films of such non-linear copolymers can more easily orient perpendicularly to the substrate have been reported, a topic that will be discussed in the following chapters more thoroughly and may be attributed to the entropic penalty that star-block copolymers have to pay for preferential wetting of an interface.

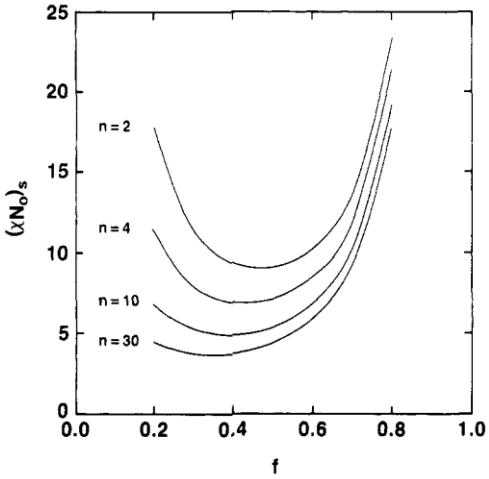

Fig.4. Variation of $(\chi N_0)_s$, with composition and arm number for $(AB)_n$ star copolymers.[73]

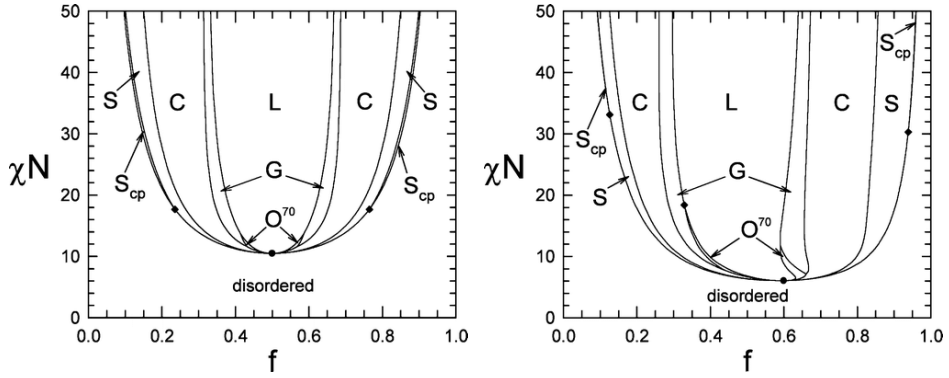

Fig.5. Phase diagrams as predicted by Matsen though SCFT. Matsen's diagrams are more accurate in SSL. (Left) Phase diagram for melts of AB diblock copolymers, showing the stability regions of the ordered lamellar (L), cylindrical (C), bcc spherical (S), hcp spherical (S_{cp}), gyroid (G), and Fddd (O^{70}) morphologies. The dot denotes a mean-field critical point, and the diamonds indicate two difficult to resolve triple points. (Right) Phase diagram analogous to that of the lower left image, but for 9-arm star block copolymers where each sample is formed by joining 9 diblocks together by their B-ends. Here N is the degree of polymerization of each diblock arm. [52]

2.3.2 Miktoarm Star Copolymers

Regarding the self-assembly of miktoarm star copolymers, large shifts on the phase boundaries are observed due to conformational asymmetry based on the complex architecture. The order-disorder transition temperature becomes lower, leading to disordered domains while the corresponding linear analogues remain ordered. In an AB_n miktoarm star copolymer the A/B interface curvature is attributed to two major parameters: the volume fraction of the single block A and the overcrowding effect due to the multiple B arms. The influence of both parameters leads to changes in the adopted morphologies compared to the linear analogues, becoming more evident as the number of arms increases. Theoretical predictions are in contradiction with the experimental results especially in the case where the number of arms increases from 2 to 3 to 5 as previously reported [88]. Careful preparation of miktoarm star copolymers, though, has allowed for integration of such copolymers in nanopatterning of ultra-small nanofeatures as will be discussed in the following section.

As early as 1986, Olvera de la Cruz [73] suggested "*graft*" copolymers of the AB_2 type exhibit a χN_{ODT}=13.5 at φ_A=0.5, slightly higher that the corresponding value for A-*b*-B or AB linear symmetric diblock copolymers (χN_{ODT}=10.5). On the other hand, symmetrical A_nB_n were reported to exhibit a χN_{ODT} equal to that of linear diblock copolymers.[73] Apart from the lower

T_{ODT} predicted, experimental data from as early as 1993, also, indicated a strong shift in the phase boundaries of miktoarm AB_2 type copolymers, since they exhibited different morphologies compared to the corresponding linear diblocks with similar molecular characteristics (molecular weight and volume fraction). This shift is attributed to effect based on the volume fraction of the single block A and the overcrowding effect due to the multiple B arms leading to respective interface curvature as already mentioned. (Fig.6)[89] These observations were thoroughly explained in the literature, providing the first phase diagram for copolymers of the A_nB_m type taking into account the asymmetry parameter ε (elastic asymmetry and architecture effect) and, also, predicting different morphologies for AB (lamellae), AB_2 (cylinders) and AB_3 copolymers (spheres) at identical volume fraction of the minority component, φ_B=0.4.(Fig.7)[90] The approach is well identified in the soft matter related scientific community as Milner's theory. Other theoretical and experimental results demonstrated the significant phase diagram shifts, while as the asymmetry due to architecture increased, the shift was larger. Furthermore, differences in the adopted morphology stability were observed(Fig.8).[52,92-98] However, it should be noted that for large architectural asymmetry, significant discrepancies from Milner's theory have been observed. There are some studies suggesting smaller nanodomains attained by AB_n star copolymers in which the decrease in d-spacing is affected by immiscibility between the blocks and overall segregation strength. Even a scaling law in the SSL was extracted, suggesting that the d-spacing decrease is dependent on the composition.[95,98,99]

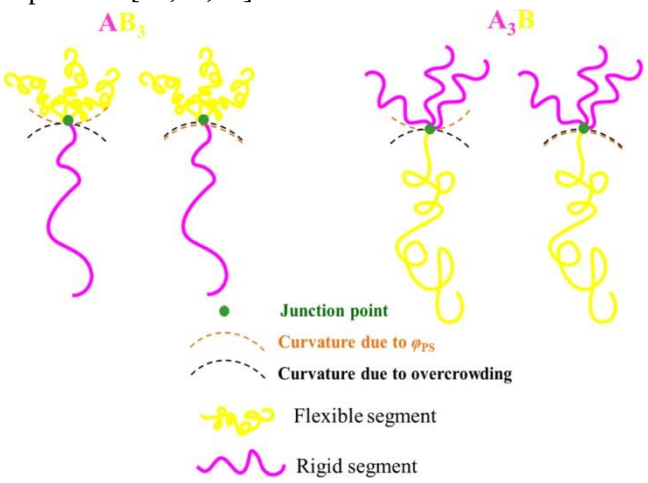

Fig.6. Model indicating the differences between the A/B interface of (a) AB_3 and (b) the A_3B miktoarm copolymer due to the f_A and the overcrowding effect. [100]

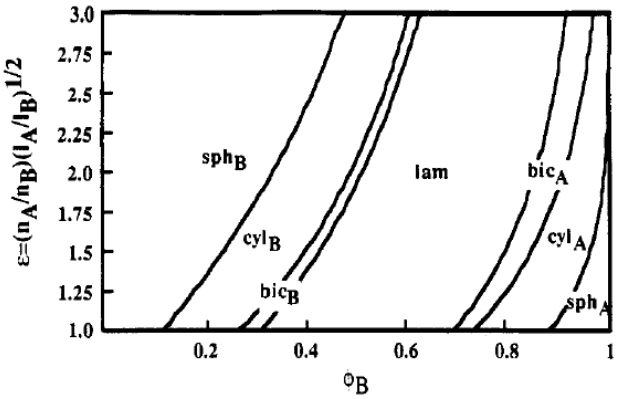

Fig.7 Phase diagram in the strong-segregation limit for star block copolymers with n_A A arms and n_B B arms (described in text) as a function of the volume fraction of the B monomer.[90]

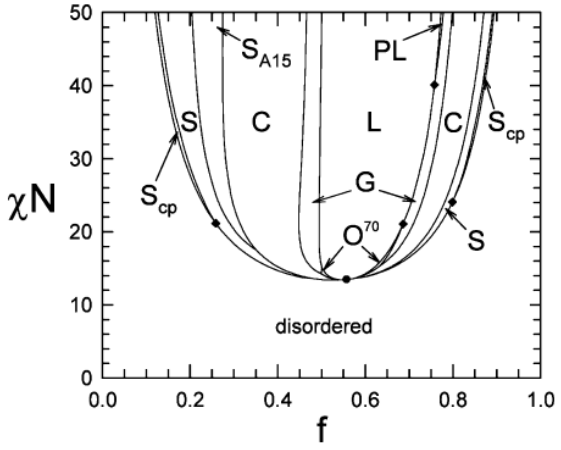

Fig.8. Phase diagram for AB_2 star block copolymers where each molecule has one A-type arm and two identical B-type arms. The change in architecture results in additional stability regions for the ordered A15 spherical (S_{A15}) and perforated lamellar (PL) morphologies. Here N is the degree of polymerization of the entire molecule.[52]

2.3.3. Cyclic Block Copolymers

Although, cyclic A-B copolymers require a slightly higher χN critical value to self-assemble, compared to linear A-B copolymers, their ability to organize in smaller nanodomains has attracted the interest of the scientific community for the fabrication of ultra-small nanofeatures. Of course, the synthetic constraints to produce such copolymers hinder this effort, but cyclic copolymers constitute a class of materials worth mentioning regarding sub-10nm nanopatterning.

In an early theoretical study in 1993, Marko et al., predicted a critical χN value equal to 17.8 (~$1.7\chi N_{c,linear}$) for symmetric diblock cyclic copolymers.[101]The ring topology and severe constraints on the block ends suppress concentration fluctuations and require higher immiscibility for microphase separation, as compared to linear diblock copolymers. However, it is also mentioned that for the same N value, cyclic copolymers would order with domain periodicities 63% lower when compared to linear diblock copolymers in the SSL. Other theoretical and simulation studies suggest that the phase diagram for such copolymers is similar to that of their linear analogues, but χN_{ODT} values are slightly higher [102-104].

Cyclic copolymers have demonstrated improved thin film stability. In general, properties such as the glass transition temperature of polymers can be altered when confined in thin films. Cyclic copolymers appear to resist such changes. For example, the absence of T_g depression that can occur on thin films, was observed in thin films of cyclic PS homopolymers.[105] Resistance to dewetting has, also, been observed,[106] as well as improved assembly dynamics.[107] Meanwhile, it is noteworthy, that they appear to have higher T_g values for a given molecular weight, which could be important for processing of low N BCPs.[93]

Although, simulations and theoretical studies predict a domain spacing reduction as high as 40%, the experimentally observed values are on the order of 18-25% when A-*b*-B and relevant cyclic copolymers are compared.[108,109,110] Recently, Goodson et al. tried to explain the discrepancy between the theoretical and experimental reduction of periodicity on cyclic copolymers by publishing a theoretical and dissipative particle dynamics (DPD) simulation study where they tried to extract a scaling law by taking into consideration chain length, segregation strength and chain architecture.[111] They concluded that d-spacing of

linear copolymers is more strongly dependent on N in comparison to cyclic copolymers, and ultimately, they successfully provided a revised scaling law. (Fig.9)

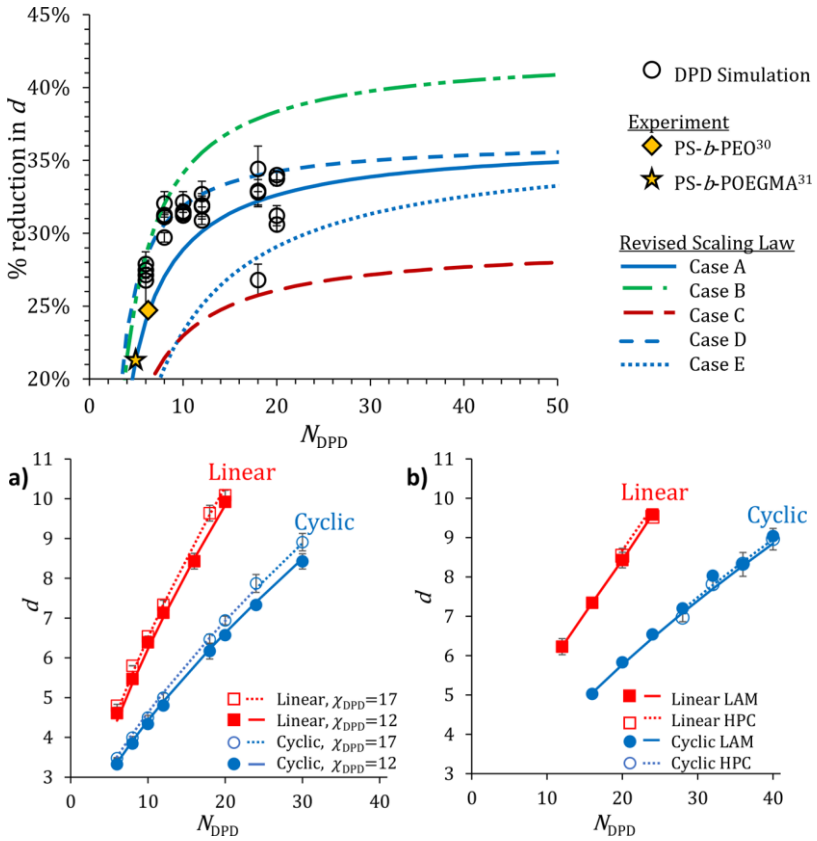

Fig.9. [111] Theoretical and dissipative particle dynamics (DPD) simulation study

Comparisons between cyclic copolymers and their linear precursors have, also been reported in the literature. Lescanel et al. synthesized PS-*b*-PDMS and PS-*b*-P2VP cyclic copolymers from their linear diblock precursors.[112] It was evidenced that cyclic copolymers exhibited a 5-10% smaller d-spacing compared to the triblock precursors (PS-*b*-PDMS-*b*-PS and PS-*b*-P2VP-*b*-PS, respectively), while periodicities as small as 12.9 nm were observed. Theoretical data were provided, predicting a 38-40% reduction as compared to A-*b*-B diblock copolymers and 2-10% reduction as compared to A-*b*-B-*b*-A triblock copolymers for lamellar morphologies. Generally, cyclic copolymers are doubly looped, whereas triblock copolymers exhibit both bridges and loop conformations. Since the cyclic copolymers form more loops per chain, their domain spacing is smaller compared to the respective triblocks. Similar results (up to 16% d-spacing reduction) were reported by Takano et al. on **PS-*b*-PI** diblock and cyclic copolymers and by Zhou et al. on **PS-*b*-PB** cyclic copolymers who reported an interface curvature away from the chain end blocks of the triblock (PS-*b*-PB-*b*-PS), when they were connected to each other in order to prepare the desired cyclic sequence.[113]

2.4 Bulk Orientation Control

Shear alignment is attributed to the differences in mechanical properties as well as viscoelasticity between the immiscible segments and is regularly employed on lamellar or cylindrical morphologies without requiring special demands. Sample shearing between two glass slides is often performed for the identification of the morphology [19,114-116].

Differences in the dielectric permittivity between BCP components lead to minimization of the orientation dependent field energy that constitutes the driving force for the electric field alignment, which even allows second order transitions beyond long-range

alignment. The studies reported in the literature have been restricted to only concentrated polymeric solutions that are quickly aligned, in contradiction to higher average molecular weight polymers that display lower chain mobility leading to dielectric breakdown. This method can be applied to polymers exhibiting high dielectric contrasts, such as BCPs constituted by neat hydrocarbon chains and heteroatom containing chains [19,117,118].

A promising tool for realizing orientation is magnetic field alignment (Fig. 10), which is advantageous towards the electric field alignment due to the absence of dielectric breakdown. In contrast to shear alignment, external stimuli, such as temperature, can be exploited, but the overall use is severely influenced by the necessity of high intensity magnetic fields (>4 Tesla). Semi and/or liquid crystalline systems having low $\bar{M}_n$ and magnetic field responsiveness are frequently processed with this method [19,119-121].

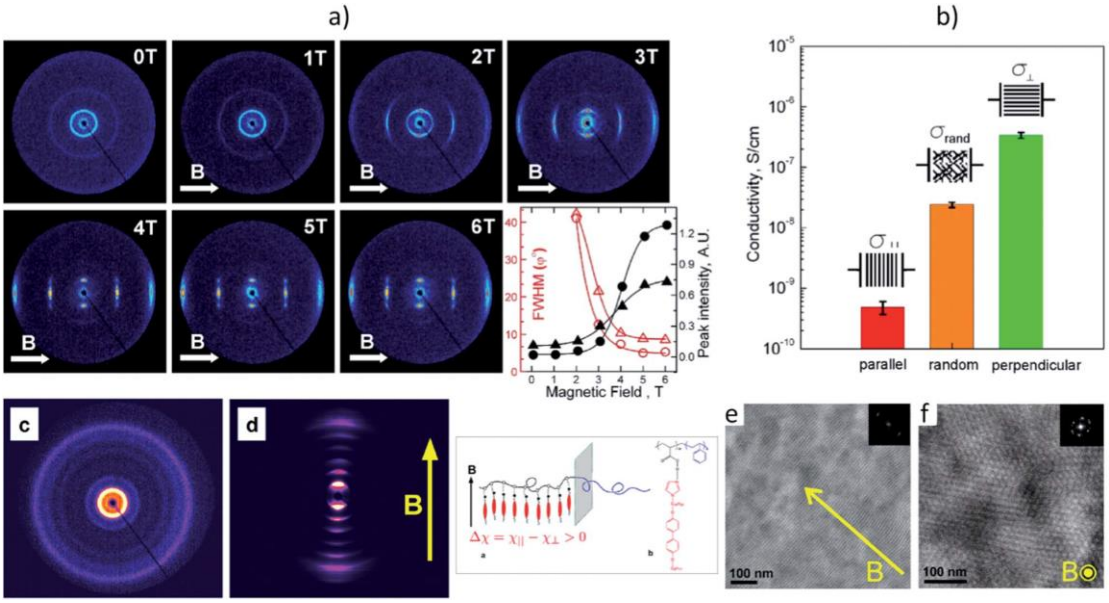

Fig.10. Magnetic alignment of a side chain Li^+ containing liquid crystalline polymer (PEO(120 EO:Li^+)-*b*-PMA/CB) as a function of field strength. (b) Comparison of the Li^+ conductivity at two orthogonal orientations to the non-aligned sample. Perpendicular sample shows an order of magnitude improvement in conductivity compared to the random sample. (c) and (d): magnetic alignment of a supramolecular side chain block copolymer system (PS-*b*-AA/LC). Imidazole mesogens are attached to the PAA units of PS-*b*-AA though hydrogen bond interactions. The as-cast random sample (c) when cooled across T_{ODT} in 5 T magnetic field results in highly oriented non-degenerate lamellae perpendicular to the applied field. (e) and (f): TEM images of the system at two stoichiometries (0.33-lamellar, 0.5 cylindrical) of the free LC to the number of binding sites after magnetic alignment. [122]

Zone annealing (temperature gradient field) yields to aligned microdomains, with the use of specified temperature gradients through solidification approach. This method takes advantage of slow motion of a polymeric melt [19]. Specifically, two temperature regions are employed; one below the T_{ODT} and one above the T_{ODT}, resulting in long-range orientation below the T_{ODT}. Even though, no specific requirements for the materials are required and the method is reconcilable with roll-to-roll processes, the overall instrumentation is rather complex. A similar technique, namely cold zone annealing, with slightly different conditions has been utilized. Both temperature regions lay below the T_{ODT}, leading to oriented microdomains due to the chain mobility attributed to the increased temperature (above T_g of all segments). Cold zone annealing is usually used for processing BCPs exhibiting high $\bar{M}_n$ and high χ [123-128].

Another orientation method is directional solidification where a block copolymer solution is subjected to an external stimulus separating, the crystalized solvent from the remaining bulk BCP. The main precondition in order to utilize the specific technique is the solubility of BCPs in crystallizable solvents. The effectiveness is dependent on several parameters such as the BCP T_g, boiling point of the solvent, BCP film thickness, crystalline structure as well as fast growth direction of the solvent, and any epitaxial relationship between the BCP and the crystalized solvent [19,114].

The roll-casting technique where the BCP solution is applied between two counter-rotating rolls, taking advantage of shear and elongational flow fields, has been developed by Albalak and Thomas. Microdomain orientation is achieved through the transition from disorder to order, due to the flow field applied to a solution where the solvent evaporates leading to well-defined and long-range order topologies. Both crystallizable, liquid crystalline and high-molecular weight copolymers can be manipulated utilizing the specific technique due to elevated but lower than the degradation temperatures [114,129-131].

3. Thin films self-assembly

Despite the direct dependence of thin films self-assembly on the Flory-Huggins interaction parameter, the degree of polymerization and the volume fraction, the obtained morphology is significantly influenced by additional factors such as: surface tension (substrate/air), film thickness and diffusivity [132,133]. Preferable interactions deriving from air and/or substrate surface have a key role in low dimensional BCP films, since they can induce wettability effects that define the domains orientation [134,135]. This parameter is strongly dependent on the chemical nature of each segment and therefore various orientations originate from different components, in contradiction with bulk self-assembly where this effect is absent. Furthermore, similarly to bulk film preparation, the film formation in the case of directed self-assembly is of major importance since it promotes the self-assembly during the solution casting methods. Dip- and spin-coating methods are frequently encountered as casting methods leading to films with different thicknesses and roughnesses [136,137]. The common method of choice is spin-coating, where a dilute polymer solution is deposited on a spinning substrate and due to centrifuge force the solution is obliged to form a thin film on the top of the substrate, while the solvent rapidly evaporates at the same time. Both spinning velocity and solution concentration determine the thickness of the final film and the solvent evaporation speed. Surface uniformity is affected by the solvent volatility, where usually volatile solvents induce high roughness.

Block copolymer self-assembly in thin films has attracted a lot of interest due to the versatile applications of the formed periodical patterns with miniaturized dimensions lying between 3-100 nm. These nanopatterns can be used as nanoporous materials [138-144] as lithographic masks for subsequent pattern transfer of features with ultra-small critical dimensions on desired substrates (Block Copolymer Lithography)[145-152], as templates for the fabrication of desired nanofeatures like metallic, or inorganic arrays[153-158], as well as for a variety of other applications. [159-162]

Interfacial interactions in thin films affect several aspects of self-assembly, as well as the orientation of nanodomains with respect to the substrate. Perpendicular orientation to attain nanodot or line/space patterns typically from nanocylinders or lamellae, respectively, is desired. However, when the surface energies of the different blocks are different, in-plane cylinders and lamellae occur, while for spherical morphologies bcc or hcp spheres parallel structures occur.

PS-*b*-PMMA is a block copolymer that has been extensively studied, due to easy low-cost synthesis, etch-selectivity and facile perpendicular orientation of nanostructures on Si wafers

upon appropriate surface treatment. However, the low inherent incompatibility among the segments, limits the obtained pattern periodicity for this specific BCP to ~22 nm. Other BCPs with higher incompatibility (represented by χ value) like PS-*b*-PEO, PS-*b*-PLA, PS-*b*-P4VP or PS-*b*-PDMS have been extensively studied as thin films.[148] Especially, PS-*b*-PDMS due to the etch-contrast provided under appropriate treatment of the polymeric material, as well as the increased immiscibility of the segments has been reported as a next-generation material for BCP lithography and is the most appropriate. The etch-contrast between PS-*b*-PDMS, as in the case for other silicon-containing BCPs, leads the silicon-based block, under oxygen plasma etching, to be transformed into silicon oxide providing a robust etch resistant mask (etch barrier) for dry etching and allowing high aspect ratio structures. However, the surface energy disparity between the segments leads to parallel orientation of ordered nanostructures with respect to the substrate under thermal treatment. Several ways to control orientation have been reported. Monolayers of parallel cylinders have, also, been exploited to obtain line/space patterns, however, the small film thickness hinder the formation of high-aspect ratio structures in block copolymer lithography, since only rarely do constituent blocks exhibit adequate etch-contrast.[163-165]

BCP periodic structures do not just form single-grain perfect lattices, but rather several defectivities, like dislocations or disclinations, often occur.[166,167] Thus, even though vertical alternating lamellae may, for example, form upon a certain volume fraction and χN value, in the long-range, fingerprint-like structures can be observed. Lateral order can be dependent on temperature, annealing time and residual solvent, while it is definitely improved under directed self-assembly or DSA.[168]

Importantly, in BCP thin films, film thickness plays a key role affecting several aspects of the self-assembly process due to confinement and interfacial interactions, such as: finally observed morphologies, order-disorder transition, d-spacing, defect density or orientation. [164,169]

In BCP thin films, the interfacial interactions determine the orientation of nanodomains, normal or parallel to the substrate, depending on the selectivity of either of the interfaces towards one of the blocks. Then, this block preferentially wets the corresponding surface and parallel orientation occurs. In symmetric wetting, where the same block preferentially wets both the substrate and free surface in lamellar films, flat films occur when the film thickness is commensurate to periodicity (nL_0), whereas for asymmetric wetting when the film thickness is given by $[(n+\frac{1}{2})L_0]$. (Fig.11) In unconfined films with thicknesses that do not adhere to these commensurability conditions, islands and holes, (i.e., terraces), are observed with step height L_0. [164,169-172]

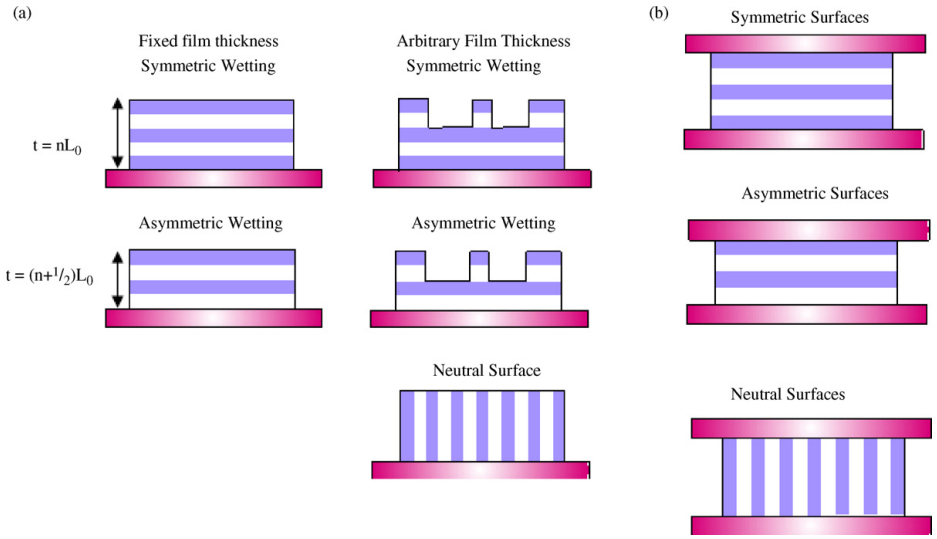

Fig.11. Configurations of lamellae in block copolymer thin films: (a) unconfined at top surface and (b) confined at both surfaces. [173]

3.1. Orientation control

To obtain normal to the substrate patterns balancing interactions between the block segments and top/bottom surfaces is required. When the enthalpic contributions from selective interactions at the interfaces are minimized, entropic contributions align nanodomains perpendicularly to the substrate to facilitate block stretching.[171] Under thermal annealing, to obtain perpendicularly oriented domains, the interfacial energies ($\gamma_{A\text{-}TOP}$, $\gamma_{A\text{-}BOTTOM}$, $\gamma_{B\text{-}TOP}$, $\gamma_{B\text{-}BOTTOM}$) are designed such that $\Delta\gamma_{TOP} \sim \Delta\gamma_{BOTTOM} \sim 0$, which, in essence, means that neither top, nor bottom interfaces show selectivity towards one of the blocks.[174] A very common approach to balance block interactions with the substrate is utilization of neutral random copolymer brushes and mats that after appropriate treatment provide an ultrathin neutral layer as a bottom interface.[175-179]

Binary homopolymer brush layers have, also, been investigated, providing a useful method to neutralize the substrate, when random A-*r*-B copolymer brushes cannot be easily synthesized.[180] Blends of homopolymer A with B brushes comprising the BCP constituents have been grafted on the substrate to neutralize it, while a short A-*b*-B copolymer acting as a surfactant was blended with the homopolymer brushes to homogenize the mixture.[181] In a different approach, self-assembled monolayers (SAMs) have been investigated to balance interfacial interactions at the bottom interface. [182,183] Several other methods to modify the bottom interface have been investigated, too.[145] However, perpendicular orientation achieved by the bottom interface modification does not necessarily propagate uniformly to the air interface in thick films, and mixed morphologies can occur near the free surface.[184,185]

Meanwhile, polymeric materials like PS-*b*-PMMA show no preferential interactions with the air free surface under typical thermal annealing temperatures, allowing for orientation control, in thin films with appropriate thickness, from the bottom modified surface. For other copolymers like PS-*b*-PDMS achieving perpendicular orientation is more complex, since the surface tensions are quite dissimilar ($\gamma_{PS} = \sim 40.7 mN\ m^{-1}$, $\gamma_{PDMS} = \sim 20.4 mN\ m^{-1}$).[148] In the case of BCPs exhibiting high χ values, disparate surface tensions usually characterize the blocks and preferential interactions with either top, bottom or both surfaces occur leading to in-plane orientation.

Of course, materials with balanced surface energies or materials requiring only facile substrate treatment to obtain perpendicular orientation do exist and several will be discussed below.

However, in most high χ BCPs this is not the case and other methods have to be exploited to provide orientation control.

Other methods targeting interfacial interactions at the top surface include deposition of SiO_x on the polymeric film to form a hard surface selective for one block, while confining the polymeric material between two hard surfaces.[186] Different strategies to impact surface interactions at the top surface include the formation of very high MW A_x-*r*-B_{x-1} films.[187][170] Blending of the BCP with surfactants like oleic acid has been examined in PS-*b*-PMMA where preferential swelling of the PMMA block by oleic acid leads to smaller surface energy difference starting from the top interface. Film perpendicular structures with high aspect ratio were obtained when the process was combined with random copolymer neutral brushes at the bottom interface.[185] Incorporation of nanoparticles can, also, lead to controlled orientation of nanodomains by mediating interfacial interactions, [158,188,189] while surface roughening has been exploited to control the orientation of nanodomains.[190] From a different point of view, surface active polymers (SAP) can be used to obtain perpendicularly oriented structures. For example, in a carbonate-based BCP, PS-*b*-PMTC-Me (χ~0.19), vertical orientation was achieved by incorporation of a neutral bottom layer and a SAP that selectively interacts with the PMTC-Me segments and after thermal annealing, segregates to the air free surface modulating interfacial interactions. [191] Another non-block-selective surface-active polymer additive that remains segregated at the top of the film during thermal annealing, has been used for PS-*b*-P2VP. The additive is a small BCP bearing a free surface selective block for the segregation to occur, as well as a block that maintains neutrality towards the main BCP. [192]

As previously mentioned, the surface energy disparity among the blocks in many high -χ copolymers leads to preferential wetting of the respective surfaces and ultimately to parallel orientation. With regard to the top surface, the block with lower surface energy segregates to the free interface. This problem is often battled by top coat materials that act as a neutral top surface. These materials complicate the overall process; however they constitute very useful means of controlling orientation in certain BCP systems. When utilizing top coat materials apart from the chemical design, the effect of BCP film thickness, topcoat molecular weight, incompatibility, as well as BCP macromolecular architecture are very important factors which should be considered.[193,194]

Partially hydrolyzed poly(vinyl alcohol) has been used as a top coat material for PS-*b*-PDMS, under solvent annealing with adequate solvent evaporation rate, to mitigate disparate surface energies. [195] Top coats consisting of neutral random copolymers on top of the BCP thin film have, also, been investigated. For example, PS-*r*-PMMA-perfluoroalkyl copolymers have been used in order to preferentially segregate at the free surface due to the perfluoroalkyl end groups. [196] In a different study, perpendicular orientation during PS-*b*-P2VP self-assembly under chemical epitaxy was achieved by polymeric top coats comprised of high MW random copolymer (PS-*r*-P2VP) or PMMA mats. The top coat mats were placed on the BCP thin film either by floating or polymer off-set pinning. Utilization of either polymeric mats or high T_g polymers in polymeric top coats is useful in obtaining a hard top coat surface avoiding mixing with the BCP thin film upon annealing.[197] PS-*b*-P2VP sandwiched between two clamped PS-*r*-P2VP coated substrates, has, also, resulted inthrough-film perpendicular structures. [198]

In general, top coat materials should be easily removed after annealing, leaving the underlying nanostructured BCP thin film unaffected. This can be a very complex task for materials design, since these top coats usually exhibit solubilities similar to that of the BCP thin film. Bates et al., employed polarity-switching polymeric top coats, that comprise maleic anhydride moieties along with moieties providing surface neutrality. Maleic anhydrite units, upon chemical transformation in aqueous basic solution dissolve and can be spin-coated by aqueous media on

top of aqueous-insoluble, non-base-sensitive high χ BCP thin films, and can be removed without affecting the underlying polymeric film. Under heating, transformation to the maleic anhydride form occurs, allowing surface neutrality. This work holds great promise for hydrophobic high χ copolymers with disparate surface energies.[174] Optimization of the process, as well as spin coating from common polar solvent (i.e., methanol) prove the versatility of the method. [199,200]

Additionally, iCVD (initiated Chemical Vapor Deposition) is another method to tune interfacial interactions by depositing a neutralizing top coat. With this method, a crosslinked top coat that grafts to the BCP chains while, also, immobilizing them, comprises the neutral top layer. The top coat can be really thin and facilitates further processing without necessarily being removed. iCVD has, also, been used to provide neutral top coat for amphiphilic BCPs.[201] Recently, a polymeric nanomosaic (PNM) was used leveraging the ability of PS-*b*-P2VP to form dot patterns during air/water interfacial self-assembly (ISA). The PNM patterns were used as a neutral bottom layer on various substrates, while placing PNM-coated PDMS-pads on the BCP films could serve as a reusable, etch-free, shear-inducible neutralizing PNM top coat. [202] Finally, plasma treatment has been used to access a neutralizing atmosphere. Through plasma treatment, the surface of disordered BCP chains could be cross-linked, thus providing a neutral layer during annealing.[13,203]

In addition, solvent evaporation and solvent vapor annealing (SVA), can direct orientation of the final nanodomains. SVA affects both ordering and orientation. For example, PS-*b*-P2VP bearing H-bonding HABA [2-(4'-hydroxybenzeneazo)benzoic acid] molecules exhibits different orientation when annealed in different solvents.[204] PS-*b*-PLA has, also, formed vertical cylinders when annealed from THF, in contrast to other annealing solvent vapors.[205] In solvent vapor annealing, the evaporation rate is critical to whether diffusion and ordering will occur, as well as to the orientation of nanodomains. Upon exposure of BCP thin film to solvent vapor two stages occur that are described in the following figure. (Fig.12) [78] In the swollen state of thin films, equilibration may or may not occur, with metastable swollen phases often observed. To obtain equilibrated states, depending on the χ and N values of BCP, prolonged exposure times may be needed.

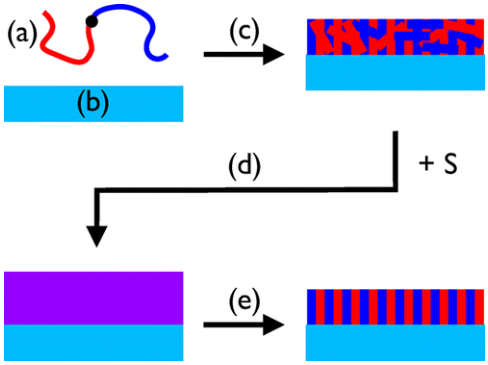

Fig.12. A schematic showing the five major considerations for SVA of block polymer thin films: block polymer selection (a), substrate preparation (b), film formation [a disorganized but ordered structure depicted] (c), solvent (S) exposure [a homogeneous, swollen film shown] (d), and de-swelling by solvent evaporation [to a perpendicular cylindrical structure as an example] (e). [3]

Interfacial interactions between BCP constituents and solvent are critical and can lead to a block preferentially interacting with the solvent vapor interface. In SVA, usually neutral or slightly selective solvents are used. Introducing a non-atmospheric neutral or preferential top surface from solvent vapors can often determine the orientation by block-solvent selective interactions. [68,206-208]

The use of a more selective solvent for one block can lead to different swelling uptake of the blocks and altered effective volume fractions, while the swelling of a block is additionally affected by its physical state. The solvent evaporation procedure is also critical and can impart long-range order. When the film is removed from the solvent vapor atmosphere, evaporation occurs and the rate of evaporation is very important. The unidirectional evaporation process provides a strong ordering field (Fig.13) [3][209]. During this process, a solvent concentration gradient occurs and as the solvent is removed the gradient propagates deeper in the film. While the solvent concentration gradient propagates in the film, the already ordered structures at the surface, where evaporation already occurred, act as a template for subsequent in-film ordering.

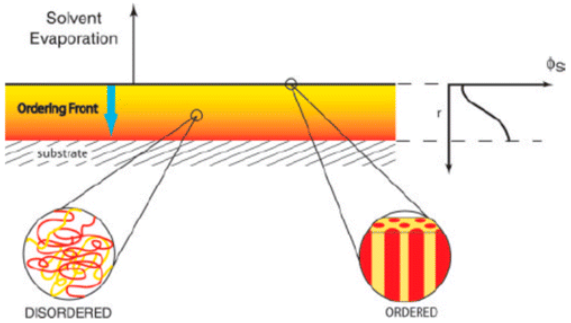

Fig.13. Schematic view of the solvent evaporation in a thin block polymer film illustrating the concept on an ordering front that propagates through the film. [3]

Overall, the presence of solvent molecules in a BCP thin film can mediate surface energies and allow perpendicular orientation, render the chains mobile lowering the T_g so as to self-assemble even at RT, and, finally, provide an ordering front through the evaporation process described. [171,210]

As previously mentioned, SVA constitutes a complex procedure affected by many experimental variables like the nature of solvent, exposure time, as well as evaporation rate. SVA also facilitates the annealing of BCPs sensitive to heating. However, it comes with many drawbacks including de-wetting, slow kinetics, difficult integration in industry procedures, while even subtle changes in temperature or vapor pressure can have a strong impact in the self-assembly process. [165,174]

Film thickness is another factor that strongly affects the orientation of nanodomains, and its value in the final film is often compared with the natural period of BCP domains to extract useful results. (Fig.14) [3,135,165,187,211-214] Electric field has, also, been used to orient nanostructures perpendicularly to the substrate, and parallel to the electric field.[215,216] Other external fields to attain controlled orientation and long-range order include directed self-assembly, zone casting, as well as optical alignment. [217,218]

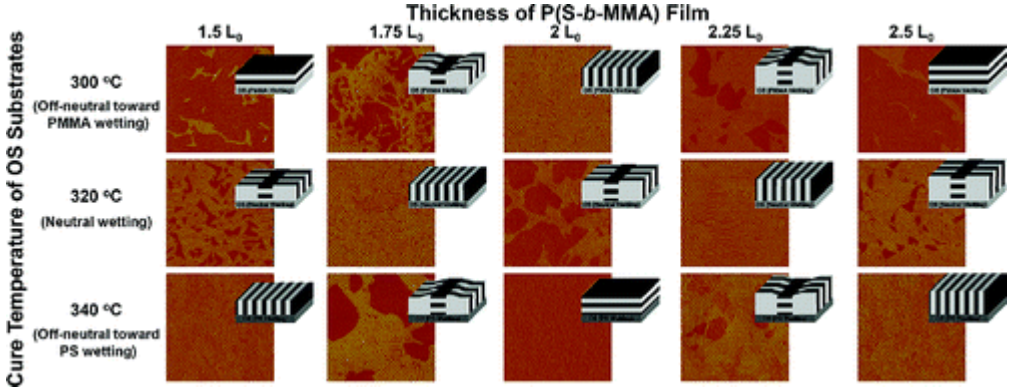

Fig.14. Film thickness influence on the orientation of the nanodomains. [214]

Zone casting is a DSA method, which provides long-range order by slow-rate deposition and slow-drying of the BCP films. The BCP solution is injected through a perpendicular placed narrow nozzle, to the vicinal moving substrate. The particular method is quite appealing for industrial use, due to the enabled large-area processing and the agility provided by the solvent selection and temperature adjustment capability. No specific requirements are necessary regarding the nature of BCPs [128,219,220] (Fig.15).

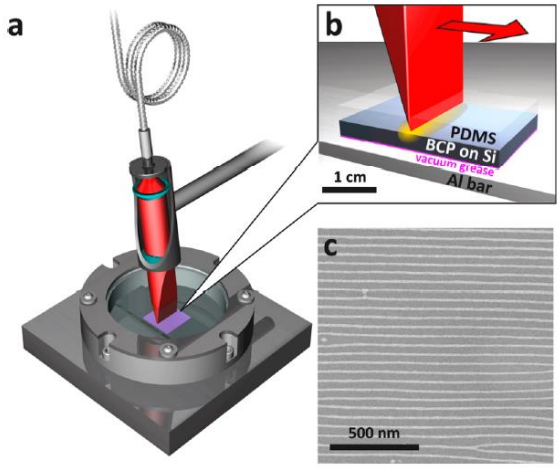

Fig. 15. Overview of the compact laser annealing setup. (a) Cutaway view of the optical head shaping the beam into a narrow line with a connected optical fiber. The beam is projected onto a sample inside a low-profile vacuum chamber mounted on a linear translation stage. (b) Block copolymer thin-film sample on a silicon substrate capped with a layer of transparent PDMS undergoing laser annealing in soft-shearing mode (SS-LZA). The line-shaped beam is continuously rastered across the sample with a PDMS cap acting as a shear-inducing element. (c) Metallic platinum nanowires on Si obtained by templated synthesis in the aligned cylindrical PS-b-P2VP diblock copolymer film after 8 cycles of photothermal annealing at 0.32 mm s−1 with 24 W beam power. Reference 128

A multilateral DSA method for depositing BCPs thin films at ordered and even equilibrium state based on electric fields, namely electro-spraying has been developed. Sub-micron droplets of dilute BCP solutions are placed onto a heated substrate by employing high-voltage laser beam to the injected solution, while simultaneously the solvent evaporates depositing BCP nanoparticles upon the substrate. Sequential depositions offered by electro-spraying (Fig.16), are considered as a major advantage compared to other techniques. With this method various materials can be deposited and the final morphology is independent from the substrate nature [221-224].

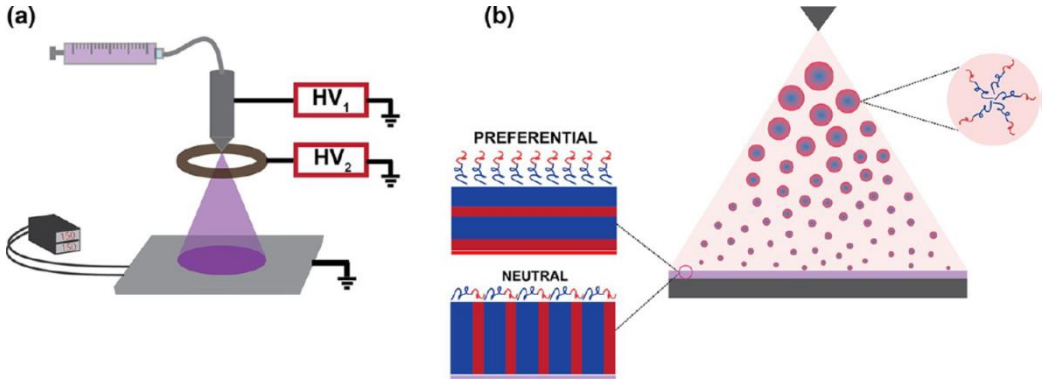

Fig. 16. (a) Schematics of electrospray setup. (b) Slow block copolymer deposition via electrospray generated droplets and equilibration in the presence of existing deposited material. A neutral surface promotes vertical growth of the microstructure while a preferential surface generates planar orientation. Micelles and/or dissolved chains of the block copolymer exist within each droplet. Reference 224

A novel promising technique that can be applied to various BCP systems such as PS-*b*-PMMA, PS-*b*-PDMS, PS-*b*-P2VP, P2VP-*b*-PS-*b*-P2VP and PMMA-*b*-PDMS inducing perpendicular orientation regardless of the molecular characteristics, the morphology and the annealing processes has been recently developed (Fig.27). The use of accelerated ion bombardment and vacuum ultraviolet/ultraviolet (VUV/UV) irradiation in plasma has been utilized to etch and crosslink a BCP leading to damaged surfaces. The newly developed method introduces a filter plasma treatment to hinter the VUV/UV irradiation and ion bombardment from damaging the BCP film allowing at the same time physical collisions by the use of neutral plasma species [13]. It should be mentioned that plasma techniques have been applied to promote the formation of perpendicular orientations in linear BCPs and complex architecture systems [203,225-227].

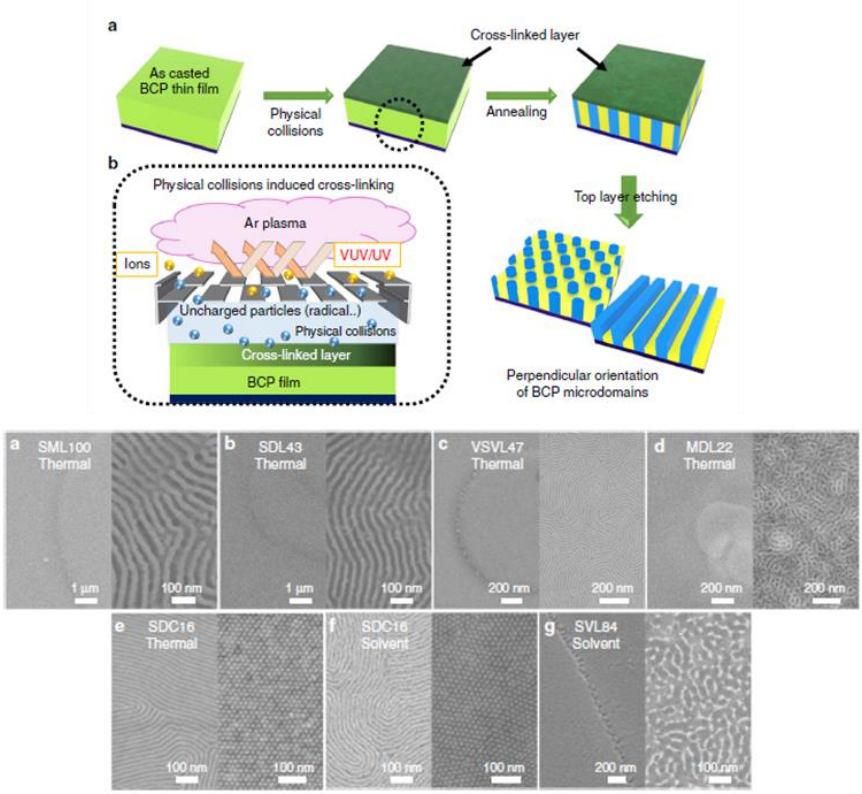

Fig. 17. Filtered plasma treatment to form the cross-linked layer for perpendicular orientation of BCP microdomains. Schematics of a. the plasma assisted process and b. the filter which blocks ion bombardment and VUV/UV generated by the argon plasma. Only the Ar neutral particles impinge obliquely on the surface of the film, forming a thin cross-linked layer without composition changes or etching. The cross-linked layer exhibits a neutral surface affinity for the BCPs, so that the perpendicular orientation of the BCP microdomains in the film after annealing can be induced regardless of the type, molecular weight, or fraction of the BCP. Reference 13

3.2. Addressing slow self-assembly kinetics in high-χ copolymers

Even though BCP systems with high χN values show more distinct, neat nanodomains with less inter-diffusivity near the domain interfaces, unfortunately, the self-assembly process can be quite slow prohibiting integration of materials in industry production lines, since annealing (Thermal or Solvent Vapor) can take up considerable amount of time.[228] The ordering process can be accelerated in higher temperatures under thermal annealing, however the maximum $T_{annealing}$ is restrained by T_{ODT} as well as thermal degradability.

Rapid thermal processing (RTP) is a method, where samples are heated with a higher rate compared to normal thermal annealing procedures. This process leverages the effect of heating rate on the degradation temperature of BCPs, like PS-*b*-PDMS, leading to a higher $T_{degradation}$ of the sample. A similar process utilizing faster heating rate, is laser spike annealing (LSA) which due to ultrafast heating in extreme temperatures, comprises a very rapid annealing process. Other exotic annealing techniques have, also, been investigated by several groups. Microwave annealing[229,230], warm spin casting (WSC)[231], or solvent-swollen PDMS gel pads have, also, been exploited to impart ordering of BCP chains, sometimes in an extraordinarily rapid way, improving self-assembly kinetics. [31,228] SVA can, also, lead to better ordering kinetics, especially when combined with heating. [232]

In SVA solvent molecules swell the nanodomains, rendering the chains more mobile and allowing for self-assembly ordering. The shortcomings of this process are the rarely eco-friendly solvents used the challenging optimization of the process, as well as the difficult scale up. However, SVA can occur under ambient temperature while the chain mobility often leads to self-assembly in otherwise hard to anneal samples. Even more, utilization of solvent molecules can alleviate interfacial interactions, as well as remove defects and provide long-range order.[165,233] Different SVA procedures like static SVA, or flow SVA have been investigated. Several methods to increase self-assembling kinetics in SVA, like preheating of the chamber can farther improve the process.[31,170]

3.3. Etch-Contrast

Directed self-assembly of BCP thin films gives rise to various structures and several wet and/or dry etching processes have been employed in order to selectively remove, either the formed wetting layer induced by the surface tension or one block's domains for the fabrication of nanoliphographic masks. Many high χ BCPs have been used to fabricate sub-10nm nanostructures for pattern transfer relevant applications. Thus, etch-contrast between the different block nanodomains is necessary to achieve pattern transfer by common etching techniques. Different etching methods have been utilized for pattern transfer of BCP structures to the desired substrates, like wet etching utilizing reagents, UV light and ozonolysis followed by solvent cleansing in order to fully remove the etched degraded segment, dry etching or ion beam etching.[148] The UV treatment has been widely exploited for the removal of polymethacrylates and afterwards the remaining traces are easily removed using an appropriate

solvent. Ozonolysis is commonly utilized in order to attack carbon double bonds and the most frequent example of treated polymers with this method is polydienes (PBd and PI). A quite commonly used reagent for the wet etching of polymers consisting of Si-O backbones is tetra-n-butylammonium fluoride (TBAF) and/or solution consisted of TBAF/n-methyl-2-pyrrolidinone followed by rinsing in deionized water. [234]

Reactive ion etching (RIE) is a very common dry etching strategy, utilizing plasma etch gases in lithographic procedures. High energy ions are accelerated through electromagnetic fields, colliding to the substrate in order to break the chemical bonds of the targeted segment [235-241].The etch-rate of organic materials is dependent on the number of carbon and oxygen atoms present in the structure.[242,243] An estimation of dry-etch resistance of polymeric materials can be extracted by the equation, $R_{etch} \propto N/(N_C-N_O)$, where N stands for the total number of atoms per segment, and N_C, N_O are the number of Carbon or Oxygen atoms per segment, respectively. The higher the R_{etch}, the higher the etch rate. This dependence of etch-rate on oxygen and carbon atoms does not change if the etch gas (O_2, Ar, H_2, CF_4) is altered, providing a qualitative indication of whether etch-contrast is present in an all-organic block copolymer material.

For most BCPs where a silicon-containing or a metal-containing segment is absent, etch-contrast is limited and has to be amplified, especially as the features are getting smaller and smaller. Several methods have been investigated towards that direction. Co-assembling of the BCP with domain selective organic or polymeric silicon-containing molecules is one of them.[144,145] Creating metallic or metal oxide nanostructures using BCPs nanodomains as a template in order to create a hard mask and facilitate etch-contrast, is another very common one etch-contrast method. For example, PS-*b*-P2VP, a block copolymer with low etch-contrast, can be doped with metal ions by solution or vapor phase deposition, and after plasma treatment yield the desired metallic structures.[246]

By solution deposition, PVP nanodomains can be protonated in dilute acidic environment and then due to electrostatic attractions interact with metal anions. Commonly by plasma treatment, the polymer is removed and metallic nanoarrays that can function as masks for pattern transfer are obtained (Fig.18). [247] Metal oxide nanoarrays can, also, be produced through solution-based deposition.[248-250] In vapor phase deposition (SIS) organometallic precursors selectively interact with a block through its functional groups (e.g., interactions with carbonyl functionality of PMMA) and ultimately under appropriate treatment yield the respective metal oxide.[251] With regard to PVP blocks, in SIS there is no need for previous protonation. [247] SIS can be used in materials comprising various blocks like PLA, PMMA, P2VP, P4VP and others.[191,208,252-254] In PS-*b*-PMMA for example, trimethyl aluminum (TMA), which is the precursor of alumina, can be selectively infiltrated in the PMMA domains through ALD technique, since TMA interacts with the carbonyl groups of PMMA. Other precursors can be used to yield TiO_2, silica, ZnO or W nanoarrays. After SIS, nanodomains with etch-contrast can be obtained.[148]

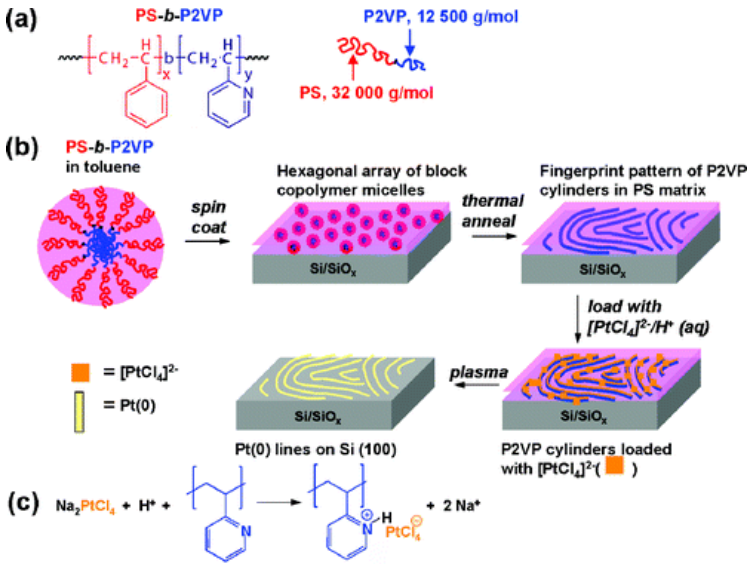

Fig.18. [247]

3.4. Directed Self-Assembly

Alignment of nanodomains in the in-plane direction and attaining BCP films with large correlation lengths can be quite difficult and although annealing can improve grain size by annihilating defects, usually other methods have to be used to attain adequate ordering. Shear, magnetic, or electric field alignment, directed self-assembly from guiding chemical or topographical patterns are only some of them. [151,165,171,172,255,256] In DSA methods utilizing guiding patterns, these patterns can typically be formed by conventional lithographic procedures, such that in essence a combined top-down and bottom-up strategy is used.

When topographical patterns are used (graphoepitaxial directed self-assembly), interfacial interactions with the edges of the topographical patterns (relief structures, e.g., trenches or ridges) as well as confinement effects are exploited to access long-range order and minimal defects.[257] In graphoepitaxy the periodicity of the BCP film can be much smaller than the characteristic length scale of the guiding patterns.[18] However, a shortcoming is that in conventional graphoepitaxy DSA, useful substrate space is occupied by the guiding templates. Graphoepitaxial DSA has been used to attain long-range order in several studies.[247,258,259]

When chemical guiding patterns are employed (chemoepitaxial directed self-assembly) their affinity towards one of the blocks is exploited. It has to be noted that the chemical guiding pattern pitch do not have to be in a 1:1 ratio towards the BCP pattern periodicity, but rather only a submultiple number of well-arranged guiding patterns can suffice to obtain long-range order. (Fig.19) This leads to a density multiplication of the patterns which is crucial to attain a higher areal density of features. Even more, in chemical epitaxy, the guiding patterns underly the BCP film and thus no substrate surface is compromised for farther processing. Relative tolerance to mismatch between guiding patterns pitch and BCP periodicity, also, simplifies the process.[260-264] The dimensions of guiding patterns and commensurability with BCP periodicity can affect the DSA process.[165,265]

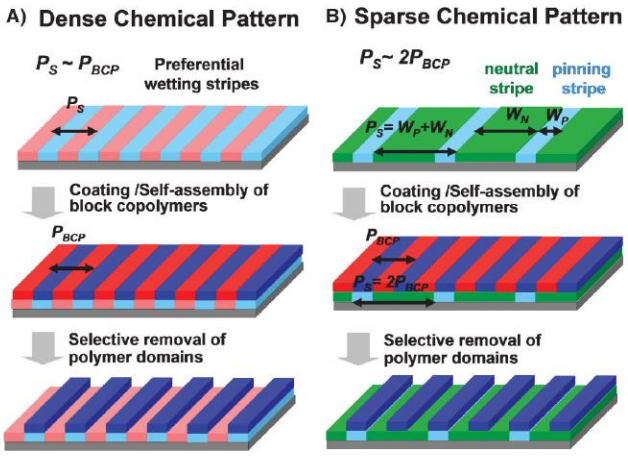

Fig.19 Density multiplication in chemical epitaxy [261]

Even more, in DSA BCP self-assembly patterns can appear rectified, leading to lower LER compared to the guiding patterns prepared by conventional lithographic methods. [266] Several studies suggest incorporation of high χ copolymers farther enhances LER, while high χ copolymers have a higher tendency for reducing defects and attaining long-range order, too. [267]

4. Towards highly immiscible diblock copolymers

4.1. Challenges

Due to recent synthetic advances quite a few possible combinations of blocks in linear and/or complex architecture copolymers, have been realized, leading to a plethora of new BCPs systems displaying quite different properties and potentials, albeit several issues still remain unresolved. The applicability of a BCP system is strongly affected by the easiness to establish a specific, sufficient, recurring synthetic protocol, which results in ample material quantities. As a result, despite the tremendous interest of several BCPs in the academic field, their practical use in industrial scale still remains ambiguous.

Challenges regarding the final processing of BCPs cannot be overlooked, such as defects and dislocations that are attributed to the grain boundaries that separate differently oriented domains and are usually evident in the self-assembled morphologies, influencing materials' properties. The lack of highly oriented and defect-free topologies is often encountered through the utilization of external fields (shear and electric fields).

For the BCP self-assembly on thin films to be integrated in nanopatterning and, subsequently, lead to high-fidelity nanofeatures, there are several prerequisites that direct materials' design. Orienting cylinders or lamellae domains to a vertical alignment is of great importance for lithographic applications and the scientific community has shifted the research towards resolving this challenge, through the utilization of predominantly external fields.

BCPs with high χ and low N values are able to produce high resolution- low feature size patterns, holding small LER. Challenges emerge when exploiting highly incompatible blocks, such as quite different interfacial energies, that conclude to planar and not perpendicular orientations, desired in several applications [268,269]. Other factors that have to be taken into consideration, however, are etch-selectivity, orientation and alignment control, mechanical and thermal properties, low-cost controlled polymerization, compatibility with thermal annealing (which is more fab-compatible), self-assembly kinetics and low defectivity.

Etch-selectivity can be induced by methods like atomic layer deposition (ALD) (e.g., to incorporate metal oxide precursors), or by integrating certain groups through

functionalization (chemical functionalization). Nevertheless, the most appealing method is to use a block that prompts etch-selectivity without additional steps. BCPs consisting of a silicon or metal containing block are compatible with oxidizing RIE techniques because the respective inorganic oxide is produced, providing an etch mask. Some representative metal-containing blocks are PFS (polyferrocenylsilane), and PSnS (Poly(4-trimethylstannylstyrene)).[270,271] However, metal-containing copolymers implicate nanoelectronics applications, thus, silicon-containing are far more well-studied.

4.2. Adjusting Driving Forces for Self-Assembly

The strong necessity for BCP systems that are well microphase separated exhibiting low periodicities for fabricating nanostructured materials has shifted the scientific community to two directions. The one direction is the synthesis of highly incompatible low molecular weight BCPs [2], to obtain well-defined patterns in the sub-10nm regime and the second direction is the synthesis of complex architecture BCPs to ensure better mechanical properties, higher T_{ODT} and lower viscosity. Various experimental techniques including absolute intensity small X-ray scattering (SAXS), small angle neutron scattering (SANS), rheology and the use of homopolymer blends have been employed for the estimation of χ value, which is critical for the assessment of the incompatibility between different segments [86,272-274].

Although the extensively studied systems such as PS-*b*-PMMA (χ~0.04), PS-*b*-PB (χ~0.06) PS-*b*-PI (χ~0.09), PS-*b*-PEO (χ~0.08), PS-*b*-PFS (χ~0.08) have provided further insight on the fundamental behavior of BCPs with respect to their microphase separation in bulk and thin films, obtaining small feature sizes (below 10nm) has proven non feasible. This fact is attributed to the chemically similar segments and their inability to self-assemble when the N value is severely diminished. This property inhibits the relatively compatible blocks for lithography. For this reason, promising BCPs have been developed that are more suitable for nanotechnology. Higher χ BCPs allow microphase separation to occur even for low N values and subsequently the domain spacing can be reduced. The ever-growing demand for lower scale lengths has led to the combination of highly incompatible compounds that can be categorized to two broad classes of materials, based on the chemical structures of the constituent segments and specifically organic and inorganic block copolymers.

As a reminder, a high χ value is an indication of a strongly-segregating BCP but direct comparisons based solely on χ can be misleading. This is due to the fact that χ value is affected by the method used to calculate it, the assumptions or reference volume values used and other factors. Further supportive evidence of a strongly-segregating system can be extracted by the smallest achievable dimensions or T_{ODT}. It should, also, be noted that a single high χ value alone cannot account for high-fidelity ultra-small nanopatterns. It has been observed that when pushing BCP to their ODT limit, weakly segregated domains are formed, resulting in bridging and other deformations after etching. This, further highlights the need for ultra-high χ copolymers to attain higher χN from low N chains, or for other ways to increase segregation strength.[200]

4.2.1. High χ PDMS Containing BCPs

The contrasting properties between two constituent blocks where at least one segment is inorganic such as PDMS, POSS, PFS, PTMSS etc. results in large segmental interactions. A considerable number of reports have been published with respect to inorganic BCPs, exhibiting higher resolution. Apart from intrinsic etch-selectivity, silicon-containing blocks are known to demonstrate enhanced immiscibility with organic constituents. PDMS, POSS-containing, PTMSS are only some of the blocks employed on that premise. [69,275-277]

One of the most extensively studied BPCs that contains an inorganic block, is the PS-*b*-PDMS system that has χ value equal to ~0.27 at room temperature [278,279]. Silicon containing PDMS segments exhibit lower surface tension than PS and as a result PDMS selectively segregate at the air/polymer interface during the microphase separation. High etch resistance properties of the PDMS segments, in addition to widely studied air/polymer surface neutralization, utilizing top-coats, neutral layers and brushes render the above mentioned system a milestone for DSA using inorganic BCPs [168,203,241].

Based on the relation of the χ value with the solubility parameters of the two blocks, an almost seven times larger χ than the PS-*b*-PDMS system has been reported for the P4VP-*b*-PDMS system, attributed to the higher hydrophobicity of the P4VP compared to the PS segment [228,280]. High ODT values due to poly(4-vinylpyridine) units prevent the χ estimation using scattering techniques. Kim et al. have studied P4VP-*b*-PDMS with regard to graphoepitaxy in Si trenches using warm solvent annealing (WSA) with ethanol in less than 10 min.[228] In-plane cylinders aligned to the trenches were created by self-assembly on a substrate pre-coated with homopolymer brushes. WSA improves the kinetics of self-assembly which is crucial for high χ BCPs where the diffusion of the highly incompatible chains can be quite slow and prohibitive for the industry standards. In this approach it is convenient to use ethanol an eco-friendly and fast-evaporating solvent. The Line Edge Roughness (LER) of the nanostructures was only 6% of the line width, a value acceptable for future semiconductor applications according to the ITRS guidelines. Importantly, it was highlighted that, high χ copolymers can significantly decrease LER, as compared to less incompatible systems. (Fig.20) The effect on pattern quality of the type of homopolymer brushes selected to precoat the substrate with, was, also, investigated in this study.

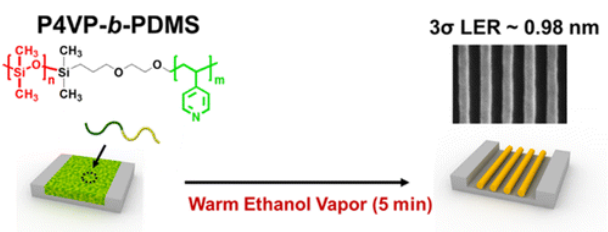

Fig.20. LER of a P4VP-b-PDMS diblock copolymer [228]

Apart from P4VP-*b*-PDMS, PDMS has been extensively studied in other BCPs with a polar block, with χ values a few times larger than PS-*b*-PDMS. Specifically, P2VP-*b*-PDMS was found to self-assemble into ultra-small nanostructures with line-widths as low as 6 nm, while it was predicted that even sub-5nm features would be obtained from this system with a lower MW.[280] By utilizing SVA, various morphologies could be formed from a single BCP through the fine-tuning of the selective swelling, while the observed d-spacing could, also, be manipulated. The BCP system has been tested for graphoepitaxy DSA and well-aligned parallel cylinders, with sharp edges (i.e., low LER) were obtained. (Fig.21)

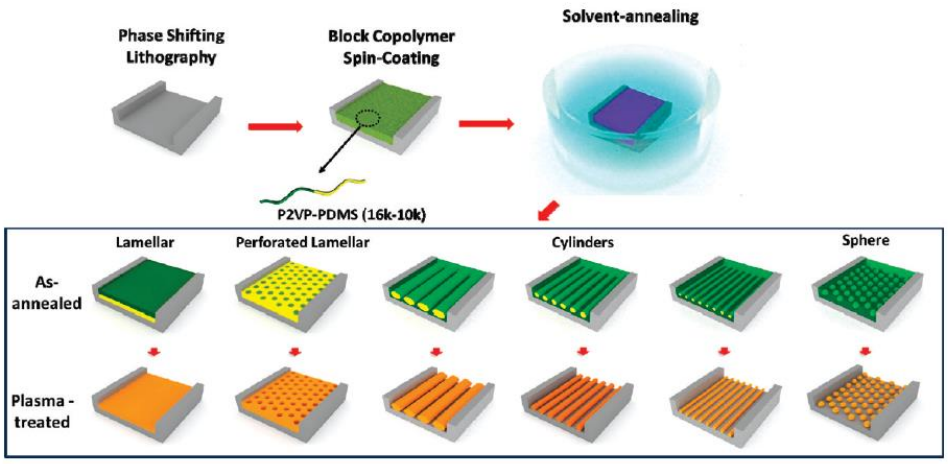

Fig.21. Schematic showing the highly tunable self-assembly process. [280]

Extraordinary immiscibility among the two components at the PDMS-*b*-PLA system, significantly affects χ inducing values as high as ~1.4 [281,282]. The combination etch-contrast, the ability to self-assemble in substantially small dimensions, and the facile synthesis contributes to the high potential of the specific copolymer for nanolithography. Chemical dissimilarity between the two blocks triggers a high difference in surface energies, a factor that favors planar orientations. PLA-*b*-PDMS-*b*-PLA triblock copolymers were studied by Rodwogin and his co-workers [282]. They managed to create nanoporous PLA or PDMS nanodots by selectively etching the appropriate block of the cylinder-forming triblock chains. The areal density of the nanodots reached the value 1Tdot/in^2. They estimated a χ value ~1 at 393K based on d-spacing. Although, other studies concerning the system suggest that this value is lower, undoubtedly, it is considered a versatile strongly segregating BCP [283]. In a subsequent work by Pitet and his co-workers, PDMS-*b*-PLA diblock copolymers were studied [281]. Parallel cylinders and spherical nanodomains were reported on thin films even for low MWs and for high compositional asymmetry. Nanodomains of approximate dimensions of 10nm were routinely observed. Lastly, this promising high χ triblock copolymer of the PLA-*b*-PDMS-*b*-PLA type has been used by Reboul and his co-workers [284]. The result was perpendicular nanocylinders of PLA (L_0=15nm) by thermal annealing. Nanodomains normal to the substrate were attained by utilizing a neutral, non-Si-containing layer.

Employing azide-alkyne click cycloaddition, PDMS-*b*-PMMA sequences were synthesized leading to high χ values equal to ~0.23 at room temperature [285]. High etching selectivity among the two components makes the specific system promising for various applications. However, the vastly dissimilar surface energies require the use of exogenous processes in order to obtain well-defined morphologies. The χ value of the PDMS-*b*-PMMA system remains approximately high (~0.2) even when the temperature rises at about 150°C in contradiction with the PS-*b*-PDMS sequence, which exhibits χ values equal to 0.1 in similar conditions. [285] (Fig.22) When studied in bulk, 8.7 nm full-pitch lamellae were achieved. In thin films, 12.1 nm full-pitch parallel cylinders were observed. These are among the smallest d-spacings both in bulk and in thermally annealed thin films. Again, in this study SVA with different solvents led to different morphologies, highlighting the versatility of SVA for ultra-high χ copolymers.

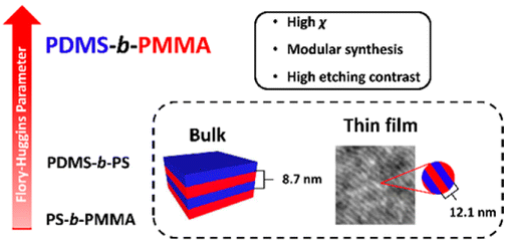

Fig.22. Graphical abstract from ref. [285]. PDMS-*b*-PMMA demonstrates improved immiscibility compared to PS-*b*-PDMS. Ultra-small nanofeatures observed.

Luo and his co-workers have worked extensively on PDMS-*b*-PEO BCPs. The Flory-Huggins interaction parameter for this copolymer was calculated to be 0.2 at 150 ^{o}C. Self-assembled morphologies with periodicities as small as 7.9 nm have been accessed. Incorporation of an H-bonding additive to improve self-asselmbly was tested, too. [286] PDMS-*b*-PEO not only exhibits a high χ value, but has, additionally, been used as a model system to test whether chemical tuning of the junction point of the blocks can further enhance immiscibility, providing a means for increasing segregation strength without altering the main BCP system.
Specifically, ionic junction points were introduced to neutral PDMS-*b*-PEO and PDMS-*b*-PMMA BCPs.[287] While, the d-spacing was slightly increased after the incorporation of the ionic junctions due to higher stretching, the T_{ODT} was significantly increased (over 50 ^{o}C), allowing even smaller nanodomains to be formed. Sub-6nm lines were easily accessed in bulk. Furthermore, successful transfer of the ionic junction to thin films yielded 13 nm full-pitch nanostructures highlighting the potential of the method for DSA applications. Apart from the aforementioned (i.e., mixing with H-bonding additive, ionic junction point), other means of increasing segregation strength will be described in detail in a following section.
An approximately two times higher χ (~0.42) in room temperature and 4 times higher (ca. 0.39) at 150 ^{o}C when compared to the PS-*b*-PDMS sequence was calculated for P3HS-*b*-PDMS system which has been synthesized using anionic polymerization with sequential monomer addition and subsequent deprotection of the THP groups [288]. Furthermore, even though corresponding thin film studies are not reported yet, small periodical dimensions equal to 7.4 nm for lamellae were evident, while it exhibited an even better etch-contrast than PS-*b*-PDMS.

4.2.2. Alkylsilyl-Containing High-χ Diblock Copolymers Thin Films

Another BCP comprising Si to induce etch-contrast with organic blocks is PTMSS. A BCP incorporating PTMSS and an oligosaccharide block (MH) led to 5 nm nanocylinders. The amphiphilic nature of the copolymer in addition to the rod like-coil configuration accounted for the increased immiscibility of the segments. However, the oligosaccharide block was prone to thermal degradation.[289]
By combining PTMSS with PLA through anionic and ring-opening polymerization, the synthetic procedure was facile and both segments showcased high glass transition temperatures. The copolymer, with an ultra-high χ (ca. 0.417, 140 ^{o}C, recalculated 0.21, 25 ^{o}C)[290] adopted lamellar morphology with a half-pitch equal to 5.7 nm, without the thermal degradation obstacle [291]. For the specific system it has been reported that the high χ parameter remains quite enlarged through a wide range of temperatures when compared to other BCPs. SVA was employed to orient nanofeatures vertically to the substrate as evident by AFM and SEM images.[292] The system is of particular interest since it exhibits high etch-contrast in oxygen plasma RIE, while PLA is, also, known to be compatible with wet acid or base etching. But SVA is accompanied by some impediments described in a previous section. In a milestone

article, the same groups described the use of polarity-switching top coats on PTMSS-*b*-PLA and PS-*b*-PTMSS-*b*-PS thin films, to produce vertical 9 nm and 15 nm half-pitch lamellae simply by thermal annealing.[174] To preserve pattern integrity, one has to use a top coat that can be spin coated by a solvent immiscible with the BCP thin film, which is the case also here. This polarity-switching top coat technique incorporating maleic anhydrite moieties has been described previously.

PS-*b*-PTMSS and PS-*b*-PTMSM have, also, been used to produce vertical lamellae with minimum periodicities 18 nm and 15 nm respectively, by thermal annealing for 1 minute or less at temperatures lower than 200 ºC regardless of film thickness (1-3 L_0).[199] For this purpose, polarity-switching top coats comprising maleic anhydride and silicon-free substrates were employed, too. It is noteworthy that a wide range of interfacial energies could be achieved by controlling the top coat composition. An optimized casting process was, also, described for the TCs, utilizing polar solvent (methanol) and trimethyl aluminum salts. Definitely, this work demonstrates a promising top coat choice for high χ, insoluble in methanol, copolymers. The problem with PS-*b*-PTMSS and PS-*b*-PTMSM, however, is that they do not really constitute high χ copolymers ($\chi_{PS\text{-}PTMSS}$=0.047, 150 ºC). Consequently, further work has been done by the same group, examining copolymers with higher χ values to obtain smaller, vertical nanofeatures. PS-*b*-PDSS (χ=0.11, 150 ºC, minimum d=14.9 nm), PMOST-*b*-PTMSS (χ=0.14, 150 ºC, d=14.4 nm), PMOST-*b*-PDSS (χ=0.2, 150 ºC) were examined in comparison to PS-*b*-PTMSS. Normal to the substrate through-film nanodomains generally form when the BCP thin film is between two neutral surfaces, which, along with the silicon oxide etch barrier formed after etching of the silicon-containing block, allows for thick nanostructures. Polymeric top coats and neutral substrates were used for orientation control. (Fig.23) RIE was subsequently applied to produce well-ordered high-aspect ratio nanopatterns. The stronger the segregation, the more improved the fidelity of nanopatterns as can be seen in Fig.24.[200]

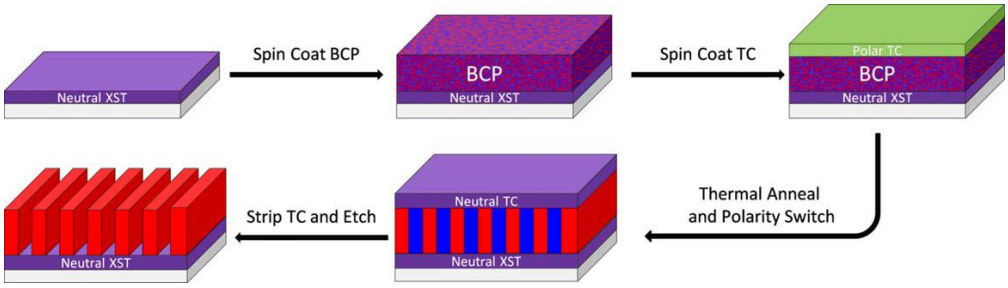

Fig.23. Schematic of TC process flow used to thermally produce perpendicular orientation of block copolymer domains.[200]

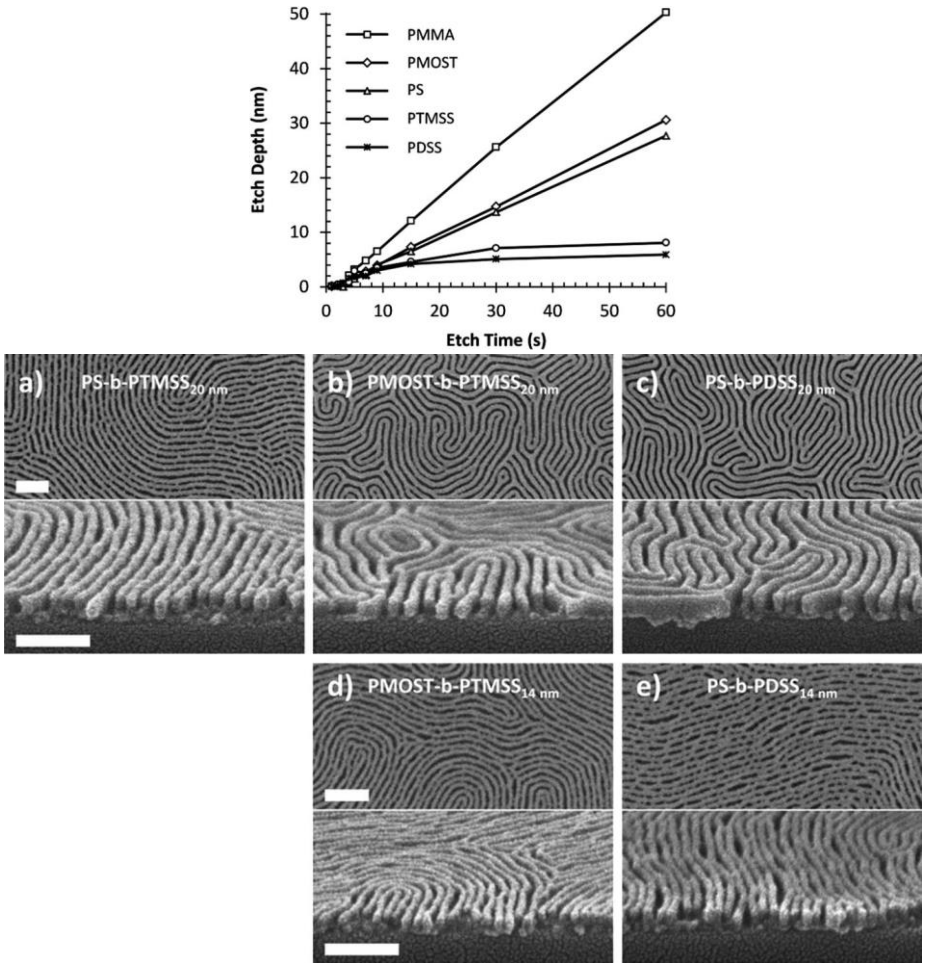

Fig.24. (Top) Etch profiles of homopolymer thin films subjected to an oxygen RIE. (Bottom) Top-down and angled SEM of (a) PS-*b*-PTMSS20 nm, (b) PMOST-*b*-PTMSS 20 nm, (c) PS-*b*-PDSS 20 nm, (d) PMOST-*b*-PTMSS 14 nm, and (e) PS-*b*-PDSS 14 nm after 13 s CO_2 RIE followed by sufficient N_2/H_2 RIE to clear the organic layer. As cast film thicknesses are ca. 1.75 L0. Scale bars are all 100 nm and apply to each row of figures, respectively.[200]

Lastly, a BCP consisting of a silicon-containing polystyrene derivative, PVDB-*b*-PDSS, was used to produce strongly segregated 5nm half-pitch nanodomains, with enhanced etch-selectivity.[293] The system was successfully subjected to a hybrid chemo-/graphoepitaxy scheme with a 4x density multiplication factor. (Fig.25) Pattern transfer was tested on a chromium hard mask with an underlying carbon layer, relieving high-aspect ratio structures. This comprehensive study could stand as a proof-of-concept for high χ, etch-selective, BCPs facilitating the DSA transition from lab-to-fab for critical dimensions as low as 5 nm.

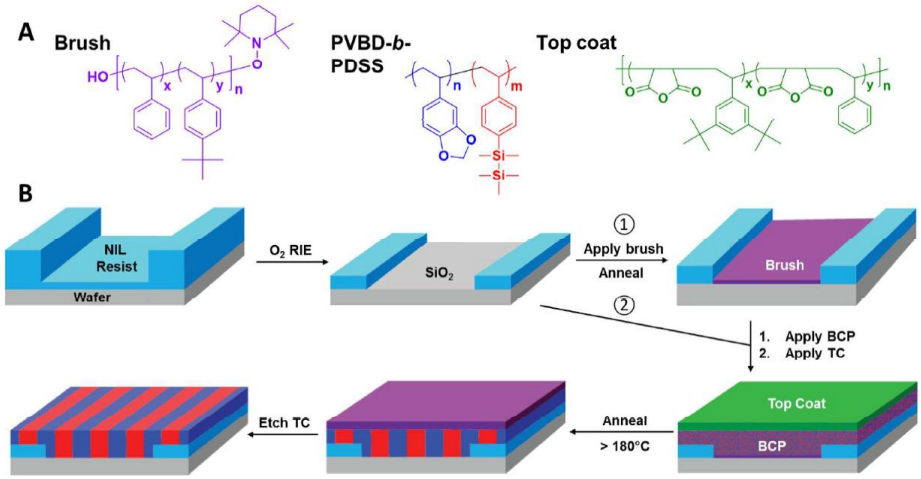

Fig.25. Schematic showing the (A) materials and (B) process steps used for producing directed self-assembly of 5 nm features. Arrow 1 and 2 describe the process with and without a grafted brush, respectively.[293]

4.2.3. POSS-Containing High χ Diblock Copolymers Thin Films

Polyhedral oligomeric silsesquioxane-POSS containing BCPs are organic-inorganic hybrid materials with desirable properties such as high glass transition temperature due to their molecular cage structure, pliable functionality and inherent high oxygen plasma etch resistance. Furthermore, semi-crystalline and crystalline nanodomains exhibit enhanced physicochemical resistance, when compared to silicones, which enable the use of the specific blocks for pattern fabrication. [200-205].

Such examples with high χ values are PMAPOSS-*b*-PS (χ=0.14, 150 ^{o}C) and PMAPOSS-*b*-PMMA (χ=0.146, 150 ^{o}C). These copolymers have proven to exhibit high etch-contrast necessary for pattern transfer.[294] (Fig.26) In a study of PMAPOSS-*b*-PMMA for chemical epitaxy after SVA, a 4x density multiplication factor and an areal density equal to 3.7Tdot/in^2 were observed.[295] Lattice spacing as small as 12.4 nm was attained. (Fig.) Careful optimization of solvent vapor annealing allowed order-order transitions due to different degrees of swelling (i.e., different effective volume fraction). Interesting is that by SVA and chemical epitaxy, as happens for thermal annealing and chemical epitaxy, self-healing of defects present in the guiding pattern was achieved in the self-assembled BCP thin film. Certain tolerance to mismatch between the guiding pattern and nanodomain periodicities was, also, observed.

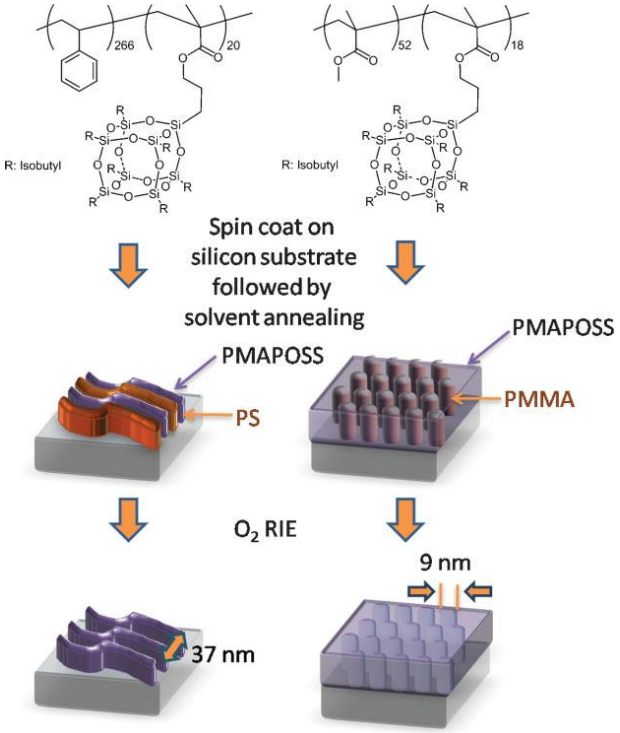

Fig.26. Schematic illustration for the fabrication of silicon oxide line arrays and nanopore arrays. Lamella forming PS-*b*-PMAPOSS and cylinder forming PMMA-*b*-PMAPOSS were spin coated onto silicon substrate and exposed to solvent vapors to induce vertical orientation of the lamellar and cylindrical domains. After oxygen-plasma treatment, silicon oxide lines and pore arrays were formed.[294]

On the other hand, diblock copolymers of the PMAPOSS-*b*-PTFEMA type were synthesized through RAFT polymerization in order to avoid back-biting reactions. These copolymers exhibit very similar surface energies facilitating the vertical orientation without any post-synthetic functionalization requirements. Overall, the specific system can be rendered a cost-effective candidate for lithographic applications since the inherent properties between the constituted blocks allow the reduction of multiple processes during patterning. [296] In general, in DSA applications, as already mentioned, it is highly desired for the self-assembled nanostructures to orient perpendicularly to the substrate in order to achieve line/space patterns from lamellae or nanodots from perpendicular cylinders. Line/space patterns can also be achieved by parallel cylinders but perpendicular lamellae are preferred due to aspect ratio issues, since for parallel cylinders the BCP thin film thickness is ~$1L_0$ for pattern transfer applications. BCP systems with a high χ value, however, usually exhibit imbalanced surface free energies on their thin films which lead to in-plane patterns. A system proven to successfully combine balanced surface free energies, etch-selectivity and ultra-high χ (ca. 0.45 at 150 ^{o}C), is PMAPOSS-*b*-PTFEMA. This system was chosen on the notion that trifluoroethyl groups of PTFEMA would serve as interfacial affinity control units balancing surface free energies (SFEs). Thin films of PMAPOSS-*b*-PTFEMA were used to fabricate lamellae with periodic dimensions as small as 11 nm and perpendicular orientation simply by thermal annealing without a top coat, additives or a neutral layer. Graphoepitaxy DSA was investigated and aligned sub-10 nm line/space patterns (L_0=15 nm) were achieved.

4.2.4. All-Organic High χ Diblock Copolymers Thin Films

As we have already mentioned, silicon containing segments can enhance immiscibility and etch-contrast. However, the considerably different surface energies in BCPs comprising hybrid inorganic-organic blocks necessitate complex additional steps to achieve the most commonly desired vertical orientation. Even more, due to their low surface energy, silicon-containing blocks often create a silicon-rich thin layer at the interface with air if a top coat is not used, complicating, thus, the subsequent processing.[297] Consequently, an all-organic scheme is sometimes preferred. To achieve high incompatibility a polar block is often combined with a non-polar, since a large difference in the solubility parameters of the blocks is associated with higher χ values. PHS-based BCP are able to microphase separate adopting well-defined morphologies by increasing the hydrophilicity or the hydrophobicity of one of the segments leading eventually to an increase in the χ value.

Kim and coworkers reported the synthesis of PDHS-*b*-PS BCPs through RAFT polymerization and found a large segment-segment interaction parameter ~0.9, attributed to the high incompatibility between the two segments, generated by the presence of two hydroxyl groups. It has been used to obtain lamellae of 5.9 nm full-pitch and cylinders of 4 nm diameter in bulk, while nanostructures of sub-10nm periodicity were achieved on thin films. The well-defined structures obtained by this system enable the fabrication of sub-5nm patterns. [298]

Although, a high χ may be an advantage, in some cases it is considered a barrier in the use of these materials in thin films. Nevertheless, PHS based materials have a strong polar character and are easily modified to alter the physicochemical properties, allowing them to be used in several applications. A significant example of an all-organic BCP is that of PDHS-*b*-PS which has one of the highest χ values (ca. 0.7, 150 ^{o}C). Via Atomic Layer Deposition, the hydroxyl groups were functionalized with metal oxide precursors to yield ZrO_2 nanowires from parallel cylinder monolayers. The incorporation of the two hydroxyl groups provides an increased polarity for PDHS. In comparison, P4HS-*b*-PS consist of one less hydroxyl group exhibited a, much smaller, χ=0.12 (150 ^{o}C) value and L_0=11.8nm lamellae in bulk.[299]

Kanimozhi and his co-workers, examined the effect increased difference of polarity would have on segregation strength for P3HS-*b*-PtBS copolymers as compared to P4HS-*b*-PS.[300]

The addition of *tert*-butyl group on polystyrene makes it more hydrophobic, allowing for much smaller nanodomains, i.e., d=8.8 nm for lamellae and d=11.5 nm for cylinders, in bulk. P3HS was preferred to P4HS due to the high T_g of the latter, necessitating very high processing temperatures that can lead to self-crosslinking of the block and thermal degradation of the other component in its copolymers. During studies of P3HS-*b*-PtBS on thin films, parallel cylinders of 14 nm periodic dimensions occurred. The films were subjected to TMA vapors, selective for P3HS, which after O_2 plasma etching led to the formation of aluminum oxide arrays.

Another *tert*-butyl containing BCP with increased immiscibility is PtBS-*b*-P2VP which exhibits a χ value equal to 0.11 (150 ^{o}C), almost 1.5 times higher than PS-*b*-P2VP, highlighting the increased hydrophobicity due to the tert-butyl groups.[246] The smallest periodicities reported in bulk were calculated to be 9.6 nm for lamellae and 14.1 nm (diameter=6 nm) for cylinders. Parallel cylinders with miniaturized dimensions were, also, prepared on thin films and used to obtain Pt nanowires of 5.8 nm diameter or alumina nanowires of 8-11 nm diameter.[246,297] (Fig.27) Alumina nanowires with a diameter equal to 11 nm were, successfully, tested as hard masks for pattern transfer, leading to promising results for pattern transfer applications of the BCP. Lastly, graphoepitaxy was exploited for long-range order and alignment of P*t*BS-*b*-P2VP nanodomains on rectangular, cyclic, or U-shaped trenches. (Fig. 28) Other BCPs incorporating PtBS, like PtBS-*b*-PMMA (χ=0.05 at 150 ^{o}C, ~1.8 times higher

than PS-*b*-PMMA) or P*t*BS-*b*-PHEMA (χ estimated over 0.4, sub-7 nm full-pitch cylinders) have manifested the increased hydrophobicity induced by the *tert*-butyl group.[301,302]

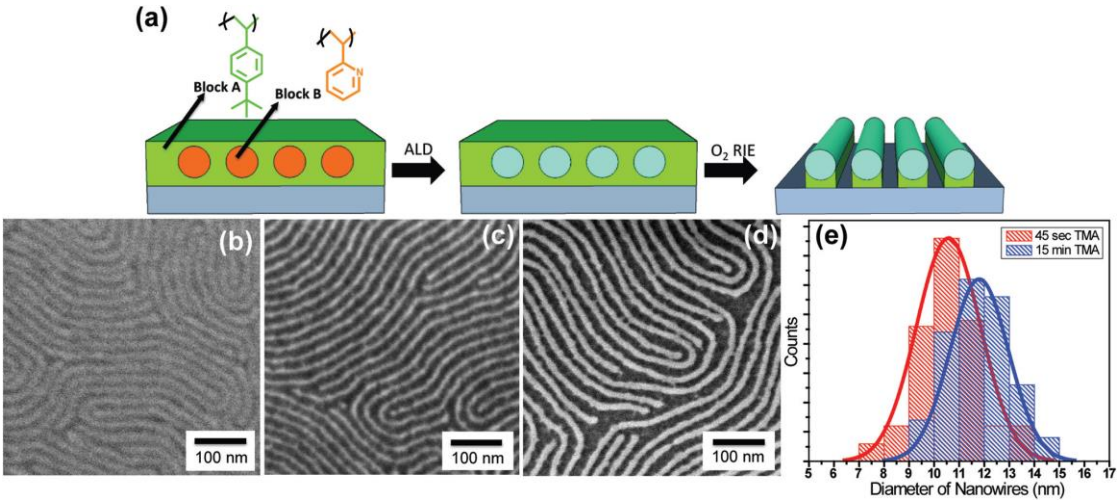

Fig.27. (a) Schematic process of metal organic precursor incorporation into selective domains of a self-assembled BCP film, followed by oxygen plasma RIE. (b–e) Top-down SEM images of self-assembled cylinder-forming P(*t*BS-*b*-2VP) (mol wt 11.9k–3.0k). (b) After polymer film self-assembly (iodine stained for imaging contrast), (c) after a total TMA exposure dose of 45 s, reaction with water vapor, and O2 RIE, (d) after a total TMA exposure dose of 15 min, reaction with water vapor, and O_2 RIE, and (e) histogram showing average nanowire diameters from 45 s total TMA exposure time (red) and 15 min total TMA exposure (blue).[246]

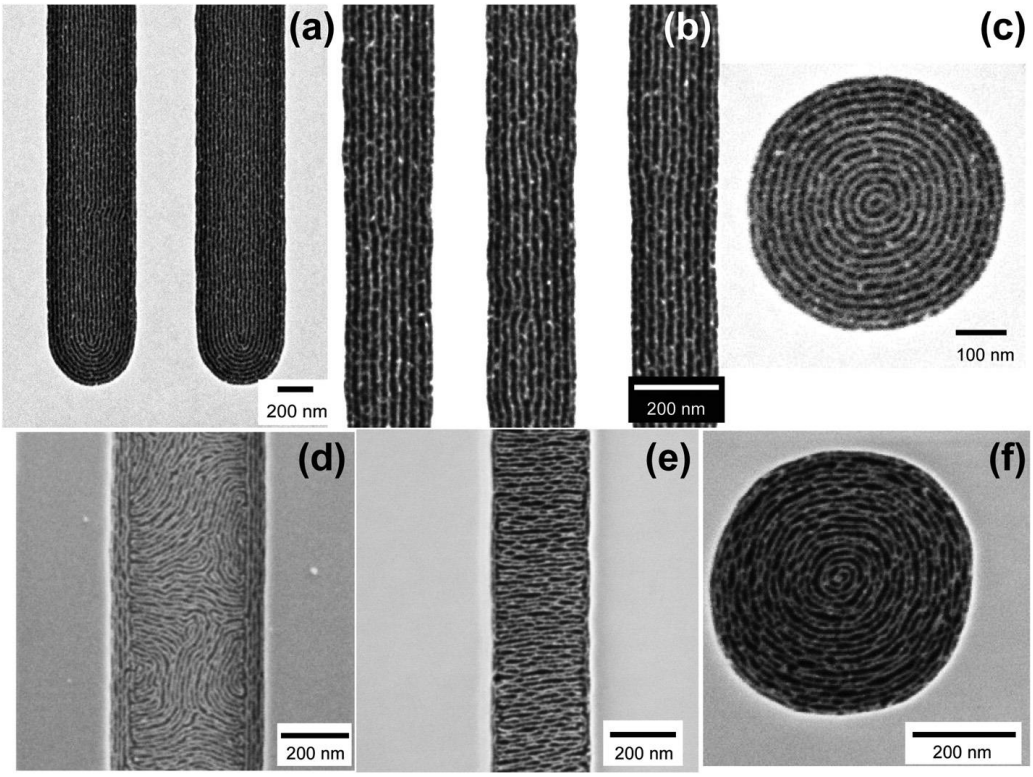

Fig.28. SEM images of 11 nm aligned ALO nanowires (a–c) with long-range ordering within ~20 nm deep trenches on silicon: (a) U-shaped channels with a width of 410 nm, (b) rectangular channels of 200 nm, and (c) circular trench with a diameter of 510 nm. SEM images of 9 nm aligned ALO nanowires (d–f) within ~20 nm deep trenches on silicon: (d) rectangular channel with a width of 410 nm, (e) narrower rectangular channels with 250 nm width, and (f) circular trench with a diameter of 510 nm.[246]

High χ PCHE-based copolymers were synthesized by Hillmyer and coworkers, through various synthetic combinations including anionic polymerization, ATRP, controlled ring-opening polymerization and heterogeneous catalytic hydrogenation. Excessively high χ values, in conjunction with the high etching selectivity exhibited in these systems, render them suitable candidates for DSA methods and nanopatterning [208,250,303].

As the significant effect of *tert*-butyl moieties on the hydrophobicity of polystyrene has been examined, the important effect of PS hydrogenation could not be omitted. Polystyrene when is being fully hydrogenated forms poly(cyclohexylethylene) (PCHE) a block that appears to be less polar, as evident by its improved immiscibility with polar blocks. For example, PCHE-*b*-PMMA demonstrates a χ value equal to 0.18 (150 ^{o}C) and self-assembled lamellae of 9 nm full-pitch have been observed in bulk, while the authors of the corresponding study suggest even 7 nm periodicities can be attained.[206] Comparatively, PS-*b*-PMMA exhibits a χ value equal to 0.022 under the same conditions. SVA was applied to BCP thin films providing 7.5 nm perpendicular lamellae as observed by AFM. PCHE-*b*-PEO, also, has a much higher χ value (0.22, 150 ^{o}C), as compared to PS-*b*-PEO.[250] Apart from the increased immiscibility, PCHE-*b*-PEO appears as a promising alternative to PS-*b*-PEO since it provides higher mechanical and thermal stability. PS-*b*-PEO, like PS-*b*-PVP, is of particular interest, because it can selectively interact with inorganic precursors and after appropriate treatment yield the corresponding metal oxide arrays. Accordingly, PCHE-*b*-PEO was used to infuse metal oxide precursors to PEO to obtain ultra-small metal oxide nanodots of 6 nm diameter. Last but not least, PCHE-*b*-PLA is another high χ cyclohecylethylene-containing BCP (χ=0.23, 150 ^{o}C, 3x $\chi_{PS\text{-}PLA}$) in which perpendicular nanocylinders of 5 nm diameter have been realized after SVA.[208] Hydrolysis of PLA led to nanoporous PCHE while, SIS was tested to yield alumina nanodots of 10 nm diameter that can induce etch-contrast to the BCP for subsequent pattern transfer. (Fig.29) Overall, it can be seen that subtle changes on the chemical structure of a block can strongly impact the immiscibility in BCP systems.

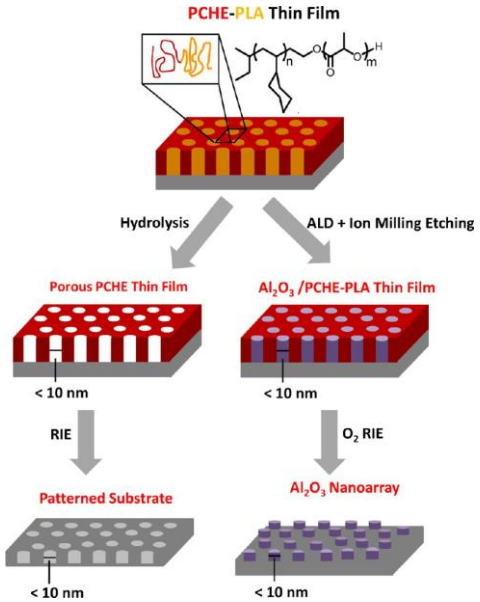

Fig.29. Illustration of the Dual Functionality of PCHE−PLA Block Polymers in Thin Film Templating ApplicationsIn one route, a nanoporous PCHE mask is produced from an organized film through hydrolytic decomposition of the PLA domain. Alternatively, the combination of domain selective ALD, argon ion milling and RIE produces an Al_2O_3 nanoarray.[208]

A block copolymer with one of the highest χ values (~0.4, 150 ^{o}C) reported is PS-*b*-PGM. [290,304] PS-*b*-PGM is produced after the acid-hydrolysis of the precursor PS-*b*-PSMA (χ=0.035, 150^{o}C) that bears two acetal-protected hydroxyl groups per repeat unit. The extraordinary increase in χ value comes as a result of the increased polarity of the PGM block. 5.4 nm full-pitch lamellae were produced in bulk from low molar mass PS-*b*-PGM, which is among the smallest nanofeatures ever achieved by BCP self-assembly. It was evident that by controlling the degree of deprotection, the χ value could, also, be tuned. Self-assembly of PS-*b*-PGMA in thin films generated 9.4 nm vertical to the substrate lamellar nanodomains by thermal annealing.[305] A random brush mat consisting of PS-*r*-PSMA with appropriate composition was used as a neutral layer. Both the PS-*b*-PSMA thin film and the underlying PS-*r*-PSMA neutral brush layer were deprotected in the solid state by acid vapors to yield PS-*b*-PGMA and PS-*r*-PGMA, respectively. Ultimately, not only did this group judiciously synthesize an ultra-high χ copolymer that self-assembles into sub-5 nm nanodomains, but also achieved the difficult task of controlling the orientation of the nanodomains on thin films by thermal annealing. Furthermore, they investigated the immiscibility of the highly amphiphilic block copolymer PS-*b*-PAA.[306] The BCP was synthesized by a two-step hydrolysis from PS-*b*-PSA. The χ value of the final BCP (ca. 0.86, 150^{o}C) was calculated to be ~15 times higher than the χ value of PS-*b*-PSA. This extraordinary incompatibility allowed for sub-7nm full-pitch nanofeatures. Carrying out only one deprotection step, the forming PS-*b*-PGA led to different morphologies as compared to the full two-step deprotection scheme that yields PS-*b*-PAA, while in both cases ultra-small nanodomains were produced. This provided a direct route to controlling morphology from a single precursor BCP.

Another carboxylic acid-containing high χ BCP has been used in a recent study lately. Enhanced segmental interaction was observed, where the χ value was calculated ~0.55, attributed to the major difference in the polarity among the two segments due to the presence of the hydroxyl group of the PMAA block [185]. The results of PS-*b*-PMAA thin films were very promising with regard to the integration of ultra-high χ copolymers for nanopatterning applications.[307] In this work, they utilized initiated chemical vapor deposition (iCVD) to prepare in situ a neutral bottom layer and a top coat for the BCP thin film. (Fig.30) For this method, vaporized monomers were polymerized directly on the respective surface and then a cross-linkable constituent of the copolymer was crosslinked to yield the top coat or neutral layer film. The composition and thickness of these layers could be tuned, whereas the use of solvents, a factor that can pose limitations to the thin film preparation process, was avoided during the top coat and neutral layer preparation. Normal to the substrate nanocylinders (diameter=4 nm) were produced with a long-range order (grain size equal to 5 L_0). It is worth mentioning that PMAA is a hydrophilic block that would hinder the design of a spin-coated top coat, since a solvent that would not affect the BCP thin film, would be required for the top coat's casting. With an amphiphilic BCP this would be a quite demanding process. In addition, the spin-coating technique, in general, can lead to defects and dewetting.

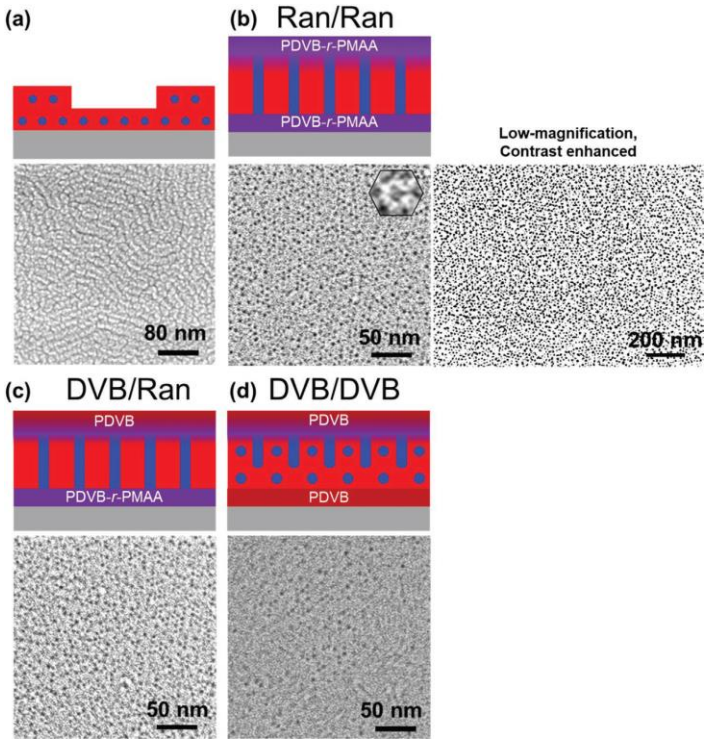

Fig.30. Top-view SEM images of PS-*b*-PMAA thin films after annealing at 180 °C for 15 h on a) bare silicon substrate and between iCVD layers; b) Ran/Ran: random top, random bottom, inset is the zoomed-in image of hexagonally close packed cylinders, image on right is a zoomed-out and contrast enhanced image; c) DVB/Ran: PDVB top, random bottom; and d) DVB/DVB: PDVB top, PDVB bottom. PMAA domains were etched via RIE prior to SEM analysis.[307]

Based on the increase of the polarity of the more polar group in a BCP enhances χ value, PS-*b*-PMMA has, also, been carefully modified by ester-amide exchange reactions with various amines to introduce a small number of polar side chains to the PMMA block.[308] (Fig.31) These slight modifications led to a remarkable increase in χ value that allowed nanostructures with L_0=11.1nm in bulk, simply by treating the commercially available PS-*b*-PMMA with the appropriate amines. Specifically, this novel type of materials exhibited χ_{eff}=0.193, which is 5 times higher than the PS-*b*-PMMA precursor. Fingerprint patterns were produced without extensive optimization of the underlayer in thin films. Graphoepitaxy DSA was, also, tested to guide the self-assembly.

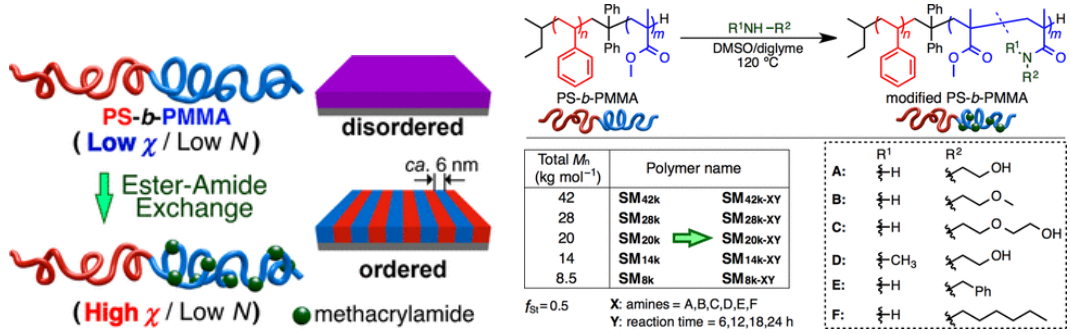

Fig.31. (Left) Schematic illustration of increased incompatibility of PS-*b*-PMMA after ester-amide exchange reactions with amines. (Right) Ester−Amide Exchange Reaction of PS-*b*-PMMA with Various Amines.[308]

In a similar manner, PSVN-*b*-PMMA [PSVN= Poly(styrene-*random*-vinylnapthalene)] is a copolymer that exhibits a double value of χ value compared to PS-b-PMMA when 29%

vinylnapthalene is included, due to intermolecular self-interactions of PSVN, with even 6.3 nm features being fabricated and perpendicular orientation preserving.[309]

4.2.5 Fluorine-Containing High χ Diblock Copolymers Thin Films

It has already been mentioned that segments with disparate polarities or hydrophilic/hydrophobic interactions can enhance immiscibility. Fluorine-containing blocks are strongly immiscible with both polar and non-polar blocks and have been utilized to produce strongly segregating block copolymers as early as more than 20 years ago. [310-313]

Recently, however, their utilization in high χ low N thin film related studies has attracted significant interest and as such this class of materials is discussed here separately. An even more intriguing factor is that fluorine-containing polymers due to lower coefficients of friction, demonstrate extremely enhanced self-assembly kinetics.

The remarkable example of PMAPOSS-*b*-PTFEMA (χ=0.45, 150 ^{o}C) which exhibits high etch-selectivity, strong immiscibility as well as balanced surface energies in thin films has been described previously.[296] One of the first recent studies regarding fluorine-containing high χ copolymers was that of Maeda et al, employing PS-*b*-PTFEMA and PS-*b*-(PTFEMA-*co*-PMMA).[314] Although χ was not experimentally calculated, from solubility parameters it was estimated that the value was rather high. PTFEMA was, also, easily degradable under E-beam, deep-UV and X-rays providing etch-contrast between the segments and allowing even for dots-in-lines patterns.

Ryu et al. reported that fluorine containing BCPs exhibiting high χ, namely PS-*b*-PTFEA diblock copolymers can be produced, after transesterification of the acrylate segments on the PS-*b*-PtBA The difference in the surface energy between the segments, required the use of top-coat surfaces to favor the perpendicular orientation of the domains, while electric field alignment was feasible due to the high dielectric contrast between the segments. The aforementioned materials exhibited a high χ value (χ=0.23, 170 ^{o}C) with L_0=10.1nm in bulk, while authors predicted even smaller achievable dimensions with lower MW. [315] Thin film studies utilizing neutral mats and top coats yielded normal to the substrate 7.9 nm lamellae, aligned by electric field DSA. The process was very rapid due to fast diffusion of the short PS-*b*-PTFEA chains and large dielectric contrast.[316]

Living anionic polymerization was utilized to prepare a PS-*b*-PGMA diblock copolymer which was post-functionalized with thiol groups leading to PS-*b*-PHFMA, another high χ copolymer (χ=0.17, 150 ^{o}C) that has been used to fabricate sub-10nm full-pitch lamellae.[317] Apart from enhanced immiscibility these two blocks exhibit balanced surface affinities in the thin film state. The mechanism behind is described as follows: the hydrophobic fluorine affinity control unit, present in the PHFMA repeat units, tunes the affinity towards the free surface while enhancing the immiscibility between the two blocks. Perpendicular lamellae have been fabricated on neutral substrates simply by thermal annealing at 120 ^{o}C for just 10 min.

In a similar study by Cummins and coworkers, PS-*b*-P2FEMA BCPs were synthesized *via* RAFT polymerization and showcased high Flory-Huggins interaction parameter (χ=0.13, 150^{o}C). These materials were used to realize 14.2 nm full-pitch vertically oriented lamellar and cylindrical nanopatterns in only 1 min by solvothermal annealing (STVA).[252] Aluminum nanowires were farther produced by sequential infiltration synthesis (SIS). It was shown that by incorporating one fluorine atom per repeat unit, χ parameter is extremely increased compared to PS-*b*-PMMA. Important was, also, the fact that comprising just one fluorine atom per repeat unit, did not strongly reduce the surface free energy, allowing thus for vertical orientation (after STVA) without the presence of a thin top wetting layer of the lower surface

energy block, as often happens for PDMS containing or perfluoroalkyl containing BCPs, that require an additional trim etching step.

A different type of fluorinated BCPs, namely PS-*b*-PPDFMA was synthesized through anionic polymerization leading to well-defined periodicities as directly visualized by TEM and SAXS studies. It is worth mentioning, that for the specific polymeric materials the notable difference in the surface energy between the constituted blocks, render the perpendicular alignment difficult without using a top-coat or other surface manipulations. The inherent properties of the fluorinated blocks, to exhibit high mobility and low coefficients of friction may ease the formation of well-defined topologies. The copolymer exhibited χ=0.353 at 150 ^{o}C resulting in 8.3 nm full-pitch lamellae in bulk, in just one minute of thermal annealing at a moderate temperature (80^{o}C) allowed by the low T_g of both segments.[318] Grapho-epitaxial DSA was employed to align parallel oriented cylinders in thin films, leading to 8 nm structures. Importantly, comparative experiments with PS-*b*-PHFBMA (a block with less fluorine atoms) led to worse self-assembly kinetics, strongly implying that the length of the fluorinated side group plays a significant role in fast ordering. This, in conjunction with the fact that more fluorine atoms lead to more disparate surface energies in the copolymers, is another proof of how important finding the gold balances in material design of high-χ copolymers is. Furthermore, comparative studies of self-assembly kinetics of the low T_g BCPs, PS-*b*-PPDFMA and PS-*b*-PDMS, led to the conclusion that utilizing a $T_{annealing}$ slightly above T_g does not necessarily suffice for fast ordering kinetics. Another fluorine-containing BCP is PPDFMA-*b*-PHS that was synthesized via RAFT polymerization and the subsequent deprotection of the PTMPOSS block, led to strong repelling force between the fluoro- and hydroxyl- groups, thus, enhanced χ values equal to 0.49 were evident. The ability to rapidly self-assemble at sub-5nm domain spacing renders the specific materials as quite promising for nanolithographic applications [319]

Another high χ copolymer comprising PPDFMA, is P2VP-*b*-PPDFMA (χ=0.387, 150 ^{o}C) with 9.7 nm full-pitch lamellar domains attained, while P2VP-*b*-PHFBMA, also exhibits a high χ value (0.347, 150 ^{o}C) with 8.3 nm full-pitch lamellar domains.[320] For reference, PS-P2VP has a χ value equal to 0.083 at same temperature meaning 4 times lower than both of the above-mentioned sequences. Thin film studies with graphoepitaxial self-assembly led to aligned, 8 nm wide, line/space patterns from parallel cylinders, while P2VP selectively complexed with metallocene to induce etch-resistance or create metallic nanopatterns.
Other fluorine containing high-χ block copolymers include DNPEPEO-*b*-PFMA,[321] PPDFMA-*b*-P6AzOMe, PHFBMA-*b*-P10AzC_5H_{11} and PPDFMA-*b*-P10AzC_5H_{11}, [322,323] as well as the block cooligomer F_{13}-*b*-PAA [324]. Overall, we can see that fluorine-containing copolymers can induce a higher immiscibility with both hydrophobic and hydrophilic segments, while fast ordering kinetics can be induced by rapid chain interdiffusion of low-N chains and low coefficient of friction of materials. Undoubtedly, we will see more fluorinated copolymers in the future high χ low N studies.

4.2.6. Increasing Effective χ Parameter

Design of BCPs with strong inherent incompatibility among the blocks, has made a lot of progress, especially in the last decade. Several ways to increase incompatibility, by incorporation of fluorine atoms, *tert*-butyl groups, hydroxyl containing blocks, etc, have already been discussed. But there are, also, some studies reporting increased effective incompatibility (χ_{eff}) without altering the main constituents of the BCP. A brief description of some of these examples follows in order to provide a more global perspective on the fabrication of sub-10nm features. The effect of macromolecular architecture on segregation strength will,

also, be discussed in a following section. To avoid the use of reagents that require demanding manipulations and time-consuming synthesis procedures, post polymerization chemical modification reactions to copolymers with facile synthetic protocols is preferred.

A synthetic approach, in which a common PMA-*b*-PtBS system was chemically modified with a $LiAlH_4$ reagent, resulted in a novel copolymer namely PPOH-*b*-PtBS. The high χ value (~0.3) of the modified material is expected to be critical to reach very low dimensions. Employing the same chemical procedure PMMA-*b*-PS and PMA-*b*-PS were chemically modified, resulting in PiBOH-*b*-PS and PPOH-*b*-PS, respectively. The increased χ values at (~0.3) after the organic transformation of the commonly used PMMA or PMA blocks, are attributed to the enhanced polarity of the hydroxyl side-groups on the former acrylic segments, as well as hydrogen bonding interactions. The above-mentioned research indicates alternative methodologies of obtaining high χ using commonly utilized monomers such as PMMA or PMA without changing drastically the dispersity indices but leading to promising results regarding the minimization of the domain spacing [325].

PDMS-*b*-PEO, as previously mentioned is a high χ system. Additionally, blends of the BCP with LTA ((l)-tartaric acid) result in significantly increased χ_{eff} (~80-120%) and suppressed crystallization of PEO. The χ value was estimated in a range between ~0.36-0.43 depending on the LTA binding sites as well as the PEO volume fraction. The increased effective χ parameter in PDMS-*b*-PEO/ LTA blends, where LTA selectively binds with PEO through hydrogen bonding, while LTA helps suppress PEO crystallinity. χ_{eff} was predicted to be higher due to the repulsive interaction between bound LTA and PDMS block, suggesting PEO/LTA is more polar than PEO[286]. (Fig.32)

PS-*b*-PEO co-assembled with domain selective organosilicate, also demonstrated, apart from etch-contrast, increased segregation strength, since short BCP chains, otherwise disordered, exhibited self-assembled, ordered ultra-small nanostructures. [326]

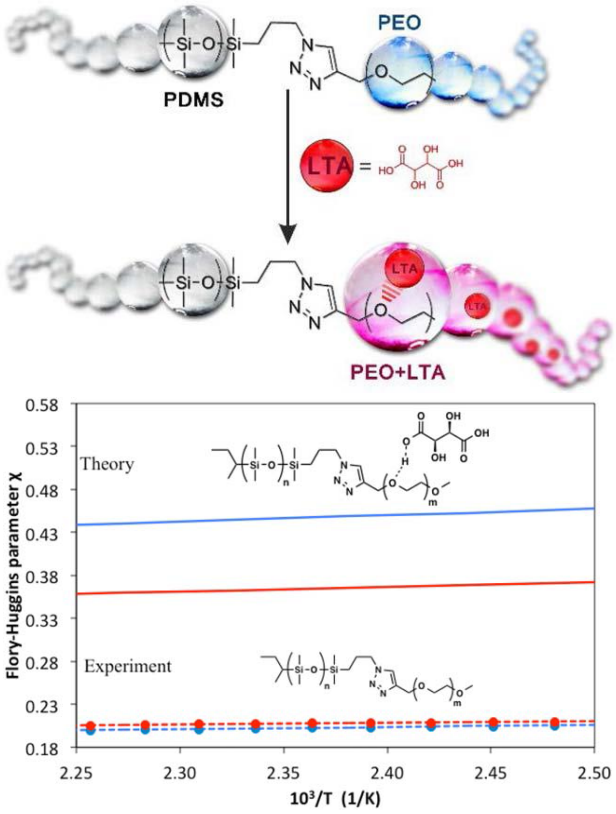

Fig.32. (Left) Schematic illustration of the PDMS-*b*-PEO (DO) block copolymer structure and the corresponding bead-spring model. A (gray), B (blue), C (red), and D (purple) circles stand for beads representing coarse-grained monomers of PDMS, PEO, (L)-tartaric acid, and PEO-tartaric acid complex, respectively. The reversible reaction of hydrogen bond is described B+C ↔C. (Right) The Flory–Huggins parameter, χ, as a function of the temperature. The experimentally measured v of PDMS-*b*-PEO from two samples $D_{1.1}O_{2.1}$ (blue) and $D_{1.1}O_{1.9}$ (red) are plotted as dashed lines with data points (lower pair) and the derived χ of PDMS-*b*-(PEO/LTA) by RPA are plotted as solid lines (upper pair). The derived χ from the higher volume fraction of PEO ($D_{1.1}O_{2.1}$) increases from the original χ of PDMS-*b*-PEO more than the smaller volume fraction of PEO ($D_{1.1}O_{1.9}$).[286]

Smaller nanofeatures, higher χ_{eff}, as well as smaller interfacial width have been reported for PS-*b*-PMMA copolymers blended with an homopolymer selectively interacting with PMMA. Several other studies, regarding the strong effect in phase separation of a BCP when blended with H-bonding homopolymers or BCPs have been reported in literature.

Selective swelling with solvent molecules during solvent annealing can, also, sometimes lead to higher χ values and ordering in otherwise disordered BCPs. Selective swelling of a block domain can lead to higher immiscibility as well as different effective volume fractions and morphological transitions. Mixtures of solvents that are both selective for different domains can lead to retaining effective volume fraction while increasing $\chi_{eff.}$ (Fig) [309,327-329]

Metal complexing in one block is another strategy to increase χ_{eff}. In a milestone study by Park et al., Au salt-complexed PS-*b*-PEO was utilized to attain down to 3 nm features with excellent lateral order through a sawtooth faceted sapphire substrate. The features observed, with an areal density up to 10.5Tb/in^2, are among the smallest achieved by BCP self-assembly.[190]

Ghosal et al., have increased the χ_{eff} of PS-b-PEO through the incorporation of lithium salt, allowing for 8 nm wide line/space patterns and after appropriate treatment iron oxide arrays were used for pattern transfer. Ordered domains were observed even at χN=7.71 due to the fact that the effective segregation strength (and T_{ODT} accordingly) has increased through the selective complexion of Li^+ ions with PEO.[249]

Other studies with salt-doped PS-*b*-PEO, also, demonstrate the increase in χ_{eff}, and morphological transitions. Similar effects apply for PS-*b*-P2VP or PS-*b*-P4VP. For example, Sun and coworkers, fabricated sub-15 nm line/space patterns from low MW copper chloride-doped P2VP-*b*-PS-*b*-P2VP that after infiltration of Pt salts and topographical guiding patterns allowed for well-aligned ultra-narrow Pt nanowires. [330,331]

Different studies, suggest that introduction of appropriate ionic liquid (IL) additives can increase segregation strength in a number of block copolymers. Incorporation of ILs impacts χ_{eff}, as well as the topology of the phase diagram and scaling of nanodomains.[332]

Blends of PS-*b*-PMMA and ILs like ([BMPR][TFSI]), ([EMIM][TFSI]) or ([HMIM][PF_6]) led to increased segregation strength, while chemical epitaxy was, also, employed requiring similar procedures as the BCP lithography workhorse, PS-*b*-PMMA. 16.5 nm full-pitch lamellar structures were observed in the thin film state. [333]

Ionic liquid (IL) additive, HMHF, was introduced to PS-*b*-PMMA resulting in selective distribution of the IL to the PMMA segment and providing for enhanced phase separation (χ_{eff}^+~0.45) depending on MW. (Fig.33) Sub-10nm features were obtained, while perpendicular orientation was preserved. Ionic liquid additives are believed to be better than inorganic salts for BCP lithography for a number of reasons like lower melting point or improved thermal stability.[334]

Another, already mentioned, example for increasing segregation strength is that of PDMS-*b*-PEO and PDMS-*b*-PMMA where the incorporation of ionic junctions between the blocks led to significantly increased T_{ODT} and reduced LER, due to the electrostatic interactions.[287]

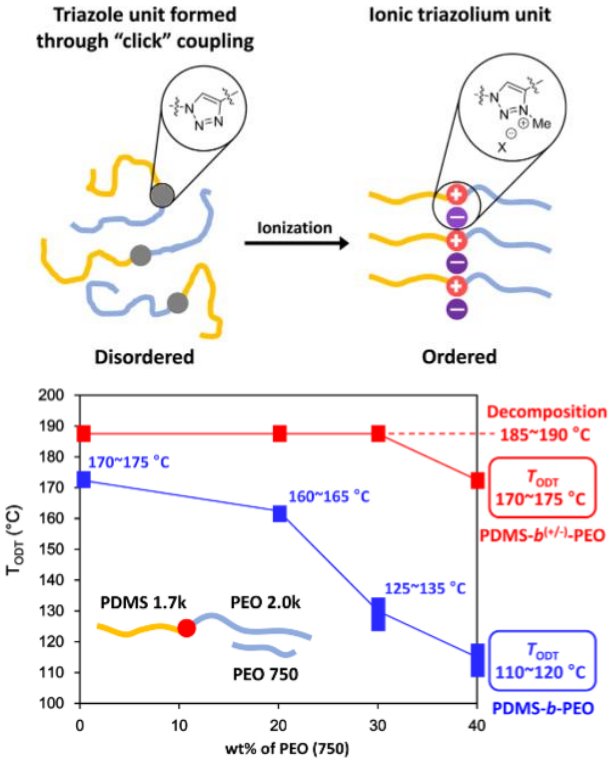

Fig.33. (Up) Graphical Representation of Enhanced Segregation Behavior for Block Copolymers through Ordering of Ionic 1,2,3-Triazolium Units Present at the Block Junctions (Down) Order−disorder transition temperatures for blends of PDMS-*b*-PEO (in blue) or PDMS-*b*(±)-PEO (in red) with varying weight percentages of PEO oligomer (Mn = 750 g/mol, Mw/Mn = 1.10)[287]

But this was not the only recent example of increased segregation strength induced simply by careful chemical tuning near the junction point. Inserting a small highly polar self-attracting PMAA middle block between PS and PMMA segments, improves phase separation while maintaining vertical orientation.[335] The improved phase separation behavior is largely imparted by the strong repulsion between PS and PMAA. As small as 16.2nm domain spacing was achieved in thin film state.

Lastly, PS-*b*-PMMA comprising hydrogen bonding U groups (Urea) along with rigid-rod groups (N-(4-amino-methyl-benzyl)-4-hydroxymethyl-benzamide, BA) at the junction point led even to 25% decrease in LER that authors attributed to a larger χ_{eff} through the lateral stacking of U-BA.[336] Importantly, the incorporation of these groups did not hinder perpendicular orientation of PS-*b*-PMMA on neutral layer. Graphoepitaxial DSA was conducted for alignment of vertical lamellae(Fig.34).

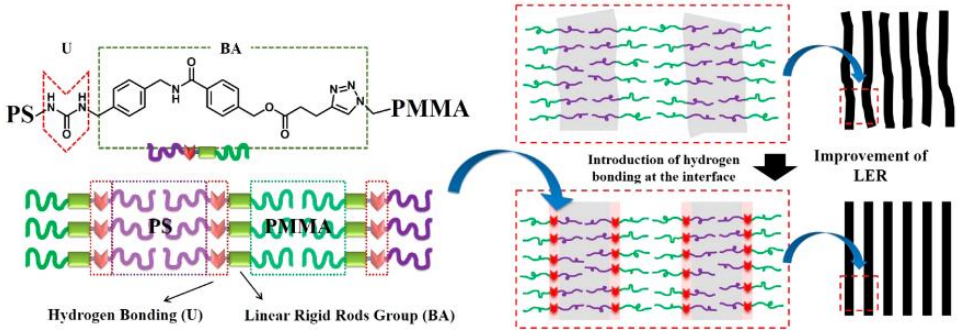

Fig.34. Chemical structure of PS-U-BA-PMMA and schematic showing sharper interface (and thus reducing LER) due to hydrogen bonding (U) and rigid rod (BA) moieties located at the junction of PS

and PMMA chains. Upper and lower right panels represent PS nanodomains prepared by neat PS−PMMA without U and BA moieties, and PS-U-BA-PMMA, respectively.[336]

4.2.7.Block Copolymers with Balanced Surface Energies

Increased segregation strength to achieve ultra-small nanodomains is of course of high importance. However, block copolymers that can self-assemble into perpendicular nanodomains via thermal annealing without the need of complicated procedures, also, appear alluring for nanopatterning applications. In high χ copolymers, however, the difference in polarity between the blocks often leads to disparate surface affinities and parallel orientation. PS-*b*-PMMA is known to exhibit perpendicularly oriented structures under thermal annealing when a neutral layer is applied, but as already mentioned the low χ value limits the critical dimensions to ~11 nm. However, BCPs with higher χ values that can easily orient perpendicularly to the substrate by thermal annealing means, exist too.

A well-studied block copolymer, with a χ value around twice that of PS-*b*-PMMA is PS-*b*-PLA that exhibits balanced surface free energies, while PLA can easily be selectively removed. Another BCP with equal block surface energies is partially epoxidized PS-PI. [337-340]

The etching selectivity in both wet and dry processes offered by polycarbonates, in addition to the facile synthetic methods, as well as easy tuning of χ and surface energies, have enabled aliphatic polycarbonates as potential candidates for their use in DSA and in pattern transfer, generally, since they are compatible with already developed methods. Specifically, a polycarbonate based BCP of the PS-*b*-PPC type was synthesized through in-situ chain transfer polymerization, using cost-effective raw materials such as CO_2 and propylene oxide and after using the SCMF, χ parameter was estimated (χ=0.079, 150 ^{o}C). The system has been used to fabricate 14.5 nm full-pitch lamellar structures in bulk, and also, exhibits balanced interfacial affinities at free surface and substrate, when a neutral bottom layer is applied, leading to perpendicular orientation in thin films(Fig.35).[254] DSA through chemical epitaxy with a 5x density multiplication factor was, also, studied yielding sub-10nm structures with long-range order. Importantly, carbonate-based blocks are sensitive to UV radiation, while amenable to metal complexation. Both properties allow for selective etching or hard mask fabrication and pattern transfer. This was, also, the case for PS-*b*-PPC, which after SIS yielded AlO_x nanowires and subsequent pattern transfer of sub-10nm lamellar motifs was successful.

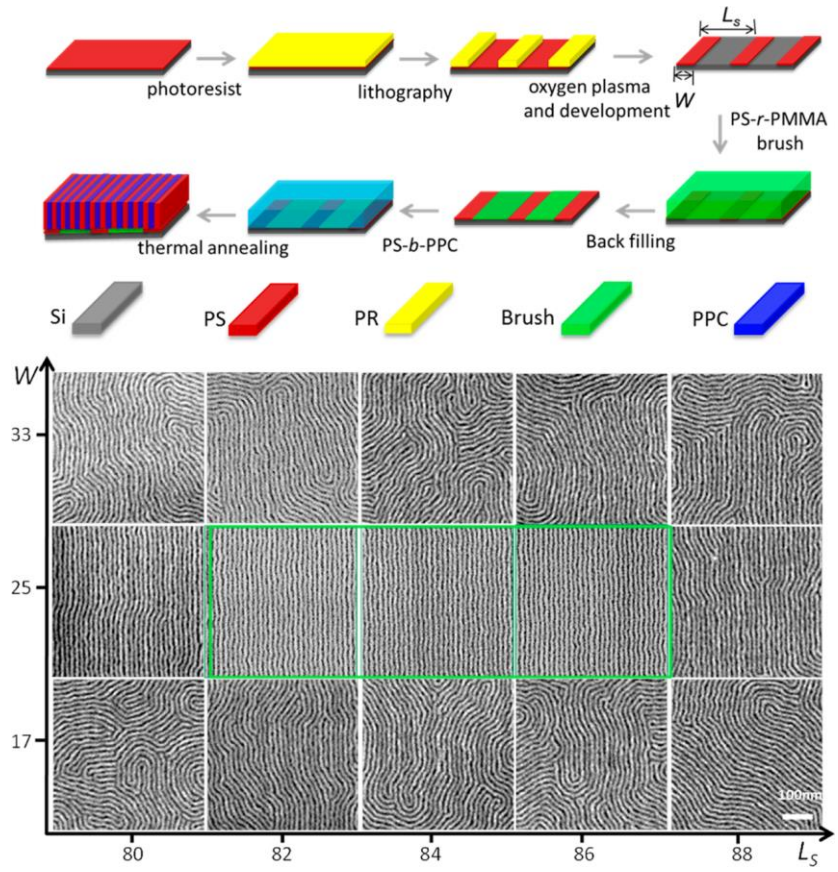

Fig.35. Schematic illustration of the procedure used to create prepatterned substrates and the DSA of lamellae forming PS-*b*-PPC system with 5 times density multiplication under thermal annealing and the top-down SEM images showing DSA results of SC (15.6, 0.47) films (17 nm in thickness) assembled on chemical patterns at Ls = 80, 82, 84, 86, and 88 nm (horizontal axis) with different PS guiding stripe widths (vertical axis). The scale bar in the image at bottom right applies to all images.[254]

A notable polycarbonate-based high χ BCP, PS-*b*-PMTC-Me was synthesized by organocatalytic ring opening polymerization followed by the addition of a surface active polymer containing hexafluoroalcohol groups that tune the orientation. The system (χ~0.19) was designed to induce perpendicular nanodomains using an optimal additive amount by preferentially interacting with only one of the segments. As a result, the PC segments were selectively etched with RIE giving rise to a 9.5 nm wide PS domain for subsequent pattern transfer (Fig.36) [191]. These materials are promising candidates for semi-conductor nodes due to their susceptibility in common lithographic techniques.

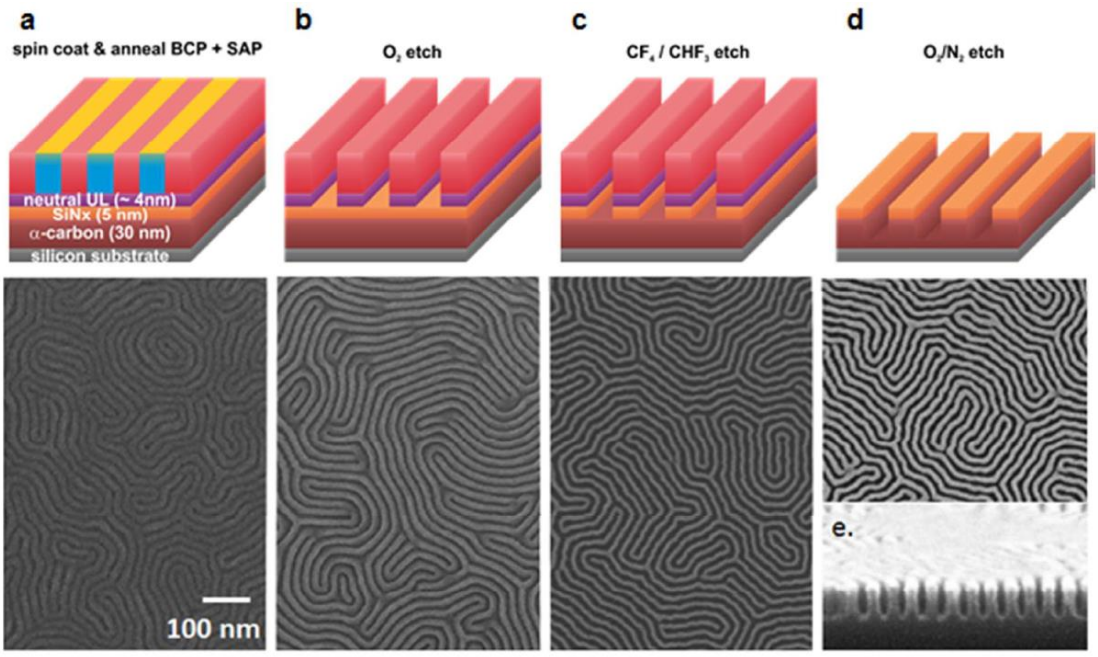

Fig.36. Etching and Pattern Transfer: Schematics and SEM images of a thin film of PS-*b*-PMTC-Me BCP with SAP additive on silicon wafer with a tri-layer stack of amorphous carbon, silicon nitride, and neutral under layer (a) after thermal annealing, (b) after O_2 etch to remove PMTC-Me block, (c) after CF_4/CHF_3 etch to remove silicon nitride, and (d) O_2/N_2 etch to remove organic hardmask. SEM cross-section after final etch is shown in (e).[191]

Smaller feature sizes can be realized using a highly segregated PS-*b*-PLA system that has a high Flory Huggins interaction parameter $\chi \sim 0.22$ [341]. Several studies have been conducted using different methods of controlling the alignment of the microphase separated domains. In addition, PLA domains can be easily etched producing nanoporous arrays [342]. Chiral BCPs of the PS-*b*-PLLA type [343], (attributed to chiral nature of the polyester) exhibit higher χ value (~ 0.19) at 110 ºC comparing to PS-*b*-PLA (~ 0.14) due to the longer persistence length of the PLLA segments. Furthermore, PS-*b*-PDLA system exhibits high χ values approximately ~ 0.23 leading to small domain spacing and also presents thermal stability, solubility in common solvents and high etching selectivity [344]. Almost identical surface energies in both room and elevated temperatures, combined with the high χ values equal to approximately ~0.38, render [345] the PS-*b*-PLGA (Poly(styrene-*b*-(lactic acid-*alt*-glycolic acid)) a better-suited system for lithographic applications instead of the conventionally deployed PS-PLA.[345] The χ value of PS-*b*-PLGA (χ=0.155, 150 ºC) is double that of PS-*b*-PLA (χ=0.077, 150 ºC), without compromising the interfacial energies. One less methyl group per monomeric unit as compared to PLA accounts for the increased hydrophilicity of the PLGA block. The applicability of the system in chemical epitaxy DSA was also confirmed leading to aligned lamellae with long-range order, perpendicular orientation and a 2x density multiplication factor. (Fig. 37)

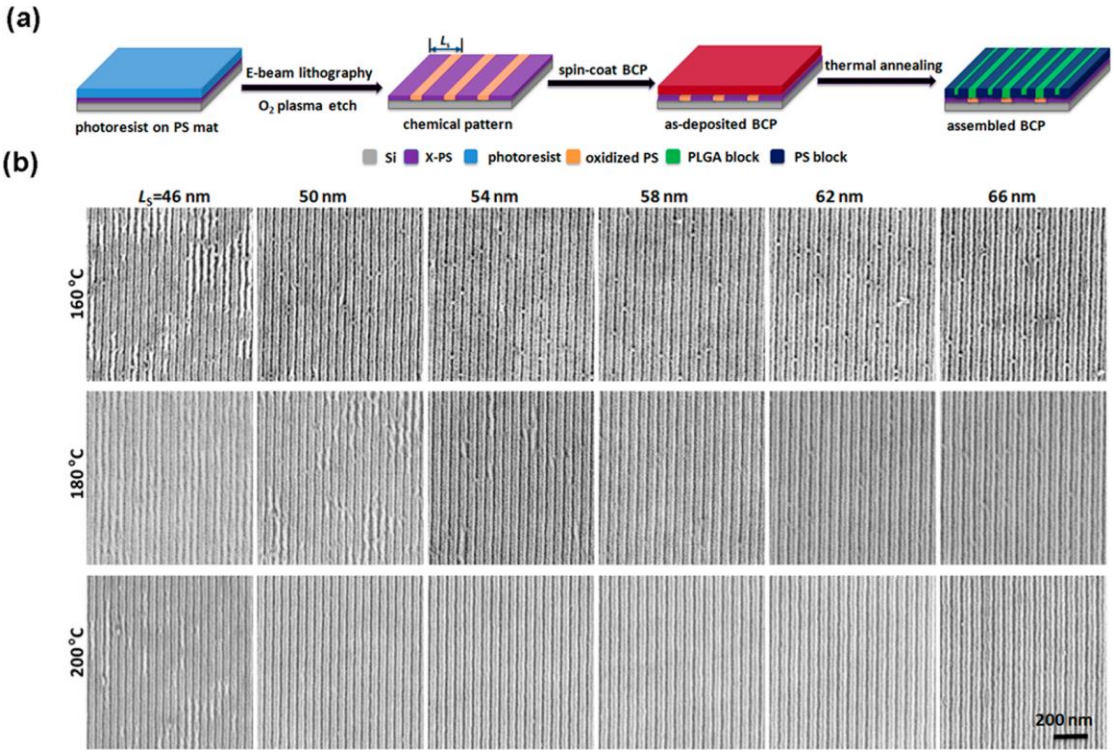

Fig.37. (a) Schematic illustration of the procedure used to create asymmetric chemical patterns and DSA of lamellae-forming PS-*b*-PLGA with 2×density multiplication under thermal annealing. (b) Top-down SEM images of SLG (9.5−13.2) films (30 nm in thickness) assembled on chemical patterns with LS = 46−66 nm under 160, 180, and 200 °C annealing.[345]

Methyl acrylate block copolymers of the PS-*b*-PMA type showcase similar properties with the PS-*b*-PMMA, regarding the etch resistance under O_2 plasma etching and susceptibility to UV treatment as well the almost equal surface energies among the two segments. [253]. In PS-*b*-PMA again a single methyl group was critical for increasing immiscibility ($\chi_{PS\text{-}PMA}$=0.068, $\chi_{PS\text{-}PMMA}$=0.029, 150 °C), while maintaining balanced interfacial energies. The χ value does not classify it into the high χ BCPs, however, ultrasmall nanodomains were obtained by PS-*b*-PMA and PMA-*b*-PS-*b*-PMA, while chemoepitaxy DSA with density multiplication led to sub-8.5nm aligned line/space patterns that after SIS allowed for pattern transfer (Fig.38). [253]

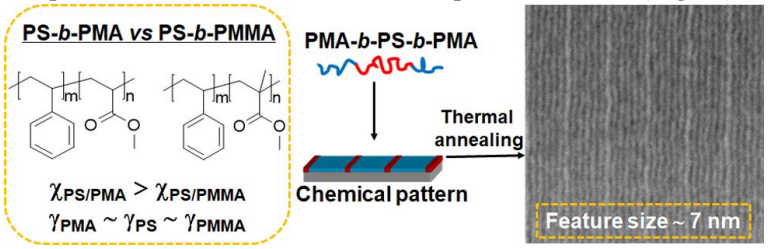

Fig.38. Graphical abstract from ref.[253]

Furthermore, PMAPOSS-*b*-PTFEMA, is an ultra-high χ copolymer that leads to perpendicular domains even without modified substrate as already mentioned above.[296] Designing BCP systems with appropriate surface affinity control side-groups has been examined in other self-assembly related works, too. The case of PS-*b*-PHFMA where the fluorinated side group mitigates the surface energy difference while enhancing incompatibility, has already been mentioned.[317] In another example, the polysiloxane block of a PS-*b*-PDMS alike BCP, PS-*b*-PMVS, was functionalized with hexanol groups.[346] The hydroxyl side groups prevented

preferential wetting of the air interface by the more hydrophobic polysiloxane block, while, both the main chain and the hydroxyl side groups of this block were incompatible with PS. Normal to the substrate 8.5 nm line/space patterns were produced simply by thermal annealing on a non-Si-containing neutral layer for just one minute under appropriate conditions, while the polysiloxane block facilitated etch resistance.

Table

BCP system	χ (25 °C)/ estimation method	Inherent Properties	How low can we go? (nm)		Reference
			Bulk	Thin films	
PS-*b*-PLA	0.22/SAXS	Chemical incompatibility, facile etching Feasible sub-10nm domain spacing	~34.0	~18.0	341,342
PS-*b*-PLLA	0.19 (T=110°C)/SAXS	Chemical incompatibility, facile etching Feasible sub-10nm domain spacing	-	~26.0	343, 347
PS-*b*-PDLA	0.23/SAXS	Chemical incompatibility, thermal stability, high etch selectivity, solubility in common solvents Feasible sub-10nm domain spacing	~15.5	~8.0/widths	344
PS-*b*-PLGA	0.38/SAXS	Chemical incompatibility, identical surface energy in wide temperature range Feasible sub-10nm domain spacing	~15.5	~46.0	345
PCHE-*b*-PMMA	0.32/DMA	Chemical incompatibility, high etch selectivity, high T_g, high T_d Feasible sub-10nm domain spacing	~9.0	~7.5/half pitch	303
PCHE-*b*-PLA	0.45/DMA	Chemical incompatibility, high etch selectivity, high T_g, high T_d Feasible sub-10nm domain spacing	~20.0 center to center cyl	~6	208
PCHE-*b*-PEO	0.41/DMA	Chemical incompatibility, high etch selectivity, high T_g, high T_d Feasible sub-10nm domain spacing	~15	~6	250
PtBS-*b*-PMMA	0.09/DMS-SAXS	Chemical incompatibility, high T_g Possible sub-10nm domain spacing	~14	-	301
PtBS-*b*-P2VP	~0.27/DSC-SAXS	Chemical incompatibility, Solvent/Thermal annealing, high T_{ODT} Feasible sub-10nm domain spacing	~9.6	-	297
PPOH-*b*-PtBS	0.3/SAXS	BCPs originated from readily available low-cost monomers, chemical incompatibility Feasible sub-10nm domain spacing	~6.5	-	325
PiBOH-*b*-PS	0.3/SAXS	BCPs originated from readily available low-cost monomers, chemical incompatibility Feasible sub-10nm domain spacing	~7.2	-	325
PPOH-*b*-PS	0.3/SAXS	BCPs originated from readily available low-cost monomers, chemical incompatibility Feasible sub-10nm domain spacing	~7.3	-	325
PS-*b*-PPC	0.2/rheology	Chemical incompatibility, high etch selectivity, use of inexpensive raw materials, identical surface energy in wide temperature range Possible sub-10nm domain spacing	~14.5	~10	254
PS-*b*-PTMC	not specified	Chemical incompatibility, easily processed Possible sub-10nm domain spacing	-	~16.4	348-350
PS-*b*-PTMC-Me	0.19/MFT	Chemical incompatibility, high etch selectivity Possible sub-10nm domain spacing	-	~19.0 full pitch	191
PGM-*b*-PS	0.438/SAXS	Chemical incompatibility, single solvent casting to sub-3nm domain spacing	~5.4	~9.4/full pitch	304,305

		Feasible sub-10nm domain spacing			
PS-*b*-PGA	0.56/SAXS	Chemical incompatibility, high etch selectivity Feasible sub-10nm domain spacing	~7.4	-	306
PS-*b*-PAA	0.88/SAXS	Chemical incompatibility, high etch selectivity Feasible sub-10nm domain spacing	~6.9	-	306
PS-*b*-PTFEA	0.26/SAXS	Chemical incompatibility, high etch selectivity, high dielectric contrast, perpendicular orientation using top-coats Feasible sub-10nm domain spacing	~10.1	~7.9	315,316
PS-*b*-PPDFMA	0.43/SAXS	Chemical incompatibility, high etch selectivity, perpendicular orientation using top-coats, high mobility, low coefficients of friction, rapid self-assembly Feasible sub-10nm domain spacing	~8.7	~5.0	318
PS-*b*-P2FEMA	0.13/SAXS	Chemical incompatibility, high etch selectivity, perpendicular orientation using top-coats, high mobility, low coefficients of friction, rapid self-assembly Feasible sub-10nm domain spacing	~7.3	~11	252
PS-*b*-PHFMA	0.191/SAXS	Chemical incompatibility, perpendicular orientation, similar surface tensions Feasible sub-10nm domain spacing	~9.6	-	317
PPDFMA-*b*-PHS	0.49/SAXS	Chemical incompatibility, high etch selectivity, perpendicular orientation using top-coats, high mobility, low coefficients of friction, rapid self-assembly Feasible sub-10nm domain spacing	~9.8	-	319
P2VP-*b*-PPDFMA	0.43/SAXS	Chemical incompatibility, high etch selectivity, rapid self-assembly Feasible sub-10nm domain spacing	~9.7	~8.0	320
P2VP-*b*-PHFBMA	0.35/SAXS	Chemical incompatibility, high etch selectivity, rapid self-assembly, enhanced χ values at elevated temperatures Feasible sub-10nm domain spacing	~8.3	~8.0	320
PS-*b*-PMA	0.16/rheology	Chemical incompatibility, high etch selectivity, identical surface energies, perpendicular orientation under thermal treatment Feasible sub-10nm domain spacing	~14.6	~13.9	253
PS-*b*-PMAA	0.55/SAXS	Chemical incompatibility, high etch selectivity, perpendicular orientation using top coat Feasible sub-10nm domain spacing	~11.7	~4.0 pore size	307
PHS-*b*-PS	0.12/SAXS	Chemical incompatibility, potential dynamic tuning of the bulk and thin films self-assembled structures Feasible sub-10nm domain spacing	~11.8	-	331
PDHS-*b*-PS	0.9/SAXS	Chemical incompatibility, high etch selectivity Feasible sub-10nm domain spacing	~5.9	~8.8	298
PS-*b*-PDMS	0.27/ODT	Chemical incompatibility, high etch selectivity, multiple self-assembled strategies for perpendicular orientation Feasible sub-10nm domain spacing	~13.5	~8.0	168,207, 241,278,279,351
P4VP-*b*-PDMS	not specified	Chemical incompatibility, high etch selectivity, rapid kinetic facilitation using environmental-friendly solvent Feasible sub-10nm domain spacing	-	-	228
P2VP-*b*-PDMS	not specified	Chemical incompatibility, high etch selectivity, pattern tunability exploiting various solvents	-	~6.0 line width	280

		Feasible sub-10nm domain spacing			
PDMS-*b*-PLA	1.4/domain spacing	High chemical incompatibility, high etch selectivity, inexpensive materials Feasible sub-10nm domain spacing	~14.4	~13.0 diameter cyl	281,282
PDMS-*b*-PMMA	0.23/SAXS	Chemical incompatibility, high etch selectivity, high χ values at elevated temperatures, exogenous processes due to dissimilar surface energies Feasible sub-10nm domain spacing	~8.7	~12.1/full pitch	285
P3HS-*b*-PDMS	0.42/SAXS	Chemical incompatibility, high etch selectivity, enhanced χ value at elevated temperatures Feasible sub-10nm domain spacing	~7.4	-	346
PDMS-*b*-PEO	0.22/SAXS	Chemical incompatibility, high etch selectivity, chemical modification ability, enhanced χ at high temperatures Feasible sub-10nm domain spacing	~7.9	-	286
PDMS-*b*-PEO/LTA	0.36-0.43/SAXS	Chemical incompatibility, high etch selectivity Feasible sub-10nm domain spacing	-	-	286
PMMA-*b*-PMAPOSS	0.146 (T=150^{o}C)	Chemical incompatibility, high etch selectivity orientation control via solvent vapor annealing, Possible Possible sub-10nm domain spacing	~20.0	~14.9	294,296,352-354
PS-*b*-PMAPOSS	0.14 (T=150^{o}C)	Chemical incompatibility, high etch selectivity, perpendicular orientation via solvent annealing, Possible sub-10nm domain spacing	~38.0	~37.0	294
PMAPOSS-*b*-PTFEMA	0.47/SAXS	Chemical incompatibility, high etch selectivity, similar surface energies, ability to be oriented without requiring post-synthetic functionalization, cost-effective Feasible sub-10nm domain spacing	~11.0	~11.0 Lo	296
PTMSS-*b*-PLA	0.46/SAXS	Chemical incompatibility, high etch selectivity, high T_g, enhanced χ at elevated temperatures, orientation control via solvent vapor annealing Feasible sub-10nm domain spacing	~12.1	~9.0 half pitch	174,291
MH-*b*-PTMSS	not specified	Chemical incompatibility, high etch selectivity, orientation control via solvent vapor annealing Feasible sub-10nm domain spacing	~8.3	~5.0	289
PMOST-*b*-PTMSS	0.047 (T=150 ^{o}C)/SAXS	Can be submitted to various DSA methods, high etch selectivity, orientation using top-coat, fast thermal annealing Possible sub-10nm domain spacing	-	~14.4	200,355,356
PVBD-*b*-PDSS	0.25 (T=180^{o}C)/SAXS	Chemical incompatibility, high etch selectivity, orientation using top-coat, fast thermal annealing Feasible sub-10nm domain spacing	-	~10.0	355
PS-*b*-PDSS	0.11 (T=180^{o}C)/SAXS	Chemical incompatibility, high etch selectivity, orientation using top-coat, fast thermal annealing Feasible sub-10nm domain spacing	-	~12.0	355

5. Beyond Block Copolymers

In the previous sections, the self-assembly process of block copolymers in bulk and thin films was described in detail. Several applications in nanopatterning along with the respective obstacles were mentioned. The effect of molecular architecture in diblock copolymers, as well as the complexity induced by the introduction of a third block was, also, discussed. It was clear that to obtain high-fidelity nanopatterns one has to use high-χ copolymers, while other methods of increasing segregation strength appear appealing. An issue, however, that has not been studied thoroughly is the utilization of high χ copolymers of complex architecture for

nanopatterning. While there is evidence that macromolecular architecture provides an extra tool for tuning block copolymer self-assembly and feature sizes, the synthetic challenges restrain experimental studies. In recent years, though, synthesis of BCPs with complex macromolecular architecture has advanced a lot. In this section, some examples of regarding works will be discussed.

5.1. Linear High χ Triblock Copolymers (ABA)

Linear triblock copolymers constitute a versatile class of materials, usually accessed by facile synthetic techniques. Their microphase separation can be different than in A-*b*-B diblock copolymers in many ways. In linear A-*b*-B-*b*-A triblock copolymers, the phase boundaries appear asymmetrical in the WSL. [80] This asymmetry is imparted by the higher difficulty to confine two A blocks in a domain, in comparison to a single B block, due to the fact that if B constitutes the matrix, then it has to deform more (and face more entropic constraints) to confine the two A end blocks in A domains.

In the SSL, Helfand and Wasserman predicted similar phase behavior for triblock and diblock copolymers, while, the nanodomains of A-*b*-B-*b*-A and A-*b*-B (assuming to be an A-*b*-B-*b*-A cut in center) were predicted with similar dimensions, or slightly larger in the A-*b*-B-*b*-A case. [32] Similar experimental results corroborate this spacing trend, while estimations report bridging conformation to be preferred in 1:1:1 composition. Looping conformation, in contrast, appears favorable in 1:2:1, even though both conformations appear in both compositions.[357] Slightly larger d-spacing has, also, been reported for A-*b*-B-*b*-A triblock copolymers because in the B domain both loops and bridges appear.

In a very comprehensive SCFT study by Matsen and Thompson, comparing symmetric A-*b*-B-*b*-A triblocks with their A-*b*-B counterparts, triblocks exhibited advanced segregation strength (higher T_{ODT}), due to less free ends [358]. Even more, narrower interfaces were predicted for A-*b*-B-*b*-A copolymers as a consequence of enhanced order.[269,359,360] Simultaneously, the B middle chain could stretch more compared to the A end chains leading to slightly larger d-spacings, while the complex phase regions shifted towards smaller f_A. They, also, predicted the fraction of B chains that adopt the bridging conformation for different morphologies, and the estimated fractions (lamellae: 40-45%, cylinders: 60-65%, spheres: 75-80%) were not highly affected by segregation strength and composition even though they were highly influenced by the morphology. [358] Overall, we can see that T_{ODT} in ABA copolymers can appear higher (lower χN_{ODT}), d-spacing can be slightly larger and narrower interfaces (i.e., lower LER) can be obtained, when compared to A-*b*-B copolymers with $N_{AB}=N/2$. These are significant properties in the pursuit of miniaturized well-defined nanofeatures. Furthermore, triblock copolymers have been reported to yield perpendicularly oriented nanostructures in their thin films more easily, while tolerance to incommensurability with guiding patterns in DSA can appear higher in ABA copolymers. [269,361-364]

Examples from the literature regarding A-*b*-B-*b*-A copolymers phase separated in domains with miniaturized dimensions both in bulk and thin films will be briefly discussed. For example, the already discussed, PS-PTMSS-*b*-PS, in conjunction with polymeric top coat and neutralized substrate was used to form vertical structures (L_0=29 nm) via 1 min annealing. Bulk studies on this highly segregated triblock copolymer, indicated the formation of lamellar morphologies with sub-30nm periodicities [174,365]. PMA-*b*-PS-*b*-PMA with balanced surface energies ordered in sub-8.5 nm nanodomains compatible with DSA techniques while lamellar morphologies exhibiting sub-16nm feature sizes were obtained when studied in bulk [253]. Li et al., used P2VP-*b*-PS-*b*-P2VP blended with polymeric additive that mitigates surface energy dissimilarity, to fabricate 8.5 nm half-pitch vertically oriented domains via chemical

epitaxy with a 5x density multiplication factor.[366] In a different study, P2VP-*b*-PS-*b*-P2VP was used in tandem with SVA to attain perpendicular sub-10nm structures, while the process was amenable to DSA procedures. SVA facilitated mitigating surface energy disparity as well as immobilizing polymer chains. In the triblock architecture, a wider process window for SVA was observed. [68] The high incompatibility due to the high hydrophobicity and the existence of a Si-containing segment at the triblock copolymer PLA-*b*-PDMS-*b*-PLA, led to the formation of lamellar, cylindrical and spherical arrangements with approximately 28 nm diameter in bulk [282]. Furthermore, in a different study, the same system self-assembled in hexagonal close-packed cylinders with sub-15nm domains [284].

Low molecular weight oligosaccharide triblock copolymers of the MH-*b*-PS-*b*-MH type microphase separated in lamellar and cylindrical morphologies exhibiting 8.4 and 10.6 nm domain spacing respectively as evident by TEM and SAXS [367]. Periodicities approximately 12 nm were obtained after SVA in mixed THF/H_2O that led to vertical and perpendicular orientation [367]. Body-centered cubic and cylindrical structures were evidenced in MH-*b*-PCL-*b*-MH triblock copolymers at different temperatures with the overall domain spacing not exceeding 13nm [368]. Potential triblock copolymers for nanopatterning consist of oligosaccharides and propylene oxide, namely MT-*b*-PPO-*b*-MT and MH-*b*-PPO-*b*-MH microphase separated in lamellar and cylindrical morphologies with domain spacing ranging from 6.4 to 11.8 nm. [369] Preferential PPO swelling during SVA and μ-wave oven annealing enabled the formation of cylindrical instead of lamellar morphologies. Thin films domain sizes were found approximately 8 nm. In a very recent work, the combination of MH oligosaccharide segments with PDL which is a bio-based polymer gave rise to cylindrical domains of approximately 13 nm both in bulk and thin film states. MH-*b*-PDL-*b*-MH triblock copolymers constitute an alternative for sustainable nanotechnology applications [370].

5.2. High χ Triblock Terpolymers (ABC)

Block copolymers of linear or complex architecture with two components generally demonstrate the same morphologies, most commonly spherical, cylindrical or lamellar. However, a wider range of morphologies, including rather exotic morphologies, like "decorated" lamellae or core-shell cylinders, can be attained when a third block is involved. In the microphase separation of such polymeric materials, the volume fraction is described by f_A and f_B, while f_C=1-f_A-f_B. Importantly, the segment-segment immiscibility is now described by three different Flory-Huggins parameters, χ_{AB}, χ_{BC}, χ_{AC}, the relative strength of which is very important. Critical is, also, the arrangement of the blocks in linear block terpolymers (ABC, ACB, BAC). [62,114,371,372] Some representative thin film studies comprising from A-*b*-B-*b*-C or ABC terpolymers follow.

Thin films of PS-*b*-P2VP-*b*-PtBMA have been used to create hexagonal perforated lamellar structures of P2VP/PS/P2VP sheets perforated by P*t*BMA channels. These, after the removal of P*t*BMA, could be used for nanolithographic applications. The P2VP sheet was, also, chemically modified to become hydrophilic something that could lead to expansion of the thin film applications. [373] In another thin film study, perpendicularly oriented core/shell cylinders of PS-*b*-PFS-*b*-P2VP led to hollow ring arrays of oxidized PFS with an outer diameter equal to 33 nm and an inner one equal to 11 nm. The patterns were successfully transferred to a PS layer. [374] Thin films of PB-*b*-PS-*b*-PMMA have, also, been used to create nanorings successfully transferred to silica films through RIE.[375] Nanopore and nanobushing arrays were, also, prepared from PS-*b*-PI-*b*-PLA and PI-*b*-PS-*b*-PLA via selective removal of the appropriate blocks.[376] Furthermore, nanoscale rings with sub-50nm diameter were obtained from PS-*b*-

PDMS-*b*-PLA. After oxygen RIE, PDMS turned into SiO_x used as a hard mask for pattern transfer on Au, NiFe, and NiCr (Fig.39). [377]

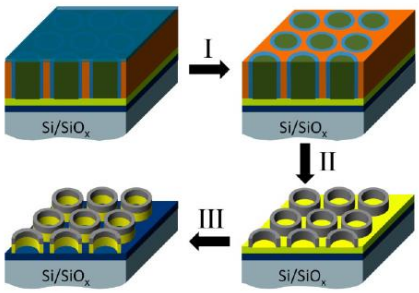

Fig.39. [377]

PI-*b*-PS-*b*-PFS and PI-*b*-PS-*b*-PFS/PS blends have been used to create structures of square lattice with long-range order on topographical substrates. Pattern transfer experiments led to 30 nm tall, 20 nm diameter silica nanopillars in a square lattice. Square-symmetry patterns can be preferred for several technological applications, in comparison to hexagonal close-packed.[378] Similar results were obtained from thin films of PI-*b*-PS-*b*-PFS blended with 15% PS utilized to fabricate nanolithography relevant, square patterns with significant in-plane ordering by controlling the surface chemistry, film thickness, solvent annealing conditions and substrate topography.[276]

An interesting approach for controlling the orientation involves the use of a short middle "sacrificial" segment in the thoroughly investigated BCPs systems such as PS-*b*-PMMA and PS-*b*-PDMS. Specifically, the introduction of a short hydrophilic PMAA block between PS and PMMA segments led to triblock terpolymers of the PS-*b*-PMAA-*b*-PMMA type. Not only did PMAA middle block promoted the phase separation, but also induced perpendicular orientation. Bulk morphologies exhibited *d* values 19.1 and 16.5 nm, respectively [235]. Most interestingly, vertically oriented lamellar domains with feature sizes as low as 8 nm were obtained further confirming the critical contribution of the sacrificial block.

A similar principal was adopted in a very recent publication where a low molecular weight "sacrificial" block was added to the extensively studied PS-*b*-PDMS system either as a first or as the middle block. Sub-15nm feature sizes for lamellar morphologies have been adopted in bulk, for the linear triblock terpolymers of the PS-*b*-$PB_{1,4}$-*b*-PDMS and $PB_{1,4}$-*b*-PS-*b*-PDMS sequences, while the layer thickness for the $PB_{1,4}$ blocks did not exceed 1.9 nm and 2.4 nm respectively [379].

Another interesting category of ABC terpolymers for DSA, is ABC miktoarms. The three different blocks are connected on a single junction point and a wider variety of complex morphologies can be attained, like tiling patterns. Again the relation between χ parameters is of primary importance. [87] For example, 3-miktoarm star (PI)(PFS)(PS) blended with PS resulted to 2D Archimedean tiling patterns. Graphoepitaxial DSA on square-symmetry tilings facilitated long-range order. The tilings were amenable to pattern transfer on the underlying substrate. (Fig.40) [380]

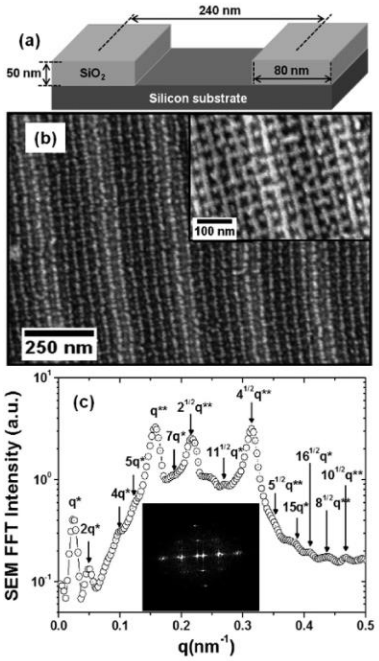

Fig.40.[380]

Recently, (PDMS)(PI)(PMMA) thin films were used to create cylindrical shells of PDMS or square arrays of nanodots after selective removal of PI and PMMA. The arrays were subsequently transferred to a silica substrate. [381] Overall, it can be seen that block copolymers comprising three constituents, can farther expand the versatility of structures attainable from microphase separation and help override critical obstacles observed in diblock copolymers.

5.3. Star-Block Copolymers

Star block copolymers self-assembly lead to high resolution, while keeping the system to a well-ordered state, since *N* values are higher than the linear diblock precursors due to the multiple diblock arms.

A remarkable work of star-block copolymers with regard to nanopatterning was published by Sun and co-workers.[274] They studied (PS-*b*-P2VP)$_n$ salt-doped star copolymers to yield nanofeatures with periodicities less than 10nm. The incorporation of salts binding to the P2VP segments increases the effective χ value allowing for even smaller domains. Furthermore, the possibility to obtain ordered miniaturized nanofeatures by taking advantage of a lowered critical order-disorder transition point, $(\chi N)_c$, attainable by star-block copolymers is, also, discussed with corroborating SAXS and STEM data. When the diblock arm molecular weight was reduced, while the arm number was increased to maintain order, smaller nanofeatures were produced. This is a study that directly links star-block architecture with smaller achievable nanofeatures, useful for future nanopatterning applications.

Sung and co-workers, have worked extensively on star-block copolymers comprising either PFMA-*b*-PS or PMMA-*b*-PS arms.[382] They employed a recently found annealing method, called Solvent Vapor Annealing with Soft Shear (SVA-SS) to obtain perpendicularly oriented, aligned lamellae in thin films. It is noteworthy, that in star-block copolymers the interfacial width was reduced as compared to the linear analogues, which facilitates the formation of nanopatterns with lower LER. The group estimated much increased χ_{eff} values for the stars (~2.5x for PFMA-*b*-PS), while the estimated lowest possible domain periodicities were

on the single-digit nanometer scale (L_0=7.8nm), based on the estimated χN_c values, lower in star-block copolymers.

In another, recent work by Isono and co-workers, an oligosaccharide-containing star-block copolymer (PCL-*b*-MT)$_n$ was utilized to obtain cylinders with domain periodicities as small as 6nm, by employing a high χ system along with complex molecular architecture.[383] Again in this study, higher T_{ODT} values were observed for copolymers of star-block architecture, while the morphology and d-spacing compared to separate arm chains remained intact. Importantly, pattern fidelity from star copolymers in thin films was much improved compared to the linear analogues, which can be extremely useful for nanopatterning applications. Even more, crystallization, a factor that disturbs microphase separation, of the inner block, PCL, was highly attenuated in stars. At last, the authors suggested that increased T_{ODT} allows for much improved self-assembly kinetics with high-temperature ultrafast annealing methods. In a different study, another oligosaccharide, MH, was combined with PBA in A-B, A-B-A and (A-*b*-B)$_n$ copolymers to produce thin films as charge trapping layers in field-effect memories for stretchable electronics.[384] It was proven that star-block architecture allowed for films with improved memory performance and enhanced mechanical properties with better tolerance to high strain.

Apart from the higher T_{ODT} values, the enhanced interfacial width between the nanodomains, the lower achievable feature dimensions and the improved mechanical properties, another reason that star-block copolymers appear as promising materials for nanopatterning is their higher tendency to form vertical nanodomains in thin films as compared to their linear analogues. This was observed in thin films of (PMMA-*b*-PS)$_{18}$ on various substrates.[385] In essence, the driving force of vertical orientation is the entropic penalty that the star-block system has to pay in order for the self-assembling chains to preferentially wet the substrate. This entropic penalty is induced by the increased number of covalently linked junction points, while the MW, also, plays an important role.[386] A schematic illustration of the mechanism is presented in Fig.41.

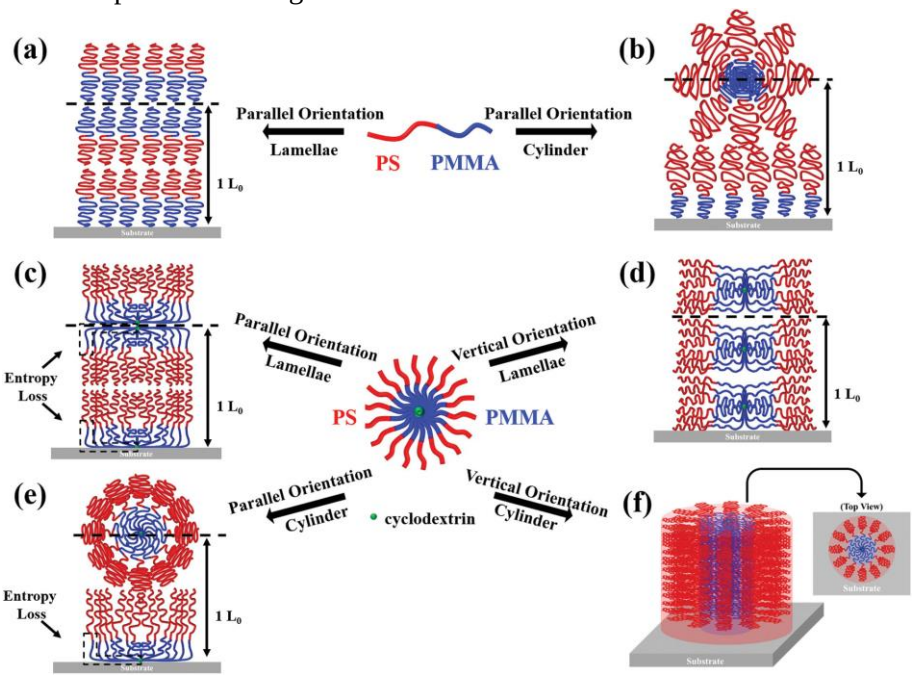

Fig.41. Chain arrangement of linear diblock copolymer on a substrate with thickness of 1.5 L 0 for a) lamellar and b) cylindrical nanodomains. Chain arrangement of lamellar nanodomains of star-shaped block copolymer on a substrate with thickness of 1.5 L 0 for c) parallel and d)

vertical orientations. Chain arrangement of cylindrical nanodomains of star-shaped block copolymer on a substrate for e) parallel and f) vertical orientations.[386]

In a very recent study, the thin film morphology of lamellar nanodomains of 6-arm star block copolymers of [(PMMA-*b*-PS)$_6$] were demonstrated leading to rectangular channels as a function of the trench width (*W*) based on DSA and graphoepitaxy. A systematic comparison between the experimentally obtained topologies, which are strongly dependent upon *W/L*0, with self-consistent field theory predictions, took place. Contributing factors such as polymer brushes or selective gold (Au) deposition severely influence the domain orientation allowing the formation of various nanopatterns(Fig.42).[387]

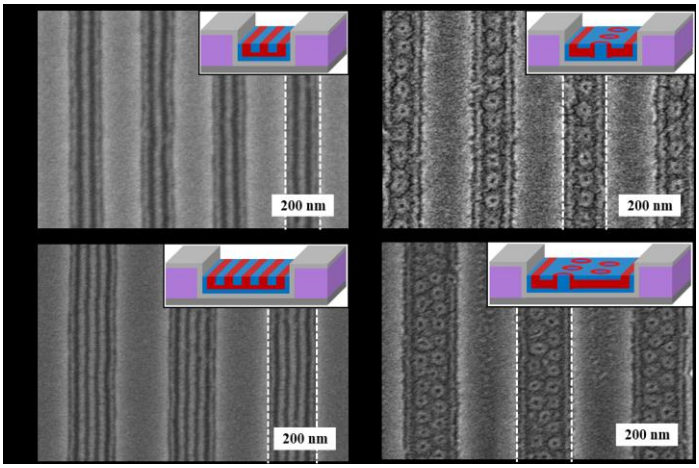

Fig.42. FE-SEM images of (PMMA-*b*-PS)$_6$ thin films with *h* = 30.0 nm (1.00 *L*0) in trenches with an Al2O3 layer with varying *W* (a: 90 nm (3.00 *L*0), b: 120 nm (4.00 *L*0), c: 150 nm (5.00 *L*0), and d: 180 nm (6.00 *L*0)). Each inset shows a schematic for the microdomain alignment of (PMMA-*b*-PS)$_6$ within the trench. Blue and red colors represent PMMA and PS blocks of (PMMA-*b*-PS)$_6$, respectively. The scale bar in the images is 200 nm. [387]

In a subsequent study, Lo et al. have used (PS-*b*-PDMS)$_n$ copolymers, with a much higher χ, to obtain vertically oriented nanostructures on thin films, that were farther used as lithographic masks for pattern transfer or as templates for nanoporous monoliths.[388] As generally known, the enthalpic interactions from the interfaces determine the orientation of nanodomains in BCP thin films. However, in star-block copolymers the increased chain end number induces an enhanced entropic contribution effect that can override the enthalpic contributions from the interfaces, providing thus a simple means for attaining vertical nanodomains initiated from the bottom interface. The entropic effect is governed by the arm number and surface energy disparity of the blocks(Fig.43). As the number of arms increases the entropic penalty for obtaining parallel nanodomains increases, too, while the surface energy disparity plays a key role as to whether few layers of parallel oriented nanodomains will occur at the thin film/free surface interface. (Fig) (PS-*b*-PDMS)$_n$ copolymers have, also, been used to obtain high-aspect ratio span-thru vertical cylinders. The entropic effect of star-block architecture, in tandem with surface air plasma treatment to mitigate preferential wetting in the top surface, led to perpendicular cylinders with the orientation control initiated simultaneously from the top and bottom interfaces, in parallel with a cylinder self-alignment process (Fig.44).[389] Examples of entropy driven vertical orientation have been observed on high χ rod-coil star-block copolymers, too.[390] The lower bulk dimensions obtained from star-block copolymers of the (PS-*b*-PDMS)$_3$ or (PS-*b*-PDMS)$_4$ type were reported in a recent study by the same group for lamellar morphology, giving rise to as low as 14 nm feature sizes [86].

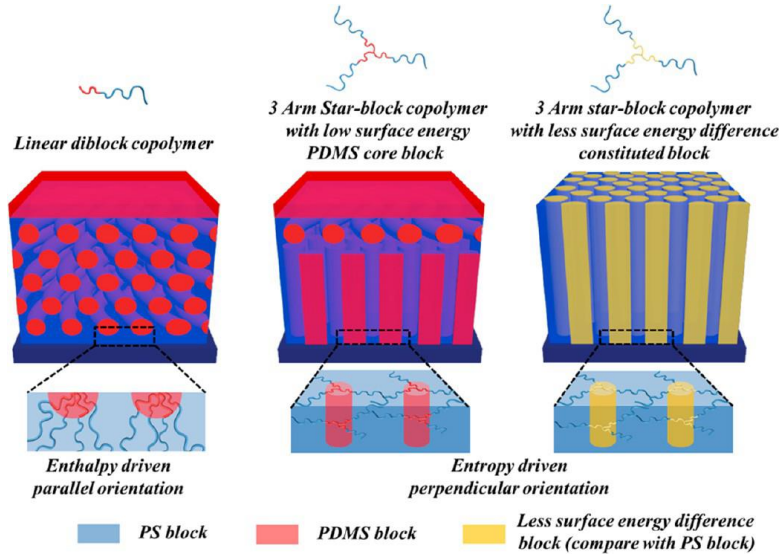

Fig.43. Schematic illustration of entropy-driven orientation of nanostructured thin films using star-block copolymer of the (PS-*b*-PDMS)$_3$ type and star-block copolymer with less surface energy difference constituted block in comparison to the enthalpy-driven orientation using a simple diblock copolymer (PS-*b*-PDMS).[388]

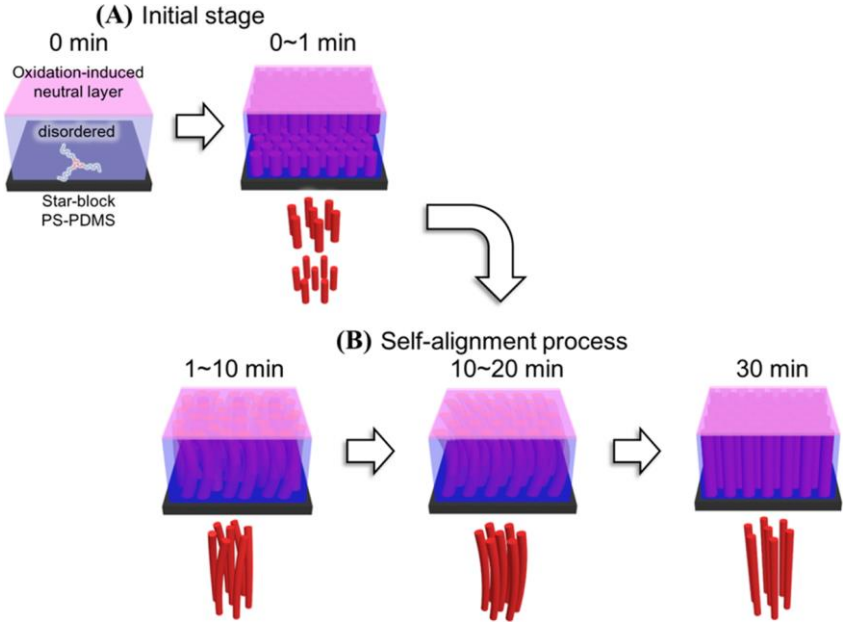

Fig.44. Schematic illustration of the self-alignment process of the perpendicular cylinder-structured star-block PS−PDMS thin film with annealing time as indicated. (A) The nucleation of perpendicular cylinders can be formed from both the interfaces of the top and the bottom at the initial stage of the thermal annealing process. (B) Span-thru PDMS perpendicular cylinders can be fabricated through the self-alignment process with the increase of the thermal annealing time as illustrated.[389]

5.4. Miktoarm Star Copolymers

As already mentioned, miktoarm star block copolymers can self-assemble into morphologies other than their linear counterparts for the same volume fraction, due to architectural asymmetry. This partial decoupling of the obtained morphology from the volume fraction, broadens farther the range of possibilities for nanopatterning through the self-assembly of block copolymers with complex architecture. Several groups leveraged this effect to obtain ultra-small nanofeatures in thin films.

Recently, Kim et al., studied the effect of architecture on $PS(P2VP)_2$ copolymers in thin films.[391] They reported, apart from changes in the observed morphologies, changes in the orientation of the block copolymers in the thin film state. $PS(P2VP)_2$ after SVA, exhibited parallel structures, whereas PS-*b*-P2VP of the same volume fraction exhibited vertical ones. Authors attributed this effect to the absence of micellar structures in the as-spun films of $PS(P2VP)_2$ as compared to PS-*b*-P2VP that ultimately led to effective anchoring of P2VP to the substrate, whereas in the linear copolymers due to micelle formation P2VP-substrate interactions were partially masked. Topographical DSA was, also, tested by utilizing sapphire faceted substrates to align the PS cylinders of $PS(P2VP)_2$ parallel to the ridge direction.

Shi and coworkers, studied the effect of molecular architecture both experimentally in PS_2PLA_2 or $PS(PLA)_2$ copolymers and theoretically through SCFT and RPA analysis. Experimental results led to nanodomains with periodicities as low as 12.8 nm, while the effect of molecular architecture on domain morphology was observed. Through the theoretical calculations spinodal curves were constructed for copolymers of all architectures for a certain N, as well as normalized for arm number. Importantly, by SCFT calculations they predicted that for certain N, A_nB_n miktoarm stars separate into domains with periodicity $(1/2)^{2/3}$ in comparison to AB copolymers and this discrepancy is even larger (i.e., even smaller nanodomains comparatively) as segregation strength increases. For definite N, they predict d-spacing to increase in the order A-*b*-B>AB_n>A_nB_n. This comprehensive study, combining both experimental and theoretical data, highlights the potential of copolymers with complex architecture for sub-10 nm nanopatterning.[392]

In another study, PS_4PLA_4 was utilized to produce cylinders and lamellae with periodicities ranging from 15.5-21 nm.[393] They concluded that in WSL, in accordance to theory, T_{ODT} increases, while d-spacing is slightly lower when comparing PS_4PLA_4 with their linear isomers. This unexpected behavior was predicted only near the ODT. In thin films vertical nanostructures with short-range order (due to weak segregation) were observed on a PS substrate, while PLA was easily removed with basic hydrolysis. All short-chain miktoarms exhibited phase separation, whereas from the linear isomers only one with the higher MW did.

Minehara et al., used a hybrid inorganic/organic copolymer comprising PDMS and PLA to study the effect of branched architecture on the microphase separation of a high χ low N (highly stretched) copolymer in bulk and in thin films.[284] Chi parameter, χ, was recalculated here by SAXS equal to 0.24 at $T>T_{ODT}$. Due to elastic and architecture asymmetry, branched copolymers (miktoarm stars) exhibited different morphologies from their linear counterparts. For example, branched copolymers with f_{PLA}=0.2 exhibited cylindrical structures with 6.5 nm diameters, whereas the linear analogues formed spherical domains. Regarding d-spacing, for a pair of architectural isomers with the same morphology it was almost the same for both copolymers. The scaling law of Matsushita for branched copolymers predicted significantly smaller nanodomains from the branched copolymer of this composition in the SSL, however this discrepancy was attributed by the authors to an effect of the segregation strength of the examined copolymers. They, also, suggested a new scaling law incorporating the effect of immiscibility should be prepared. The authors, also, mentioned that branched copolymers exhibited higher correlation length which they attributed to less entanglements and enhanced diffusion kinetics under annealing. Overall, this extensive study indicates how important it is to study farther and more thoroughly the effect of macromolecular architecture when considering BCP thin films for nanopatterning.

Worth mentioning is, also, the case of PS(hv-PS')-*b*-P2VP and PS(hv-PS')-*b*-PMMA.[394] These are miktoarm copolymers with a photocleavable arm that after UV irradiation lead to a blend of diblock copolymer and arm homopolymer chains, providing access to morphology

tuning and dual nanopatterning from a single starting material. Dot or line patterns were attained at specific substrate areas depending on whether the areas were UV irradiated or not, while the procedure was tested in topographically prepatterned substrates, too. P2VP was, also, utilized for metal deposition yielding Pt nanowires and nanodots. (Fig.45)

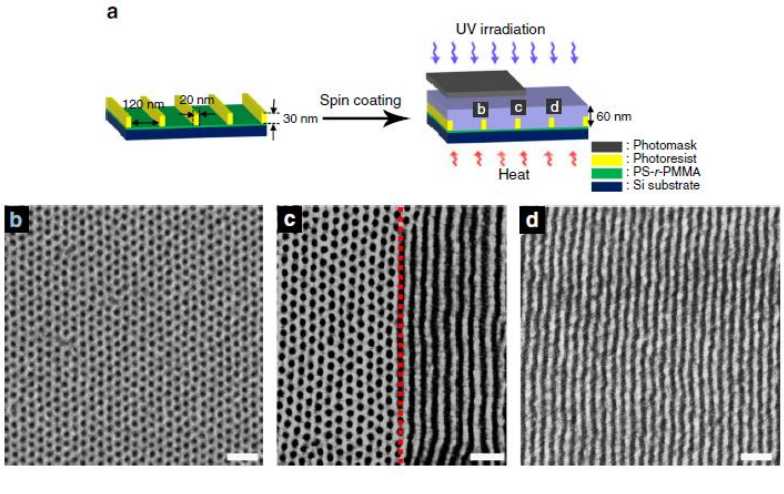

ς

Fig.45. Directed self-assembly of PS(hv-PS′)-*b*-PMMA after selective UV exposure. a Scheme of directed self-assembly using topologically pre-patterned substrate. SEM images of PS(hv-PS′)-*b*-PMMA on a patterned substrate at b unexposed, d exposed, and c boundary regions. Dark holes and lines in SEM images represent PMMA nanodomains that were etched out by O2 RIE. The red dotted line represents the boundary. Scale bar is 100 nm. [394]

Recently, as previously mentioned, much work has been done on oligosaccharide-containing block copolymers for fabrication of sub-10nm structures, due to their strong incompatibility with conventional organic blocks because of the hydrophilic/hydrophobic interactions present as well as the rod-like configuration of saccharides.

In a cornerstone study it was found that d spacing was decreased by increasing the branching degree in saccharide-based miktoarm copolymers of the MH-*b*-$(PCL)_2$ and MH-*b*-$(PCL)_3$ types. Bulk assembly led to body-centered cubic phases with sub-10nm feature sized, which is smaller than the obtained nanodomains of the corresponding linear precursors (Fig.46). [273] Conformational asymmetry in conjunction with multiple arms number is beneficial to the shrinkage of the domains.

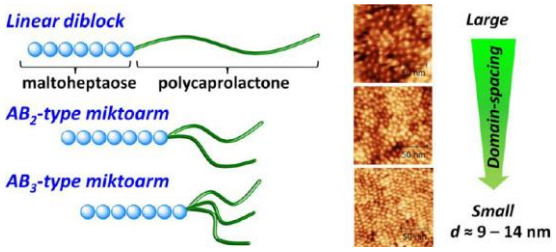

Fig.46.

The same constituents but this time with different topology, namely $(MH)_2PCL$ and MH-*b*-PCL-*b*-MH, were investigated again by Isono and coworkers. Triblock copolymers exhibited essentially the same morphology as their diblock isomers.[368] Importantly, lamellar structures not achievable by the linear analogues were observed in $(MH)_2PCL$ of f=0.27 and f=0.16. Thermal caramelization of the MH blocks was, also, investigated, leading to order-order transitions and lower d-spacing values. Miktoarm star block copolymers showed higher periodicities than triblock copolymers of the same MW and volume fraction which was attributed to bilayer MH structures in contrast to interdigitated chains in the triblocks. The results from these two previous studies are summarized in the following figure. It can be seen

that for a certain volume fraction, bcc, hex, and lamellae morphologies can be attained simply by tuning macromolecular architecture.

In a subsequent study, $(MH)_2PS$, MH-*b*-PS-b-MH and MH-*b*-PS were again investigated regarding their microphase separation and sub-10 nm feature sized formed.[367] Morphology tuning was farther facilitated by macromolecular architecture. In accordance to other experimental studies, lamellar domains formed from triblock copolymers oriented vertically to the substrate in thin films after SVA, whereas the A_2B analogue formed parallel lamellae. Domain periodicities between 7.6-10.5 nm were obtained in all cases.

Lastly, in a more nanopatterning focused study, Katsuhara et al. synthesized PVFc-*b*-MH and $PVFc(MT)_2$ to achieve sub-10 nm nanodomains (d~8nm) with enhanced thermal stability and etch-selectivity (PVFc:poly(vinyl ferrocene), MH:maltohexaose, MT:maltotriose).[395] Better long-range order was observed for $PVFc(MT)_2$ in comparison to PVFc-*b*-MH, because the lower T_g of MT facilitated enhanced chain mobility and grain coarsening, proving how versatile the utilization of macromolecular architecture can be for nanopatterning. By comparison, PVFc-*b*-MT did not form ordered structures due to lower MW. Lamellar structures were obtained, too, when $PVFc(MT)_2$ was blended with glucose to increase $\varphi_{saccharide}$. Importantly, thin film studies were conducted with $PVFc(MT)_2$ with sub-10 nm full periodicity parallel cylinders being prepared that could allow for line/space patterns.

XPOSS-*b*-$(PS)_2$ miktoarm BCPs presented lamellar and cylindrical morphologies with feature sizes smaller than 10 nm [396]. In this study the influence of segments composition and conformational asymmetry on the self-assembly behavior was determined and led to the conclusion that miktoarm copolymers showcased advanced nanophase separation to the respective linear precursor.

Previously we mentioned that apart from asymmetry due to architecture, important is, also, the effect of conformational asymmetry. Some studies regarding miktoarm stars incorporating high conformational asymmetry have been conducted. Goseki et al. investigated the effect of architectural asymmetry but in a copolymer with high conformational asymmetry, too. Rod-coil $(PS)_2$-*b*-PMAPOSS [397] copolymers were used to fabricate ellipsoidal cylinder-like PMAPOSS nanostructures when vol % PS was 60%, whereas the corresponding linear block copolymers yielded lamellae. Similarly, different morphologies were formed in AB_2 rod-coil copolymers containing π-conjugated blocks $(P3DDT)_2$-*b*-PMMA [398] when compared to linear isomers, while the effect of architecture, also, impacted the crystallization behavior and fibril structure formation of the conjugated block, which is particularly important for organic electronics.

5.5. Cyclic Block Copolymers

Cyclic copolymers can self-assemble in nanostructures with much lower domain spacing compared to their linear analogues. However, the utilization of this property to fabricate ultra-small nanodomains on thin films directed for nanopatterning has not been extensively studied. This is mainly attributed to the fact that cyclic copolymers demand for difficult synthetic procedures. Considering, though, the remarkable progress on cyclic copolymer synthesis, this complex architecture could ultimately find its niche in nanopatterning applications, too.[108]

Two comprehensive recent studies addressed this issue utilizing cyclic copolymers on thin films. In the first study, by Poelma and co-workers, thin films of PS-*b*-PEO cyclic copolymers were compared to linear A-*b*-B diblock copolymers of the corresponding full or half molecular weight.[109] A large reduction, around 25%, in d-spacing was observed for the full molecular

weight analogue, whereas the copolymer of half molecular weight remained disordered. Importantly, sub-20nm periodicities were attained through the ring architecture.
In the second study, Gartner et al., used PS-*b*-POEGMA cyclic copolymers along with their linear counterparts to make direct comparisons with a view to integrating cyclic copolymers in nanopatterning and templating applications.[110] Salt-doping with different amounts of lithium salt was employed to examine a range of segregation strengths utilizing a single initial copolymer. A ~20% reduction of d-spacing was observed for the cyclic copolymers in comparison to linear AB diblock copolymers at all segregation strength values. Additionally, both experimental and simulation data indicated less sensitivity of cyclic copolymers to χ_{eff} changes for a standard MW. It should be noted, however, that less distinct domains, i.e., slightly higher interfacial mixing, which implies higher LER, were reported for the ring chains. However, this discrepancy was mitigated at high χ_{eff}Ns. Corroborating data from molecular dynamics simulation were provided. Overall, farther work would expand our knowledge on thin films of cyclic block copolymers, but the reduced domain spacing of their microphases seem to provide an alternative route to ultrasmall nanofeatures.

6. Future Perspectives

Although significant scientific research has already been conducted concerning the fundamentals of polymer science and technology with respect to nanotechnology, new emerging applications are expected to have a significant role to next generation lithography. BCPs self-assembly constitutes a cost-effective nanofabrication method which is complementary to optical lithography techniques. The miniaturization of feature sizes in the sub-5nm scale is a prerequisite to the current social need for low-dimension opto-electronics, nanodevices, nanoporous membranes, drug delivery, nanostructure networks and nanoparticle templates.

Block copolymers with high χ/low N characteristics have received tremendous attention for the above-mentioned applications. Nevertheless, the inherent properties of each copolymer limit the resolution to a bottom level, shifting the attention towards the enhancement of χ parameter utilizing exotic segmental combinations. A different approach involves the use of complex architecture systems, because of the minimization of defects induced by the multiple arms as well as the ability to adopt periodicities with lower d-spacing. Innovative synthetic procedures and post-polymerization modification reactions have enabled the preparation of novel linear and complex architecture BCPs capable of forming even lower dimensions.

The facile processability, etching selectivity, spontaneous self-assembly and low-cost treatment render the fabrication of block copolymer masks feasible. Grapho-epitaxial methods are then applied in order to obtain perpendicular oriented cylindrical or lamellar morphologies. Long-range order is essential to the final manufacturing process, since the perfectly oriented, defect-free patterns are critical for the successful outcome of DSA. The susceptibility of polymer materials to external stimuli provides the ability to align the nanodomains depending on their intrinsic properties.

This review article emphasizes the significant progress made regarding the exploitation of BCP self-assembly in nanotechnological applications in an effort to move towards the much desired “plenty of room at the bottom”. The recent advances concerning novel synthesis as well as the analogous applications have been covered highlighting the potential future perspectives.